Distribution Agreement

In presenting this thesis or dissertation as a partial fulfillment of the requirements for an advanced degree from Emory University, I hereby grant Emory University and its agents the non-exclusive license to archive, make accessible, and display my thesis or dissertation in whole or in part in all forms of media, now or hereafter known, including display on the world wide web. I understand that I may select some access restrictions as part of the online submission of this thesis or dissertation. I retain all ownership rights to the copyright of the thesis or dissertation. I also retain the right to use in future works (such as articles or books) all or part of this thesis or dissertation.

Signature:

_____

Dillon Graham Patterson Date

IRF4 controls cell fate outcomes during the initial stages of B cell differentiation

By

Dillon Graham Patterson
Doctor of Philosophy

Graduate Division of Biological and Biomedical Science
Genetics and Molecular Biology

Jeremy M. Boss, PhD

Advisor

William G. Kelly, PhD

Committee Member

Roger B. Deal, PhD

Committee Member

Ignacio Sanz, MD

Committee Member

Joshy Jacob, PhD

Committee Member

Accepted:

Lisa A Tedesco, PhD

Dean of the James T. Laney School of Graduate Studies

Date

IRF4 controls cell fate outcomes during the initial stages of B cell differentiation

By

Dillon Graham Patterson

M.S., University of South Alabama, 2015

B.S., University of South Alabama, 2014

Advisor: Jeremy M. Boss, PhD

An abstract of

A dissertation submitted to the Faculty of the

James T. Laney School of Graduate Studies of Emory University

in partial fulfillment of the requirements for the degree of

Doctor of Philosophy

in

Graduate Division of Biological and Biomedical Science

Genetics and Molecular Biology

2021

Abstract

IRF4 controls cell fate outcomes during the initial stages of B cell differentiation

By: Dillon Graham Patterson

Naive B cell (nB) differentiation to antibody-secreting plasma cells (ASC) requires significant transcriptional and epigenetic reprogramming events that are coupled to cell division. Following antigen stimulation, considerable heterogeneity exists between responding activated B cells (actB), such as their cell division capacity and ability to differentiate. However, a complete understanding of the factors that drive such heterogeneity are unknown. Here, we identified the transcription factor interferon regulatory factor-4 (IRF4) as one molecular determinant controlling cell fate outcomes. Using an *in vivo* model system and single cell RNA-sequencing, we identified a bifurcation event that occurred during the earliest stages of B cell differentiation, with only one trajectory leading to ASC formation. This differentiation branch, termed the ASC-destined branch, required IRF4 induction and could be distinguished from non-ASC cells by loss of CD62L expression. Comparing bulk RNA-sequencing data from actB that followed each branch indicated the non-ASC cells contained a pre-memory B cell transcriptional signature, indicating they may be destined to become memory B cells. Additionally, these data indicated the IRF4-dependent ASC-destined branch upregulated gene sets necessary for proliferation. To explore the role of IRF4 on proliferation, we performed an adoptive transfer time course covering three days using IRF4-sufficent and -deficient B cells. We found that IRF4-deficient B cells divided but stalled during the proliferative response, indicating IRF4 also controlled the proliferative capacity of responding B cells. To better understand the cell division-coupled IRF4-dependent reprogramming events that occurred during the initial stages of B cell differentiation, CellTrace Violet (CTV)-labeled IRF4-sufficient and -deficient B cells were sorted in discrete divisions for RNA- and ATAC-sequencing. Transcriptional analyses revealed that IRF4 was critical for inducing MYC target genes and metabolic gene sets during the earliest cell divisions. Complementary chromatin accessibility analyses suggested a hierarchy of IRF4 binding activity and identified broad networks of dysregulated transcription factor families, including E-box binding family members. Indeed, IRF4-deficient B cells failed to induce *Myc* and displayed altered cell cycle distribution. Furthermore, IRF4-deficient B cells exhibited reduced mTORC1 signaling and were unable to increase in cell size. *Myc* overexpression in IRF4-deficient cells was able to rescue the cell growth defect, indicating an IRF4-MYC-mTORC1 relationship that controls cell growth and the proliferative capacity of actB in the earliest cell divisions. Taken together, we identify IRF4 as a key factor that instructs cell fate outcomes during the initial stages of B cell differentiation, including differentiation, proliferation, and cell growth.

IRF4 controls cell fate outcomes during the initial stages of B cell differentiation

By

Dillon Graham Patterson

M.S., University of South Alabama, 2015

B.S.., University of South Alabama, 2014

Advisor: Jeremy M. Boss, PhD

A dissertation submitted to the Faculty of the

James T. Laney School of Graduate Studies of Emory University

in partial fulfillment of the requirements for the degree of

Doctor of Philosophy

in

Graduate Division of Biological and Biomedical Science

Genetics and Molecular Biology

2021

Acknowledgements

First, I'd like to thank my advisor, Dr. Jerry Boss, for his mentorship, friendship, and support during my tenure in the lab. This mentorship includes both rigorous scientific training as well as the development of professional and leadership skills that I can implement in the future. Additionally, I would like to thank Dr. Chris Scharer for his mentorship, friendship, and continued direction through the duration of my time in the lab. Without Chris' expertise and encouragement, the work herein would not be possible. I would also like to thank the many scientists with whom I've overlapped in Jerry's lab, including: Ben Barwick, Lex Bally, Royce Butler, Jake Fontaine, Bhanu Gandham, Lou-Ella George-Alexander, Muyao Guo, Mansi Gupta, Sakeenah Hicks, Gaurav Kumar, Joshua Lee, Parimal Majumder, Jeff Maurer, Tian Mi, Dennis Neeld, Mike Powell, Andrew Rahmberg, Jim Rose, Qing Wang, Keenan Wiggins, and Zhihong Zuo. Importantly, I'd like to give a special thank you to fellow graduate students Bob Haines (GMB), Madeline Price (IMP), and Anna Kania (GMB) who helped make my time in the Boss lab a fun and productive training experience. We all pushed, encouraged, and assisted each other, and I am forever grateful for our overlapping time in the lab together. I would also like to thank my committee members Drs. Roger Deal, Bill Kelly, Iñaki Sanz, and Joshy Jacob for their time and direction throughout the duration of this project. Thank you to my Emory cohort for their encouragement and assistance during my coursework at Emory, as well as Dr. Tamara Caspary for her professional guidance and advice. Additionally, I would like to thank my family: Mike and Mary Patterson (father and step-mother), Sharon and Steve Cross (mother and step-father), Christy St. John (mother-in-law), Chris Caldwell (father-in-law), Megan and Nate Bush (sister-in-law and brother-in-law), Sterling Cross (step-sister), and Kaylen and Jonathan Beard (sister and brother-in-law) for their unwavering support. Lastly, I would like to thank my amazing wife, Alexandria Patterson, for her support and encouragement, even when pursuing a career in science was a distant goal when we met in undergrad. Thank you for your sacrifice and support; without you, none of this would be possible.

Table of Contents

List of Figures and Tables

Chapter 1

Chapter 2

Chapter 3

Chapter 1. Introduction

Dillon G. Patterson*[1], Anna K. Kania*[1], Zhihong Zuo*[1], Christopher D. Scharer[1], and Jeremy M. Boss[1]

*These authors contributed equally

[1]Department of Microbiology and Immunology, and the Emory Vaccine Center, Emory University School of Medicine, Atlanta, GA 30322, USA

Correspondence: jmboss@emory.edu

Author Contributions

D.G.P. and A.K.K. made figures and wrote the review. Z.Z. participated in writing and figure design. All authors edited the manuscript.

Chapter Notes

Components of this chapter were previously published and have been modified or expanded for the purposes of this chapter.

Components of this chapter were originally published in *Immunological Reviews*. Dillon G. Patterson, Anna K. Kania, Zhihong Zuo, Christopher D. Scharer, and Jeremy M. Boss. 2021. Epigenetic gene regulation of plasma cells. *Immunol Rev.*

I. B CELL DEVELOPMENT AND DIFFERENTIATION

Revolutionary discoveries contributing to our understanding of humoral immunity

The discovery that immunity exists is attributed to Edward Jenner, who published observations in 1796 that individuals infected with the mild disease of cowpox seemed to be protected against the more severe disease of smallpox. In fact, Jenner demonstrated this experimentally by inoculating subjects with pus from cowpox-infected milkmaids and showing it conferred protection against the related disease of smallpox [1,2]. This discovery inspired additional work, including research from Louis Pasteur, who discovered that attenuated organisms can prevent infectious disease [3]. However, it was not until a century later that the mechanism of protection afforded by vaccination began to be uncovered.

In 1890, Emil von Behring and Kitasato Shibasaburō published reports that serum – or as they call it, "cell-free blood fluid" – could cure infected animals or prevent healthy animals from being infected [4]. This work was the first to recognize that serum from previously infected animals contained the "antitoxins" needed for protection, establishing the existence of an adaptive and humoral component of the immune system. Paul Ehrlich built on these observations and described the "side-chain theory" that explained the antitoxins as receptors, or "antibodies", that he envisioned were shed by cells into the bloodstream. While antibodies clearly provided protection from pathogens, their origin remained unidentified.

The plasma cell theory of antibody formation [5] evolved in the 1940s and 1950s after it was discovered that plasma cell levels correlated with an increase in antibody [6], which was later supported by *in vitro* studies [7]. Thus, plasma cells were established as the cellular

source of antibodies, but their origin remained elusive. A breakthrough occurred when Max Cooper and colleagues later discovered the cellular source of plasma cells – B cells – after removing the Bursa of Fabricius from chickens and demonstrating that B cells controlled a "Bursa-dependent follicle in the spleen" (now recognized as germinal centers) and antibodies [8-11]. In the years that followed, biomedical research has built upon these findings to better understand the cellular and molecular mechanisms that control B cell mediated diseases [12], antibody diversity [13], and plasma cell differentiation [14,15]. Despite these advances, many components of B cell differentiation remain uncovered and continued efforts are needed to fully understand the events that transpire during plasma cell formation.

B cell formation

In mammals, B cell development for most B cells begins in the bone marrow [16,17] (**Figure 1-1**). Bone marrow multipotent hematopoietic stem cells (HSC) first differentiate into multipotent progenitor cells (MPP) that can give rise to both lymphoid [18] and myeloid cells [19,20]. MPP express the FLT3 receptor [21,22] that interacts with FLT3 ligand [23,24] on bone marrow stromal cells, ultimately resulting in signaling that promotes the differentiation of common lymphoid progenitor cells (CLP) [17]. The first committed B cell-lineage cell (the pro-B cell) arise from CLP. Transcription factors (TF) E2A [25,26] and early B cell factor (EBF) [27] instruct transcriptional programs that determine the pro-B cell state and are dependent on the expression of other TF, including Ikaros [28,29] and PU.1 [17,30,31]. One key TF that is induced by E2A and EBF is Pax5 [17,32]. Deletion of Pax5 results in B cell arrest

at the pro-B cell stage and is an essential TF for reinforcing the B cell transcriptional program throughout B cell maturation [33].

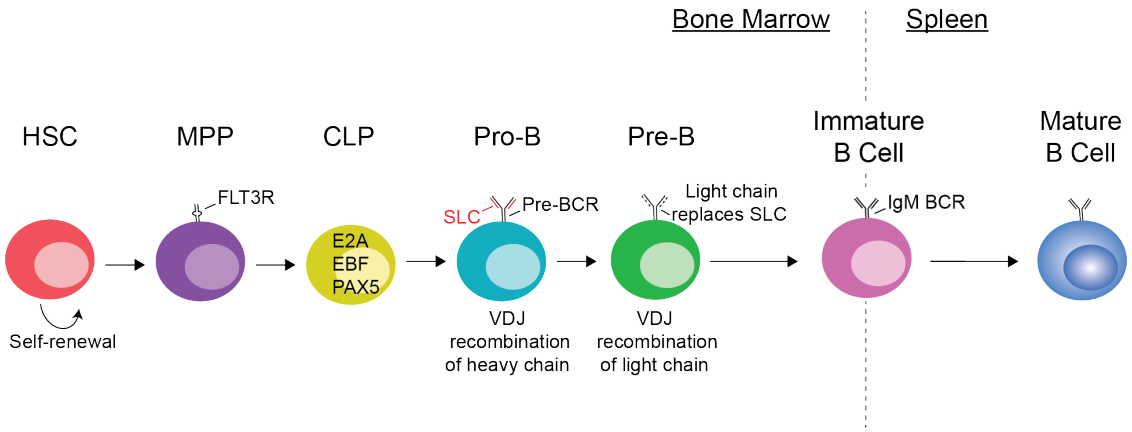

Figure 1-1. **B cell development**. Hematopoietic stem cells (HSC) give rise to multipotent progenitor cells (MPP) that can commit to common lymphoid progenitor cells (CLP). CLP then progress through B cell differentiation stages and eventually migrate to the spleen to complete maturation. Transcription factors critical for commitment of Pro-B cells are shown inside the cell representing CLP. SLC; surrogate light chain.

The proceeding B cell development stages are structured around rearrangement of immunoglobulin gene segments (**Figure 1-1**). E2A and EBF are critical for this process and induce expression of RAG enzymes that promote the rearrangement [34]. Heavy chain gene segments are rearranged in a fixed order [35], and include variable (V_H), diversity (D_H), joining (J_H) and constant regions. During the early pro-B cell stage, D_H to J_H rearrangement occurs followed by V_H-DJ_H in the late pro-B cell stage [36]. The rearranged heavy chain, which has the μ constant region, joins with a surrogate light chain [37] to form the pre-B cell receptor [38]. The pre-B cell receptor tests for successful rearrangement of the heavy chain, which signals [39] pro-B cells to halt additional heavy chain rearrangement and proceed to the next stage of B cell development [40]: the pre-B cell stage. During this stage, rearrangement of the light chain begins. The light chain is comprised of variable (V_L),

joining (J_L), and constant regions. Upon rearrangement of V_L to J_L, the bona fide light chain replaces the surrogate light chain to form a complete IgM molecule on the surface of the developing cell, forming an immature B cell [16,41]. At this stage, autoreactive immature B cells that exhibit strong reactivity to self-antigen are identified and prevented from continued development [42,43]. Immature B cells that demonstrate no autoreactivity migrate from the bone marrow to the spleen where they continue their maturation to a mature naive B cell. Mature naive B cells remain quiescent until encountering an immune challenge [44] and exhibit an average lifespan of 5-7 weeks [45]. This remarkable process of B cell development results in the generation of mature naive B cells with a theoretical B cell receptor diversity of more than 10^{13} different potential specificities [46]. In this dissertation, splenic mature naive B cells are the cellular source used to study B cell differentiation to antibody-secreting plasma cells (ASC).

B cell activation

The humoral arm of the adaptive immune system relies on robust differentiation of naïve B cells (nB) into ASC. Upon antigen encounter, nB become activated, rapidly proliferate, and undergo substantial epigenetic reprogramming events, with a subset differentiating to ASC (**Figure 1-2**). B cell stimulation with T cell-independent (TI) antigens, such as lipids and polysaccharides, leads predominately to the formation of short-lived plasma cells (SLPC). TI antigens can be subdivided into two types [47]. TI type I antigens include pathogen-associated molecular patterns that bind pattern recognition receptors, such as toll-like receptor recognition of bacterial cell wall components or DNA. TI type II antigens have highly repetitive, multivalent structures that activate B cells by crosslinking of their

B cell receptors (BCR) [48]. TI type I antigens elicit large polyclonal responses, whereas TI type II antigens engage the BCR and thus induce antigen-specific B cell response. Intriguingly, TI type II antigens can generate memory B cells (MBC) [49] and long-lived plasma cells (LLPC) [50-52].

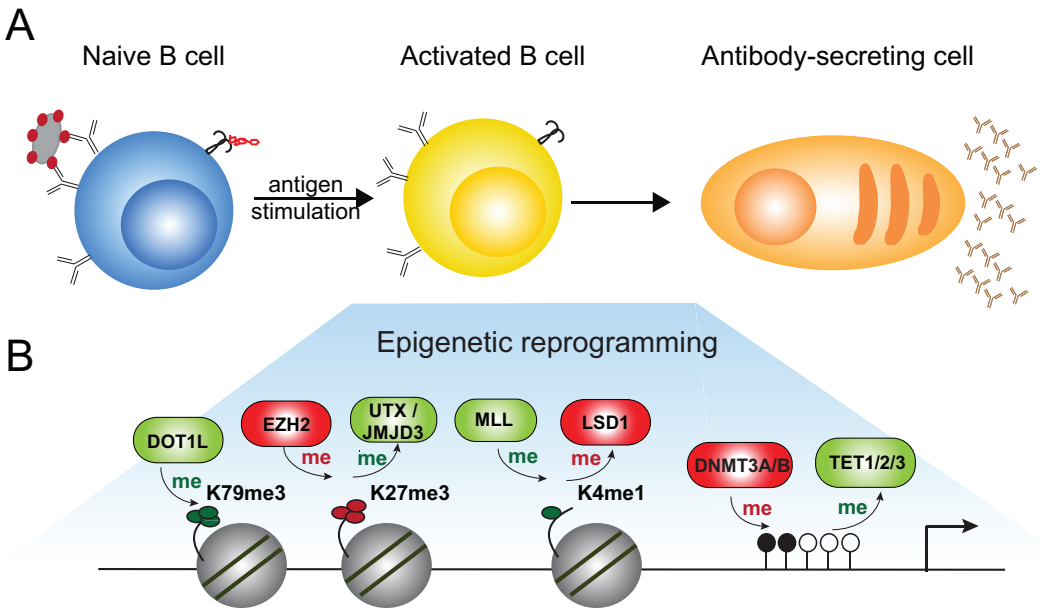

Figure 1-2. B cell differentiation to ASC requires epigenetic reprogramming. (**A**) Following stimulation with T-cell independent or T-cell dependent antigen, naïve B cells become activated and differentiate into antibody-secreting cells. (**B**) The process of naïve B cell reprogramming requires substantial changes to the epigenome. Enzymes that catalyze the addition or removal of DNA methylation and various histone modification are depicted in the shaded box. Enzymes that promote gene expression are colored in green, while enzymes promoting gene repression are colored in red.

Stimulation with a protein antigen induces a T cell-dependent (TD) response in which B cells migrate to germinal centers (GC) and undergo somatic hypermutation (SHM) and affinity maturation, ultimately resulting in the generation of BCR with higher antigen affinity [53-55] (**Figure 1-3**). In the GC, interactions with CD4 T cells play a major role in

determining the cell fate choices, antibody specificity and isotype class, and ultimately longevity of the response [56,57].

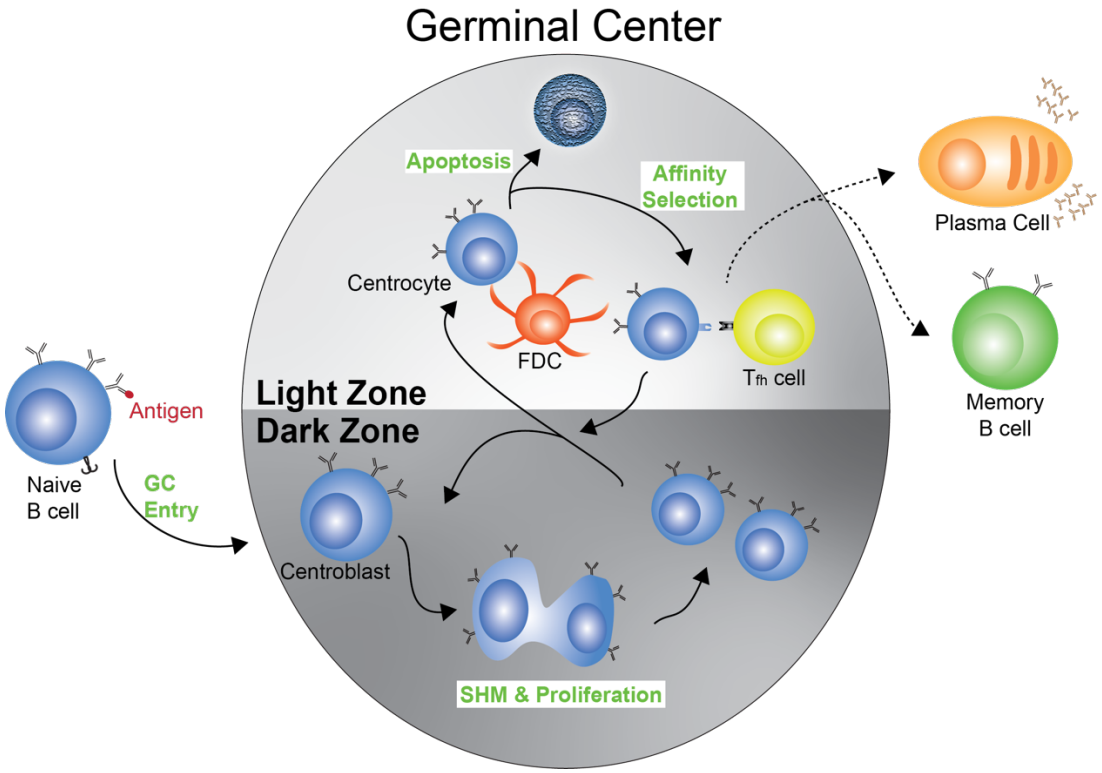

Figure 1-3. The germinal center response. The germinal center is canonically divided into two compartments – the light zone (LZ) and dark zone (DZ). In the DZ, germinal center B cells (termed centroblasts) undergo rounds of somatic hypermutation (SHM) and proliferation. Centroblasts then enter the LZ as centrocytes where they capture antigen from follicular dendritic cells. Centrocytes with improved affinity for the antigen capture more antigen, whereas those that are unable to capture antigen undergo apoptosis. This process of affinity selection is also regulated by T follicular helper cells (Tfh) that instruct centrocyte survival, differentiation, and control their proliferative burst in the dark zone. This microevolutionary process ultimately results in effector B cells, such as antibody-secreting plasma cells and memory B cells, with high affinity for an antigen.

Briefly, the GC is divided into two distinct compartments - the light zone (LZ) and dark zone (DZ) [53,58] (**Figure 1-3**). This nomenclature was established because the DZ of the GC consists predominately of B cells with a high nucleus-to-cytoplasm ratio, thus appearing

darker than the LZ by light microscopy [58]. Within the DZ, GC B cells (termed centroblasts) undergo SHM and proliferation [53]. Recent work has separated DZ B cells into proliferating DZ GC B cells (which they call the "gray zone") and differentiating DZ GC B cells [59]. GC B cells then enter the LZ (now designated as centrocytes) where they capture and internalize antigen for presentation to T follicular helper cells (Tfh) [60]. Tfh select for B cells with high affinity BCR because of their ability to capture more antigen [61-64]. In fact, signals received from Tfh are directly proportional to the amount of antigen they capture and present [65,66]. This dynamic process drives clonal expansion of affinity-matured GC B cells by inducing *Myc* levels proportional to the amount of antigen captured, which regulates the proliferative capacity of GC B cells in the DZ [67,68]. The final output of the GC reaction is long-term immunological protection provided by the generation of LLPC and MBC [69,70]. Whether derived from TI or TD responses, antibodies secreted by ASC provide protection from pathogens [71].

Although there are differences in the cell types that emerge and the timing of TI and TD B cell responses, few differences in SLPC or LLPC have been identified, suggesting that the processes that leads to ASC formation are likely similar [72-74]. Indeed, SLPC contribute to early protective antibodies to influenza [75], and more recent work demonstrated that extrafollicular responses correlated with early neutralizing antibodies in critically ill COVID-19 patients [76]. Thus, SLPC contribute to early protection from infection and can be induced during both TD and TI antigen responses. In this dissertation, lipopolysaccharide (LPS), 4–hydroxy–3–nitrophenylacetyl (NP)-ficoll, and influenza strain A/HK–X31 (X31) are used to model ASC formation to TI type I, TI type II, and TD antigens, respectively.

Adaptations necessary to support ASC physiology and function

The primary function of an ASC is the manufacturing and secretion of antibody molecules. Thus, transitioning from a quiescent naive B cell to an ASC capable of secreting up to 10,000 antibodies per second [77] requires significant morphological and bioenergetic changes [78]. This change in metabolism is essential to meet the energy demands required for rapid proliferation of responding B cells and the translational requirements of ASC [73,79]. Responding activated B cells (actB) utilize both glycolysis and oxidative phosphorylation (OXPHOS), whereas GC B cells also utilize fatty acid oxidation [80,81]. As actB divide and differentiate towards ASC, they gradually increase their capacity to perform OXPHOS [80]. This shift towards OXPHOS is in part due to an increase in transcription of more than 100 components of the electron transport chain and tricarboxylic acid cycles [80], as well as activity mediated by Protein Kinase C β, which is induced in actB following antigen stimulation [82,83]. ASC primarily rely on OXPHOS to support antibody secretion, and this metabolic switch is dependent on BLIMP1, one of the master transcriptional regulators of ASC fate. Experimentally, promoting OXPHOS metabolism in responding B cells using dichloroacetate [84-86] results in increased ASC formation, demonstrating a role for OXPHOS in promoting differentiation [80].

In addition to upregulating metabolism to support antibody secretion, ASC also support their energy needs by autophagy, a process that allows cells to degrade proteins and reuse the resulting metabolic intermediates [87]. This process involves engulfing cytoplasmic contents in a double-membraned vesicle that is delivered to the lysosome for degradation and recycling. When evaluating autophagy in ASC differentiation from murine B cells, significant autophagic induction was observed in both *in vitro* and *in vivo* generated

ASC, independent of the initial stimulation [88]. The importance of this pathway is illustrated by the fact that deletion of *Atg5*, an essential component of the autophagy pathway, resulted in increased ER stress, reduced cellular ATP, and a decrease in ASC survival [89]. Surprisingly, an increase in antibody secretion on a per cell basis was observed, suggesting that autophagy may be necessary to limit antibody secretion, thus reducing the ATP expenditure and promoting cell survival.

The high rate of antibody production also requires substantial adaptations of the secretory apparatus and unfolded protein response (UPR), which is normally induced during stress and initiated by the accumulation of misfolded proteins in the endoplasmic reticulum (ER) [90]. The UPR consists of three highly conserved signal transductions pathways triggered by three main UPR-inducing ER stress sensors: 1) PKR-like endoplasmic reticulum kinase (PERK), 2) activating transcription factor 6 (ATF6), and 3) inositol-requiring enzyme 1α (IRE1α) [91]. The PERK pathway leads to an overall suppression of protein translation [92,93]; however, very limited PERK activation in ASC is observed *in vitro* [94]. In fact, genetic ablation of PERK or CHOP (C/EBP homologous protein), a downstream component of the PERK pathway, has no impact on plasma cell survival *in vitro* [95,96]. ER stress that exceeds the capacity of adaptive UPR leads to activation of the apoptotic program partially induced by CHOP [97]. However, it has been reported that LLPC are less sensitive to ER stress associated apoptosis [98], although the underlying mechanism remains to be elucidated. The ATF6α pathway can augment ER quality control processes and drive ER expansion, but deletion of ATF6α did not impact antibody secretion or survival *in vitro* and *in vivo* [99].

The response initiated by IRE1α is best understood in ASC. IRE1α is a ribonuclease and splicing factor that promotes the splicing of X-box protein 1 (XBP1) mRNA to a more stable *Xbp1* isoform [100]. Once generated, XBP1 promotes the expression of genes necessary for the expansion of the secretory apparatus [101,102]. The importance of XBP1 is highlighted by *in vivo* studies, where deletion of *Xbp1* impeded the ability of ASC to secrete antibodies. XBP1-deficient ASC exhibited normal protein folding but altered glycosylation and lipid synthesis, leading to the failure to mount a proper UPR [103]. These findings indicate that XBP1 is not required for ASC formation but rather for antibody secretion [102,104]. While XBP1 is typically thought of as the master transcription factor regulating the UPR response initiated due to the high antibody secretion, a recent study demonstrated that actB upregulate UPR-related genes prior to becoming an ASC [105]. Upregulation of the actB UPR program was regulated by mammalian target of rapamycin complex 1 (mTORC1) signaling and the adaptor protein Raptor and occurred prior to XBP1 activity [105]. This important finding indicates that part of the actB program is to prepare for subsequent antibody synthesis by initiating and building the transcriptional networks necessary to deal with the stress of protein production and secretion. Thus, the transition from a quiescent nB to an ASC is a requires substantial physiological alterations, including a shift in metabolism, ER stress pathways, and autophagy to sustain immunoglobulin production.

Initiation of the antibody-secreting cell transcriptional program

B cells and ASC express mutually exclusive gene expression programs [15]. As a result, B cell differentiation into ASC requires significant transcriptional rewiring that is coordinated by TF [15]. For example, *Pax5* [33,106], *Bach2* [107-109], and *Ebf1* [110] are important for establishing or maintaining the nB program, while *Bcl6* [111-115] and *Irf8* [116,117] regulate actB

fate. Interferon regulatory factor 4 (IRF4) controls key components of the actB and ASC program, and initiates the transcriptional switch to an ASC through its unique concentration-dependent activity in selecting motifs and motif binding partners [118-120] (**Figure 1-4**).

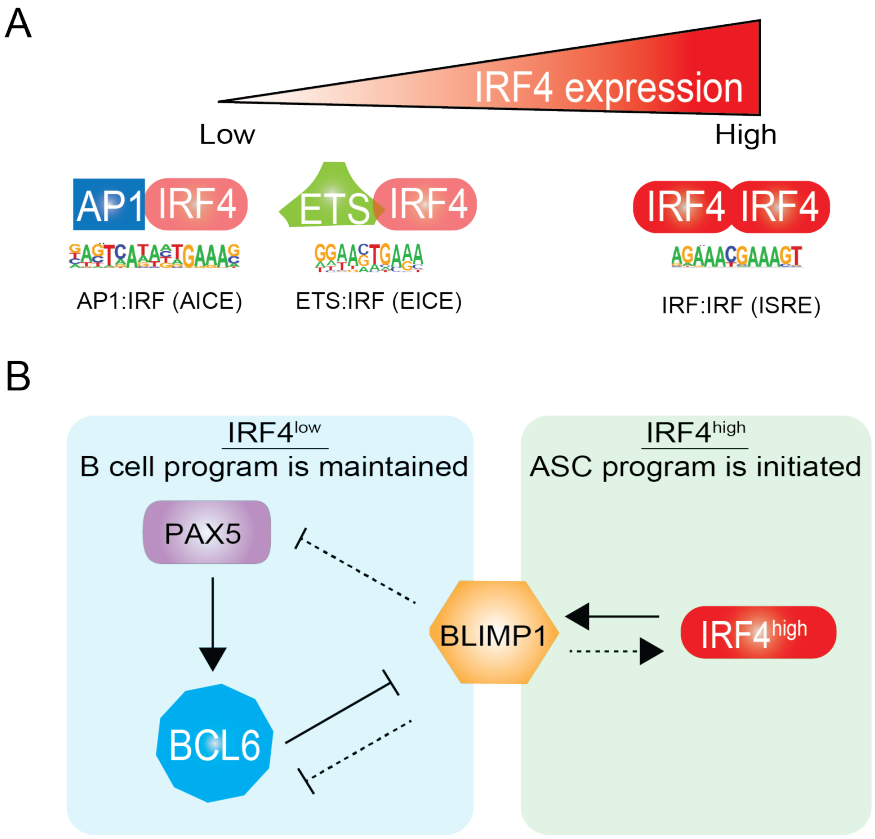

Figure 1-4. Specificity and gene regulatory activity of IRF4. (**A**) IRF4 DNA binding is concentration dependent. At low levels, IRF4 partners with AP1 or ETS family members to bind high affinity AICE and EICE motifs, respectively. At high levels, IRF4 homodimerizes with itself to bind the low affinity ISRE motif. (**B**) In naive B cells and activated B cells, PAX5 induces expression of BCL6, which represses *Blimp1* expression - the master transcription factor for initiating the ASC program. In B cells differentiating to ASC, IRF4 is expressed at high levels, which induces *Blimp1*. Blimp1 reinforces the ASC program by augmenting expression of *Irf4* and repressing expression of *Pax5* and *Bcl6*.

At low levels, IRF4 partners with ETS and AP1 factors to bind high affinity DNA binding sites termed ETS:IRF composite elements (EICE) [121-124] or AP1:IRF composite elements (AICE) [125-127], respectively (**Figure 1-4A**). As IRF4 levels increase, IRF4 can homodimerize to bind a low affinity DNA binding sequence called the interferon-stimulated response element (ISRE) (**Figure 1-4A**). This "kinetic control" model is used to describe IRF4 regulatory functions, where the levels of IRF4 control variable transcriptional programs [119,120,128,129]. The closely related IRF family member, IRF8, competes with IRF4 to regulate cell fate [116]. This mutual antagonism between the two factors, which is centered around competing concentration levels, has the capacity to influence immune outcomes [116,130].

The B cell program is maintained by PAX5 and BCL6. PAX5 induces expression of BCL6, which in turn represses the expression of the master ASC regulator *Blimp1* [118,119] (**Figure 1-4B**). B cell activation leads to progressive upregulation of IRF4, which induces expression of *Blimp1* [131]. BLIMP1 then extinguishes the B cell program through repressing key regulators of the B cell state, such as *Pax5*, *SpiB*, *Bcl6*, *Id3*, and *Myc* [131-134]. Furthermore, BLIMP reinforces the ASC program by augmenting expression of *Irf4* [135,136]. BLIMP1 alone coordinates many distinct phenotypes associated with ASC, including division cessation through repression of *Myc* [132], loss of MHC class II antigen presentation by repressing expression of the class II transactivator (CIITA) [137], and establishment of the ASC program via repression of PAX5 [134,138]. Moreover, BLIMP1 directly regulates membrane bound versus secreted form of immunoglobulin, the hallmark of ASC function [138,139]. While recent work has demonstrated that repression of *Pax5* is not essential for formation of *bona fide* ASC, normal ASC gene expression programs are significantly

dysregulated when PAX5 remains expressed in ASC [140]. These studies highlight the essential role of IRF4 in controlling cell fate outcomes during the later stages of B cell differentiation; however, less is known regarding the impact of IRF4 during the initial stages of B cell activation and its impact on final immune outcomes.

II. THE ROLE OF IRF4 ON B CELL DEVELOPMENT AND DISEASE

Development

In the above section, the impact of IRF4 and IRF8 on ASC formation was highlighted. In opposition to this antagonizing role, these factors are functionally redundant during the early stages of B cell development. IRF4 and IRF8 have been identified as a direct target of PAX5 at the pro-B cell stage [141]. Similarly, IRF4 and IRF8 binding sites have been shown at the PAX5 enhancer [142], suggesting these factors reinforce the program essential for B cell identity and function. While IRF4 and IRF8 single knockouts develop B cells, B cell development is blocked in IRF4/IRF8 double knockouts (IRF4/IRF8-/-) [143]. Detailed characterization of hematopoiesis in IRF4/IRF8-/- revealed B cell development was halted at the pre-B cell stage, the stage in which light chain rearrangement and expression occurs (**Figure 1-1**) [143]. Indeed, IRF4 and IRF8 bind enhancers of light chains to regulate their expression [121,122,144-146]. Overexpression of either IRF4 or IRF8 was sufficient to overcome the developmental defect, confirming these factors were functionally redundant at this stage of B cell development [146].

Upon assembling a functional BCR, immature B cells are tested for autoreactivity before exiting the bone marrow and maturing in the spleen (**Figure 1-1**). This process is called central tolerance [147]. The mechanism of central tolerance involves receptor editing [148], which modifies the specificity of B cells carrying autoreactive BCR. IRF4 has been implicated as a critical factor for central tolerance because it promotes receptor editing [149,150]. Deletion of IRF4 perturbed secondary rearrangements of the immunoglobulin receptor that could not be overcome by IRF8 [149]. Intriguingly, IRF4 was found to be more critical for lambda chain rearrangements than kappa chain rearrangements [149]. Collectively, these studies indicate that IRF4 and IRF8 play critical roles in governing B cell development with context-dependent redundancy [151].

Differentiation

As detailed in the above section, IRF4 is an essential TF needed for terminal differentiation of B cells to ASC [118,119,152]. IRF4-deficient B cells fail to form ASC because they are unable to initiate the ASC program (**Figure 1-4**). In addition to this role, IRF4-deficient B cells control other key aspects of B cell differentiation. This includes class switch recombination [118,119], SHM [118], and GC formation [120,153] due to insufficient induction of *Aicda* and *Bcl6* (**Figure 1-3**). AID (encoded by *Aicda*) is essential for class switching and SHM [154], whereas BCL6 is the master regulator for the GC reaction [111,114,155]. Indeed, transient expression of IRF4 is sufficient to induce GC B cells expressing BCL-6 and AID [120]. While IRF4 is necessary for GC formation [118,153], it is dispensable for GC maintenance [118]. Deletion of IRF4 in GC B cells prevents ASC differentiation, but does not impact early MBC formation [118]. Intriguingly, IRF4 is required for long-term maintenance of the MBC

pool [118], despite being expressed at very low levels [156,157]. This suggests IRF4 may play a pro-survival role in MBC. Indeed, IRF4 was demonstrated to be indispensable for long-term survival ASC [139]. While deletion of IRF4 in ASC leads to apoptosis, IRF4 did not regulate the apoptotic pathway directly [158]. Instead, IRF4 was critical for mitochondrial homeostasis [158]. This included regulating mitochondrial mass, reactive oxygen species (ROS) production, and maximal metabolic capacity [158]. Thus, IRF4 plays critical cell-type specific roles that control cell fate outcomes.

Disease

Consistent with the diverse role of IRF4 during B cell development and differentiation highlighted above, dysregulation of IRF4 expression/activity is involved in the pathogenesis of many B cell diseases [151]. IRF4 functions as a tumor suppressor in murine models of B cell acute lymphocytic leukemia (B-ALL) [159]. Eμ-Myc mice express *Myc* at high levels at the pre-B cell stage (**Figure 1-1)** and develop B-ALL at about 20 weeks of age. However, IRF4 heterozygous mice (*Irf4*+/-EμMyc) develop B-ALL within just 8 weeks. Similar to the role of IRF4 in preventing progression of B-ALL, two independent mouse models have demonstrated that low levels of IRF4 accelerate the progression of chronic lymphocytic leukemia (CLL), which is derived from mature B cells (**Figure 1-1**) [160,161]. Indeed, higher IRF4 levels correlated with better clinical outcomes in CLL patients [162]. In addition to this role in developing and mature B cells, IRF4 has also been implicated in the development of non-Hodgkin lymphoma, including diffuse large B cell lymphoma (DLBCL). DLBCL is a diverse group of B cell malignancies that can be divided into subtypes resembling transcriptional programs of normal stages of B cell differentiation

(**Figure 1-2**, **Figure 1-3**). These subtypes include activated B cell-like and germinal center-like DLBCL [163]. In both cases, dysregulation of IRF4 activity results in an inability of DLBCL to complete the differentiation process [164,165], and this is reflected in the transcriptional program used to identify the subtypes. IRF4 has also been implicated in Hodgkin's lymphoma (HL), which is a GC-derived malignancy [166]. HL cells depend on IRF4 for survival and continued proliferation [167]. Finally, IRF4 is also involved in the formation and survival of multiple myeloma (MM) [168], which is an aggressive plasma cell-derived malignancy. Similar to HL, knockdown of IRF4 results in reduced proliferation and survival of MM cells [169]. Characterization of the molecular targets of IRF4 identified the *Myc* promoter as a direct target, which is central to the pathogenesis of MM [169]. This is intriguing given the role of IRF4 in inducing *Blimp1* [131] (**Figure 1-4**), which normally represses *Myc* expression [132]. Thus, MM cells have broadened IRF4 activity that includes IRF4 binding to regions that are typically silenced [169]. Collectively, these data indicate inappropriate control of IRF4 expression/activity can result in a myriad of B cell malignancies (**Figure 1-5**).

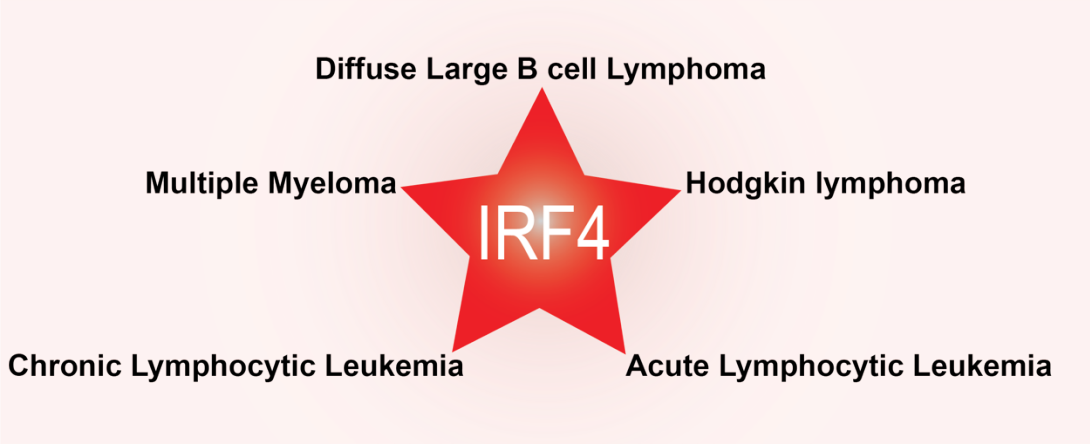

Figure 1-5. IRF4 is associated with the pathogenesis of many B cell-based malignancies. IRF4 is central to the development of many diseases involving developing and mature B cells (chronic lymphocytic leukemia and acute lymphocytic leukemia),

activated/germinal center B cells (diffuse large B cell lymphoma and Hodgkin lymphoma), and plasma cells (multiple myeloma).

III. B CELL DIFFERENTIATION IS A COORDINATED MULTISTEP PROCESS

Cell division is an essential process during B cell differentiation

Inhibition of proliferation after stimulation of peripheral blood mononuclear cells with pokeweed mitogen prevented the generation of ASC, implicating cell division as essential for B cell differentiation to ASC [170]. The development of carboxyfluorescein succinimidyl ester (CFSE) [171] or CellTrace (CT) dyes allowed for the relationship of cell division and ASC formation to be assessed. These dyes covalently bind free amines on the surface and inside of cells and become diluted through cell proliferation. Application of these dyes has led to the appreciation that cell division is intimately linked to reprogramming events leading to ASC formation [172-176].

The modeling of B cell differentiation kinetics in the context of cell division has largely been performed using *ex vivo* stimulated cells [177-184]. This has led to a stochastic model of differentiation, where a simple probabilistic division-based framework can accurately predict ASC formation and isotype class switching [179]. *Ex vivo* stimulation of CT-labeled splenic naive B cells using the TI antigen LPS demonstrates this concept (**Figure 1-6A**). Over a time course spanning three days, a consistent frequency of CD138+ASC are observed at each time point and each division (**Figure 1-6B-D**). Notably, a consistent proportion of cells in the same division differentiate, regardless of the time taken for the

cell to enter that division (**Figure 1-6B,6C**). Thus, stochastic modeling of differentiation predicts population-level immune responses while accounting for heterogeneity for an individual cell.

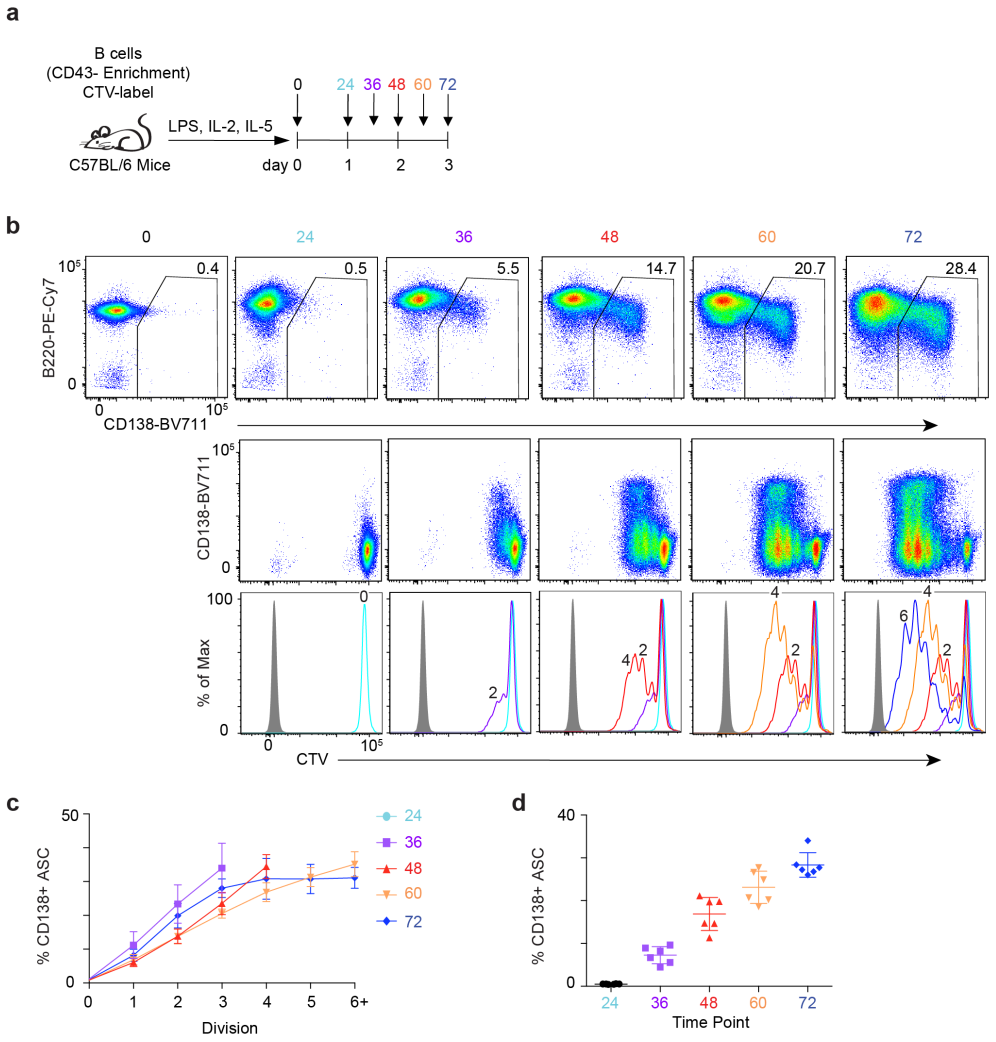

Figure 1-6. B cell differentiation kinetics *ex vivo*. (**a**) Schematic of experimental design. Briefly, CD43– splenic naive B cells from C57BL/6J were isolated, labeled with CellTrace Violet (CTV) and cultured in the presence of LPS, IL2, and IL5. Downward pointing arrows indicate the hour samples were harvested after culture for flow cytometry. (**b**) Representative flow cytometry plot of B220 versus CD138 (top), CD138 versus CTV (middle), and CTV histograms (bottom) at indicated time points. The solid grey histogram represents an unstained control. (**c**) Percentage of cells that are $CD138^{+}$ at each division across each time point from **b**. (**d**) Total $CD138^{+}$ cells at each time point. Data in **c**, **d** represent mean ± SD and were derived from two independent experiments with 6 mice.

This quantitative approach to predict and describe B cell differentiation was extended using TD antigens [180]. TD modeling of cell division and ASC formation resulted in a graded model, where changes in stimulation impact the time in which cells start dividing and the proportion of cells that differentiate at each division [180]. In contrast, TI stimulation results in a quantal all-or-none response, where the concentration of stimulation changes the proportion of cells that enter the response but does not impact the frequency of cells that differentiate at each division [180]. While *ex vivo* studies have served as a suitable microenvironment to study many components of B cell differentiation, principal components of ASC formation are different, including the division in which differentiation occurs [174]. These concepts will be explored experimentally later in this dissertation using an *in vivo* model of B cell differentiation described below.

Cell division-coupled hypomethylation and gene regulation coordinate B cell differentiation

The methylation of cytosine at CpG dinucleotides is a central epigenetic modification that controls gene expression by recruiting proteins involved in gene repression or by inhibiting the binding of TF to DNA [185]. DNA methylation localized to promoters or enhancers results in gene repression. Alternatively, methylation across the gene body coupled with loss of methylation at promoters or enhancers supports gene expression [186]. DNA methylation is mediated by one of three DNA methyltransferases (DNMT). DNMT3A and DNMT3B promote *de novo* DNA methylation [187], while DNMT1 maintains DNA methylation during cell division [188]. Loss of DNA methylation can occur either via passive loss of methylation during cell division or an active process mediated by Ten-eleven translocation methylcytosine dioxygenases (TET1, TET2, TET3). TET

enzymes promote DNA demethylation in a step wise manner by conversion of mCpG into 5-hydroxymethylcytosine (5hmC), 5-formylcytosine (5fC) and 5-carboxylcytosine (5caC), which leads to unmethylated DNA [189].

A model system can be employed to investigate the relationship between cell division and differentiation [174]. In this system, CT-labeled splenic nB cells are transferred into the B cell-deficient mouse host strain μMT [190]. One day later, hosts are inoculated with LPS to stimulate differentiation. Using this *in vivo* model system, DNA methylation and transcription were examined in discrete divisions leading to ASC formation [174]. These included cells in division 0, 1, 3, 5, and 8, with cells in division 8 further delineated based on CD138 status to separate ASC ($CD138^+$) from non-ASC ($CD138^-$) [135,191]. This study revealed that B cell differentiation is associated with a progressive loss of DNA methylation, with only a small number of loci gaining *de novo* DNA methylation during ASC formation [174]. Differentiation of human B cells observed similar trends and indicated the reconfiguration of the DNA methylome was connected to the cell cycle [192]. Importantly, loss of DNA methylation occurred at many key genes essential for ASC formation, including *Blimp1*, *Irf4*, *Xbp1*, and was enriched at enhancer regions [174,192]. TFs critical for the differentiation of ASC were enriched within demethylated enhancer regions and included IRF family members, BATF (AP-1 family member), NF-kB, and E2A [193]. Selective demethylation at regulatory regions critical for ASC differentiation suggests that these regions are targeted. Examination of 5hmC, an intermediate step during active demethylation, suggests active demethylation contributes to ASC formation [192]. Furthermore, inhibition of DNA methylation [174] or enhancement of TET enzymes via

ascorbic acid (vitamin C) [194] led to an increase in ASC, thus providing functional evidence for the essential role of DNA demethylation in ASC formation.

Despite *de novo* DNA methylation occurring only at a small number of loci, those changes are necessary for restraining the commitment to the ASC fate [195]. B cell conditional deletion of *Dnmt3a* and *Dnmt3b* led to an increase in GC B cells, as well as ASC with an aberrant transcriptional profile. DNMT3A/B-deficient ASC upregulated genes associated with lysosome function, transcription, as well as various metabolic pathways [195]. However, despite the well-established role of DNA methylation in ASC formation, how these enzymes are recruited to the specific loci remain to be determined. Additionally, more work is needed to uncouple passive and active demethylation events and determine the timing in which these processes occur.

Chromatin accessibility changes indicate epigenetic control of B cell differentiation

Epigenetic mechanisms, such as DNA methylation and histone modifications, function to prevent or promote accessibility of DNA to TF [196]. Therefore, identifying the regions that change accessibility during B cell differentiation can reveal critical regulatory elements and factors that control B cell reprogramming to ASC. The development of the assay for transposase accessible chromatin-sequencing (ATAC-seq) [197,198] has revolutionized the study of accessible chromatin landscapes. Using the *in vivo* model system described above, ATAC-seq was applied to discrete divisions during B cell differentiation to better define the cis-regulatory changes that occur during ASC formation [175]. These included actB cells in divisions 0, 1, 3, 5, and $CD138^{+}$ASC [135,191] in division 8. Differentially accessible regions (DAR) were determined for all samples compared back

to division 0 and revealed that progressive changes in chromatin accessibility occurred as the cells divided, with the majority of chromatin accessibility changes occurring in ASC. TF essential for ASC formation were enriched in ASC DAR including NF-κB, AP1:IRF heterodimers (AICE; high affinity IRF site) [125], and IRF:IRF homodimers (ISRE; low affinity IRF site) [120,199]. Accessibility surrounding NF-κB and AICE sites increased progressively as cells divided, whereas accessibility surrounding ISRE was unique to ASC. These data are consistent with the concentration-dependent activity of IRF4 and high levels of IRF4 expression promoting ISRE binding in ASC [119,120,128,199]. Furthermore, these data described a hierarchy of TF activity that is linked to cell division during B cell differentiation. Strikingly, comparing undivided cells to ASC revealed a subset of promoters that was accessible in division 0, but not expressed until ASC formation in division 8, suggesting that epigenetic mechanisms play a role in regulating this "primed" set of genes. These primed genes showed strong enrichment for the gene ontology terms "cell cycle" and "DNA replication" indicating that they might allow the cells to rapidly respond after stimulation [175]. Indeed, a subset of these primed promoters were enriched for the repressive histone modification H3K27me3, and pharmacological inhibition of the enzyme responsible for H3K27me3 deposition (EZH2) resulted in increased expression of primed genes, such as *Blimp1*. These data indicate that proper control of H3K27me3 is critical for appropriate expression of ASC-inducing genes and point towards the role of the epigenome to control the timing and magnitude of gene expression during B cell differentiation.

Cell divisions represent distinct stages during in vivo B cell differentiation

Significant advances have been made in our understanding of the transcriptional and epigenetic events that coordinate ASC formation, and it has become clear that cell division and epigenetic reprogramming are intimately intertwined, with discrete divisions representing distinct stages of B differentiation (**Figure 1-7**) [174-176].

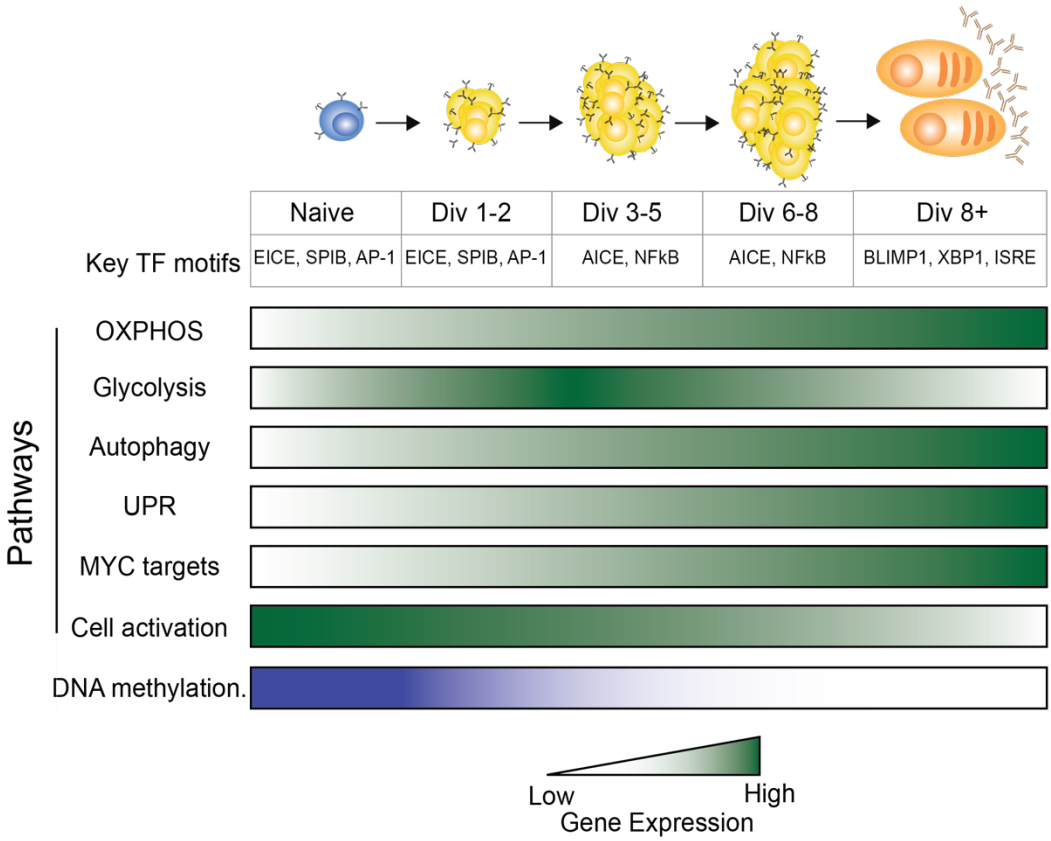

Figure 1-7. Cell divisions represent distinct stages during *in vivo* B cell differentiation in response to LPS. Genome wide accessibility at discrete divisions revealed a hierarchy of transcription factor activity[175]. Transcription factor motifs enriched at each cell division stage are indicated. RNA-seq of cells in precise divisions revealed a progressive change of gene sets throughout differentiation[174]. Shaded boxes represent the expression level of genes in the indicated pathways that change as the cells divide during ASC differentiation. Darker color represents higher expression. DNA methylation levels are represented by color with the darker color indicating more methylation.

In divisions 1-2, accessibility changes at promoters and distal elements are observed and transcriptional amplification is initiated for essential ASC gene sets, including Myc target genes and OXPHOS [80,174]. In divisions 3-5, DNA hypomethylation occurs around enhancer regions containing NF-κB and AP-1 motifs, and cells continue to upregulate / repress pathways initiated in the initial divisions [174,175]. At 72 hr, cells that continue to divide are observed in division 8, with a subset differentiating to ASC (Div 8+) (**Figure 1-8**) [174].

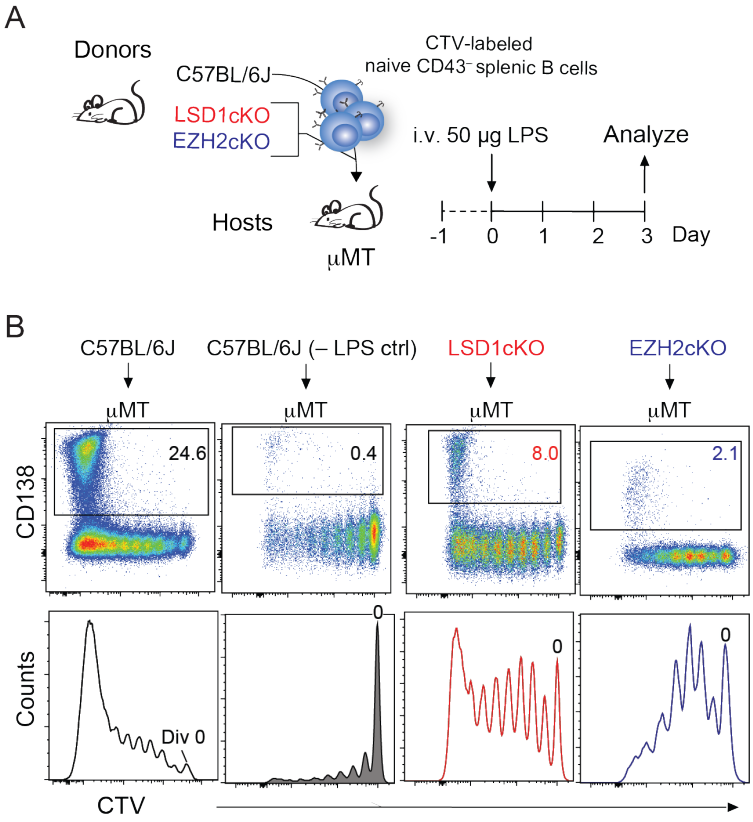

Figure 1-8. B cell differentiation is coupled to cell division and regulated by epigenetic factors. (A) Schematic of an adoptive transfer experimental design. Naïve B cells from the indicated mice were isolated, stained with CellTrace Violet (CTV), and transferred into B-cell deficient µMT hosts. After one day, host mice are stimulated with LPS or PBS (– LPS ctrl) and sacrificed three days later for analysis via flow cytometry. Transferred cells are recovered from host spleens. **(B)** Representative flow cytometry plots depicting CD138 expression versus CTV (top) and histograms of CTV (bottom) with division 0 indicated. The donor:host mouse combination is indicated. Representative examples were from previously performed and published experiments: C57BL/6J into µMT (Figure 1 [176]), LSD1cKO into µMT (Figure 5 [200]), EZH2cKO into µMT (Figure 7 [201]). cKO, conditional knockout.

During these final divisions before ASC formation is observed, massive epigenetic and transcriptional changes occur. Cell division defects following the deletion of LSD1 and EZH2 that contribute to actB reprogramming are often observed in these divisions [200,201] (**Figure 1-8**). Remarkably, substantial differences in epigenetic and transcription reprogramming exist in actB and ASC in division 8. This includes >50,000 demethylated loci and >1,500 differentially expressed genes [174]. Additionally, low affinity IRF:IRF (ISRE) and E2A motifs are uniquely enriched in accessible regions in division 8 ASC and positively correlate with predicted target gene expression, implicating these as a major contributor to the final reprogramming events [175]. Collectively, studying chromatin accessibility and gene expression changes in discrete divisions during B cell differentiation, combined with genetic dissection of epigenetic enzymes, has revealed the step-wise reprogramming events that occur during B cell differentiation. These data can be exploited to understand the timing, mechanism, and scope of reprogramming by factors that impact ASC differentiation.

IV. RATIONALE AND OVERVIEW

As detailed above, it has become clear that cell division is an essential process during B cell differentiation that represents distinct stages of reprogramming. Examining the fate of individual responding B cells – whether they will divide, die, or differentiate – indicated that sibling cells had similar outcomes compared to unrelated cells in the same division [183,184]. Thus, considerable heterogeneity exists among responding B cells. This heterogeneity is reflected in the observation that cells are distributed across all divisions at

the peak of the LPS response, with only a fraction of cells in division 8 differentiating (**Figure 1-8B**) [174,175]. However, it remains to be determined what factors control such heterogeneity and the cell division in which cell fate is instructed. This dissertation identified IRF4 as one molecular determinant contributing to such heterogeneity.

Collectively, we found IRF4 controls cell growth and proliferation as well as the path to an ASC. In Chapter 2, we employed single-cell RNA-sequencing to characterize the heterogeneity of *in vivo* B cell differentiation. We uncovered a bifurcation event in actB that occurred around divisions 3–5 during B cell differentiation, with one branch leading to ASC. These data indicated that B cell fates were instructed by IRF4, in tandem with BATF, during the earliest stages of B cell activation and that a subset of B cells are destined to become ASC. ActB that followed this branch were designated "ASC-destined", while cells that followed the alternative branch were denoted "non-ASC". Cells along this IRF4-dependent branch upregulated critical gene sets for differentiation, including gene sets essential for proliferation. In Chapter 3, we explored the impact of IRF4 on cell proliferation, as well as the cell division-based IRF4-dependent reprogramming events that occur during the initial cell divisions. This was achieved by sorting cells in discrete divisions by CTV dilution for RNA- and ATAC-seq analyses. These data revealed an IRF4-MYC-mTOR relationship that controlled cell growth and the proliferative capacity of responding cells, as well as generated a road map of reprogramming events dependent on IRF4. In Chapter 4, we began to explore the fate of cells along the non-ASC branch using RNA-sequencing. These data showed that cells along this branch express markers of pre-memory B cells, indicating that B cell fates (ASC and memory) may be instructed

during the early stages of differentiation. Finally, Chapter 5 encompasses a broad discussion of the work.

Chapter 2. Antibody-secreting cell destiny emerges during the initial stages of B-cell activation

Christopher D. Scharer*[1], Dillon G. Patterson*[1], Tian Mi[1], Madeline J. Price[1], Sakeenah L. Hicks[1], and Jeremy M. Boss[1]

*These authors contributed equally

[1]Department of Microbiology and Immunology, and the Emory Vaccine Center, Emory University School of Medicine, Atlanta, GA 30322, USA

Correspondence: jmboss@emory.edu

Author Contributions

C.D.S. and D.G.P. designed and performed experiments, analyzed the data, and wrote the manuscript; T.M. performed bioinformatic analysis of the datasets; M.J.P. performed the BLIMP-1 adoptive transfer experiments; S.L.H generated sequencing libraries; and J.M.B. designed experiments, wrote the manuscript, and oversaw the project. All authors participated in editing the manuscript.

Originally published in *Nature Communications*. Christopher D. Scharer, Dillon G. Patterson, Tian Mi, Madeline J. Price, Sakeenah L. Hicks, and Jeremy M. Boss. 2020. Antibody-secreting cell destiny emerges during the initial stages of B-cell activation. *Nat Commun* 11, 3989 (2020).

I. ABSTRACT

Cell fate programming and heterogeneity during antibody secreting cell (ASC) differentiation were investigated using T cell-independent models. We demonstrated that maximal ASC formation required at least eight cell divisions *in vivo*, with BLIMP-1 being required for differentiation at division eight. Single cell RNA-sequencing of responding B cells and construction of differentiation trajectories revealed an early cell fate bifurcation. The ASC-destined branch required induction of IRF4, oxidative phosphorylation, and MYC-target genes, but lost CD62L expression, which provided an early marker of ASC fate destiny. The non-ASC branch expressed an inflammatory signature and maintained B cell fate programming. ASC were subdivided further by differences in responses to ER-stress, indicating multiple differentiation branch points. Thus, these data define the cell division kinetics of B cell differentiation *in vivo* and identify the molecular trajectories of B cell fate and ASC formation.

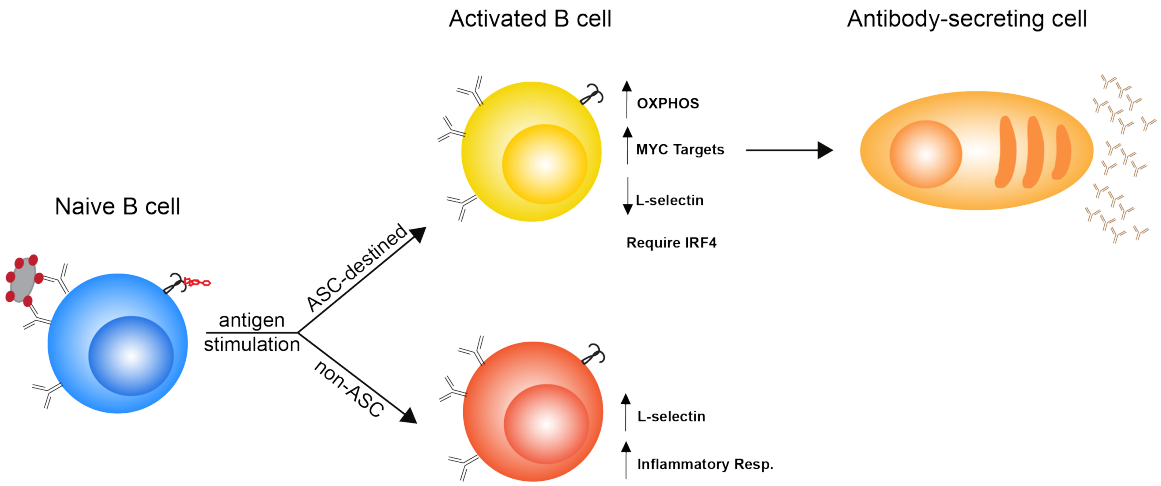

Figure 2-1. Graphical abstract depicting the bifurcating trajectories of activated B cells during B cell differentiation. Upon antigen encounter, naive B cells (left) become activated (actB), rapidly proliferate, and progress down two different differentiation trajectories. ASC-destined actB cells depend on IRF4 and upregulate oxidative phosphorylation (OXPHOS), MYC target genes, and can be distinguished by loss of L-

selectin. ActB cells that progress down the non-ASC branch maintain an inflammatory signature and maintain L-selectin expression. Transcription factors distinguishing each cell type are depicted.

II. INTRODUCTION

Many pathogens are subject to immunological control via the generation of antibody secreting cells (ASC) or plasma cells. After being activated by external stimuli, resting naïve B cells rapidly proliferate, and it is now appreciated that cell division is an essential component of ASC differentiation [170,173]. A core feature of the humoral immune response is the predictable kinetics of B cell expansion and differentiation [172]. *Ex vivo*, a stochastic model of differentiation predicts population level immune responses, while accounting for differentiation heterogeneity between individual cells [179,183,184,202]. Part of the mechanism is dependent on the expression levels of MYC, which is influenced by immune stimulation, where MYC functions as a division-independent temporal timer controlling the number of cell divisions [68,180,181]. Importantly, examination of the cell fate outcomes of individual cells indicated that sibling cells have similar fates compared to unrelated cells that have undergone the same number of divisions [183,184]. Thus, considerable heterogeneity exists between responding B cells but the differences in transcriptional programming that drives this heterogeneity is unknown.

In addition to cell division, ASC differentiation requires the coordinated regulation of hundreds of genes, ultimately demanding differentiating cells to extinguish the B cell program and initiate the ASC program [14,15]. *In vivo*, transcriptional rewiring and epigenetic remodeling [203] occurs within the framework of cell division [80,174,175,193,201]. For example, DNA hypomethylation events occur in ASC predominately at enhancers and this is

accompanied by a change in chromatin accessibility and gene expression [174,175]. Reciprocally, *de novo* DNA methylation is critical for limiting B cell activation and plasma cell differentiation [195]. Epigenetic chromatin modifiers, including EZH2 and LSD1 alter the division and differentiation kinetics of B cells *in vivo* [200,201]. While these studies underscore the importance of epigenetic reprogramming during B cell differentiation and how these reprogramming events help coordinate the appropriate ASC transcriptional program, they have not examined how cellular division and differentiation occur at the single cell level.

Recent advances in single cell RNA-sequencing (scRNA-seq) [204,205] now allow for a molecular characterization of heterogeneity within immune populations during an immune response. This can be leveraged to gain a better understanding of cellular transitions or trajectories that may provide insight into the processes that govern B cell fate decisions. Here, we employed an *in vivo* model system [174] to better assess the relationships between cellular heterogeneity, cell division, and B cell differentiation. We report that B cell differentiation *in vivo* requires a minimum of 8 cell divisions. However, only a fraction of responding B cells differentiate, indicating that additional guidance cues ultimately decide B cell fate decisions. Using scRNA-seq, we defined a path to ASC that revealed an early decision point, with one branch leading to ASC differentiation that was dependent on IRF4. Cells that followed this branch induced gene sets that included oxidative phosphorylation, cell proliferation based on MYC and ultimately ER-stress responses. Cells that followed the second branch induced inflammatory gene sets and failed to downregulate L-selectin (CD62L) and form ASCs. Thus, we provide a molecular path that defines the variation in cell fate decision making that is required to form an ASC.

III. RESULTS

Cell division is a critical component of B cell differentiation in vivo

The modeling of B cell differentiation kinetics in the context of cell division has largely been performed using *ex vivo* stimulated cells [177-184]. To better understand the kinetics of cell division with the timing of B cell differentiation *in vivo,* we used an adoptive transfer model. Here, CellTrace Violet (CTV)-labeled splenic $CD43^-$ B cells from $CD45.2^+$ donor mice were transferred to $CD45.1^+$ μMT mice. After one day, host μMT were inoculated with 50 μg of LPS and cell division/differentiation was assessed by the expression of the surface proteoglycan molecule Syndecan-1 (CD138) [135,191] in a detailed time course over the next three days [174]. At 24 hr, no division was observed, defining a minimum lag time before responding cells begin dividing (**Fig. 2-2a**). Between 48 and 54 hr, a maximum of 7 cell divisions was observed with no significant increase in the percentage of $CD138^+$ cells. However, by 60 hr, a small fraction of the cells divided at least 8 times and the first $CD138^+$ cells were observed (**Fig. 2-2a**). At 72 hr, more cells reached or exceeded the 8^{th} division, corresponding to a peak in $CD138^+$ cells or ASC (**Fig. 2-2b**). As such, ASC differentiation corresponds with the time it takes for responding B cells to reach division 8 (**Fig. 2-2c**). Mice that received CTV-labeled cells and no LPS displayed background, homeostatic levels of proliferation and differentiation at 72 hr (**Fig. 2-2a**).

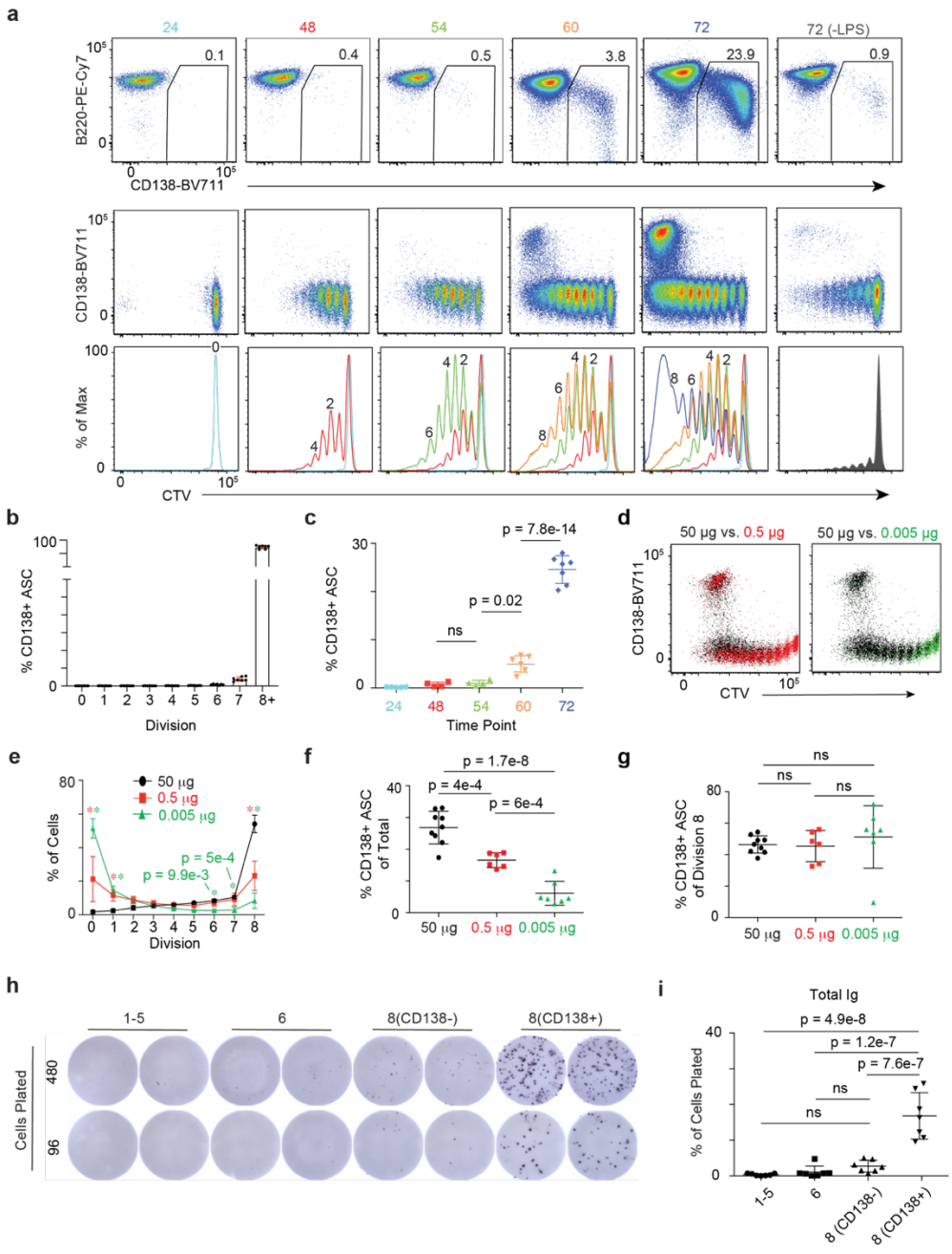

Figure 2-2. Cell division mapping of ASC differentiation *in vivo*. (**a**) Representative flow cytometry plots of B220 versus CD138 (top), CD138 versus CTV (middle), and CTV histograms (bottom) at the indicated time points following *in vivo* LPS inoculation. The percentage of total CD138$^+$ cells is indicated in the top row. (**b**) Frequency of CD138$^+$ cells at each division at 72 hr. (**c**) Frequency of CD138$^+$ cells at each time point. (**d**) Representative flow cytometry of CD138 versus CTV plots 72 hr after µMT hosts were challenged with 50 µg (black), 0.5 µg (red), or 0.005 µg (green) of LPS. (**e**) Frequency of transferred cells at each division for each dose. Asterisk indicates significance of $p<0.05$ between 50 µg versus 0.5 µg (red) and 50 µg versus 0.005 µg (green). (**f**) The percentage of total CD138$^+$ cells is shown for samples from **e**. (**g**) The percentage of division 8 cells

that are CD138$^+$ is shown for samples from **e**. (**h**) Representative images of total Ig ELISPOTs on cells sorted from divisions 1-5, 6, or 8(CD138$^-$ or CD138$^+$) 72 hr post-LPS challenge from one mouse. (**i**) ELISPOTs from **h** were quantitated as the percentage of total cells plated that formed ASC. Data in **a-c** are representative of three independent experiments containing 24 hr (n = 5), 48 hr (n = 4), 54 hr (n = 4), 60 hr (n = 6), and 72 hr (n = 7) mice. Data in **d-g** were derived from three independent experiments with 50 μg (n = 9), 0.5 μg (n = 6), and 0.005 μg (n = 7) mice. Data in **h-i** were derived from two independent experiments from 7 total mice. Data in **b**, **c**, **e-g, i** represent mean ± SD. Statistical significance in **e** was determined by a two-way ANOVA with Tukey's post-test for multiple comparisons. Statistical significance for **c**, **f, g, i** was determined by one-way ANOVA with Tukey's post-test for multiple comparisons.

To determine whether LPS dosage influenced *in vivo* ASC differentiation, a dose comparison covering a 10,000 fold range was performed. At all doses, a minimum of 8 divisions were still required for ASC formation (**Fig. 2-2d**). Similar to *ex vivo* differentiation [180], lower dosages impacted the magnitude of the overall response, ultimately resulting in fewer cells reaching division 8 and forming ASC (**Fig. 2-2e-f**). However, for cells reaching division 8, the same proportion differentiate to ASC (**Fig. 2-2g**). Thus, these data indicate that *in vivo* LPS dosage affects the number of responding B cells, but not the requirement of 8 divisions for ASC formation. Finally, to confirm that only the CD138$^+$ cells at division 8 were indeed ASC, we performed ELISPOT assays on cells sorted from divisions 1-5, 6, and 8. Division 8 cells were split based on CD138 expression. Only cells that had reached division 8 and were CD138$^+$ secreted robust levels of antibodies (**Fig. 2-2h-i**). Although not all CD138$^+$ cells formed spots, this was not unexpected as a loss in secretion of some cells has been observed in ELISPOT assays following cell sorting [206].

Cell division kinetics of B cell differentiation are similar for T independent Type I and II antigens

To determine whether similar division and differentiation kinetics were observed in a wild-type (WT) host setting, CTV-labeled B cells from CD45.1$^+$ donor mice were transferred into CD45.2$^+$ C57BL/6J WT hosts. After one day, hosts were inoculated with 50 μg LPS and division/differentiation was assessed on day 3. In WT hosts, we found the cell division kinetics of ASC differentiation to be altered such that CD138$^+$ cells were predominantly observed in division 8 but were also observed as early as division 3 (**Fig. 2-3a**). To determine if the observed differences in differentiation kinetics were due to cell extrinsic effects from host cells also responding to LPS, the adoptive transfer was repeated using *Myd88*-deficient hosts (MYD88$^{-/-}$) that cannot respond to LPS [207]. In MYD88$^{-/-}$ hosts, cell division and differentiation kinetics closely resembled what we observed for μMT hosts, with CD138$^+$ cells in division 8, as well as a similar distribution of cells across all divisions (**Fig. 2-3b**). This suggests that cell extrinsic effects from LPS-responding host cells can impact the division in which differentiation occurs.

To determine whether similar division kinetics were observed for other stimuli, adoptive transfers using WT and μMT hosts were performed followed by challenge with the T cell independent type II antigen 4-hydroxy-3-nitrophenylacetyl (NP)-Ficoll. Here, a similar division/differentiation requirement in these mice as seen in μMT and MYD88$^{-/-}$ hosts challenged with LPS was observed (**Fig. 2-3c**). Collectively, these results indicate that there is a similar cell division requirement during B cell differentiation in response to T cell independent type I and II antigens.

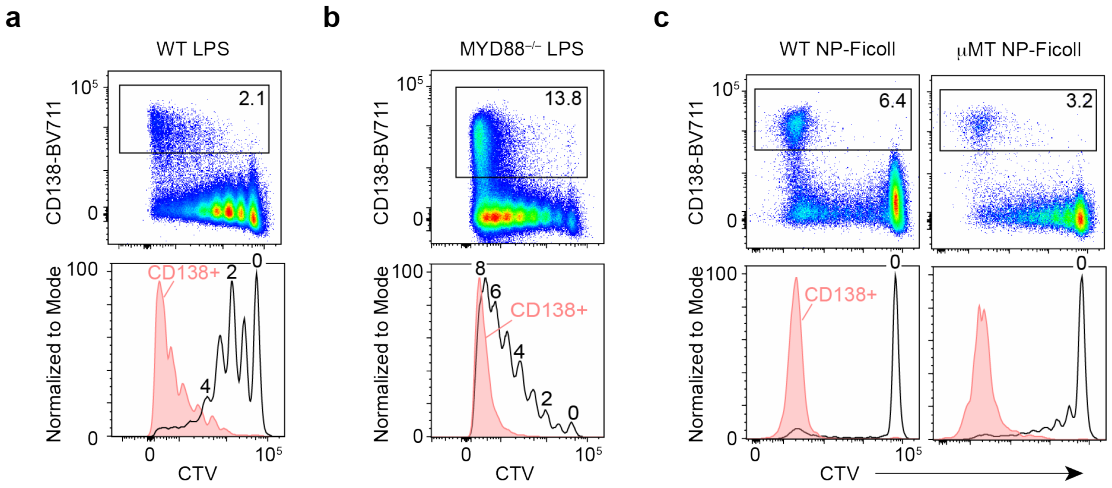

Figure 2-3. B cell differentiation to T independent type I and II antigens reveal similar division requirements. Representative flow cytometry of CD138 versus CTV plots (top) and CTV histograms (bottom) 72 hr post-immune challenge for (**a**) WT hosts challenged with 50 μg of LPS; (**b**) MYD88$^{-/-}$ hosts challenged with 50 μg of LPS; (**c**) WT hosts (left) or μMT hosts (right) challenged with 50 μg of NP-Ficoll. Black CTV histograms represent distribution of total transferred cells, while solid red CTV histograms represent CD138^{+} cells. Gating and percentage of CD138^{+} cells are indicated in the top row. Data in **a**, **c** for WT hosts are representative examples from three independent experiments and 6 total mice each. Data in **b** is representative of two independent experiments with 6 total mice. Data in **c** for μMT host is representative of two independent experiments with 6 total mice.

BLIMP-1-dependent reprogramming is defective at division 8

The transcription factor BLIMP-1, encoded by *Prdm1*, is essential for ASC differentiation [131] but is dispensable for the early proliferative phase of activated B cells [80]. Similar to previous results [80], adoptive transfers using CTV-labeled *Cd19*$^{Cre/+}$*Prdm1*$^{fl/fl}$ (BcKO) or *Prdm1*$^{fl/fl}$ (Ctrl) splenic B cells followed by stimulation with LPS as above, revealed that BcKO B cells divided the same number of times and were distributed similarly across the divisions compared to Ctrl B cells (**Fig. 2-4a**). However, no CD138^{+} ASC were observed in the BcKO adoptive transfer, despite cells reaching the 8th division. To explore the timing and extent of BLIMP-1-dependent reprogramming with respect to division number, we

FACS isolated and performed RNA-seq on Ctrl and BcKO responding B cells from divisions 0, 1, 3, 5, as well as cells in the 8th division that were CD138^{-} (8-) and from Ctrl mice, CD138^{+} division 8 (8+) cells. Similar increases in total mRNA content were observed irrespective of BLIMP-1 status (**Fig. 2-4b**). *Prdm1* expression was first detected in 8- and peaked in 8+ B cells following differentiation [174]. Consistent with this expression pattern, the majority of differentially expressed genes (DEG) between Ctrl and BcKO were observed in 8- B cells (**Fig. 2-4c**). Principal component analysis (PCA) of all DEG separated samples primarily by division status with the largest variation between Ctrl and BcKO occurring in 8- cells. (**Fig. 2-4d**). Examples of genes that failed to be induced in BcKO 8- cells included those that are known to be critical for ASC differentiation and regulated by BLIMP-1 such as *Xbp1*, *Irf4*, and *Ell2* [138,139] (**Fig. 2-4e**). Thus, BLIMP-1-dependent reprogramming is initiated no earlier than division 5 with molecular defects observed in division 8 cells.

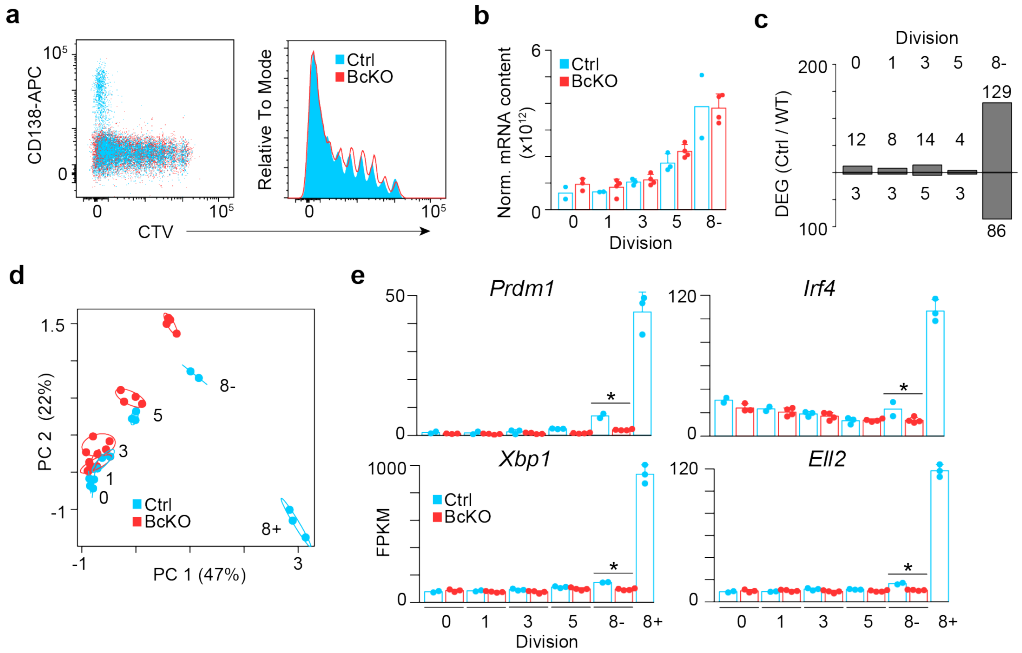

Figure 2-4. BLIMP-1-dependent transcriptional reprogramming is defective in division 8. (**a**) Representative flow cytometry analysis of *Prdm1*$^{fl/fl}$ (Ctrl) and *Cd19*$^{Cre/+}$*Prdm1*$^{fl/fl}$ (BcKO) B cells 72 hr after LPS inoculation. (**b**) ERCC normalized total mRNA content for samples from the indicated divisions sorted from **a**. (**c**) Bar plot showing the number of differentially expressed genes (DEG) for the indicated division between Ctrl and BcKO B cells. (**d**) Principal component analysis of samples from **b** using all DEG. The location of cells in each division is labeled. Circles denote 99% confidence intervals for samples in each division. (**e**) Bar plot of expression of select genes from divisions 0, 1, 3, 5, 8^{-} and for Ctrl 8^{+}. FPKM, fragments per kilobase per million. Data in **b**, **e** represent mean ± SD and statistical significance in **e** was determined by edgeR [208]. Data were derived from 2-4 individual mice as follows: Ctrl division 0 (n = 2), 1 (n = 2), 3 (n = 3), 5 (n = 3), 8- (n = 2), and 8+ (n = 3); BcKO division 0 (n = 3), 1 (n = 4), 3 (n = 4), 5 (n = 4), 8- (n = 4).

Single cell RNA-sequencing captures a continuum of LPS-responding B cells

Molecular analysis of discrete divisions highlights the progressive epigenetic and transcriptional reprogramming that occurs as B cells divide [174,175]. However, B cells respond asynchronously and only a fraction of B cells that make it to division 8 differentiate, indicating there may be additional mechanisms that instruct B cell fate decisions. To resolve B cell differentiation at a finer molecular resolution, we performed scRNA-seq on adoptively transferred cells in μMT hosts at 72 hr post-LPS challenge (**Fig. 2-9**). In total, mRNA from 8,368 B cells was sequenced from two independent mice. In agreement with the previous division data [174], overall mRNA content increased among responding B cells (**Fig. 2-10**).

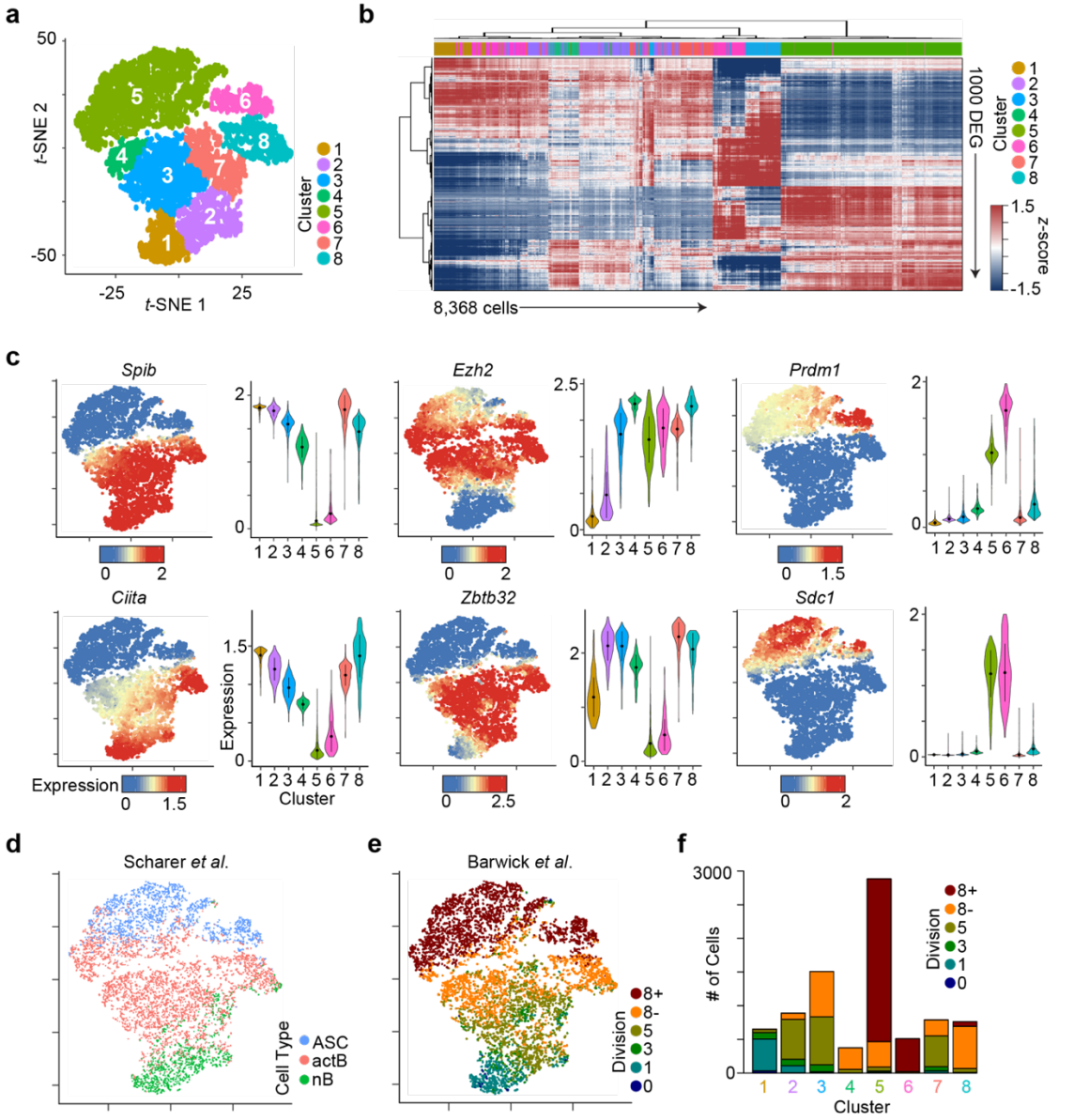

Figure 2-5. scRNA-seq reveals a continuum of heterogeneous LPS-responding B cells. (**a**) *t*-SNE plot of 8,368 WT cells responding to LPS showing eight distinct clusters of cells. (**b**) Heatmap showing hierarchical clustering of the top 1,000 differentially expressed genes (DEG) between cells in each of the 8 clusters from **a**. Data represent *z*-score normalized MAGIC expression values. (**c**) *t*-SNE plot (left) from **a** and violin plots (right) for each cluster showing the MAGIC gene expression data for the indicated gene. For violin plots, the dots represent the mean and lines represent 1st and 3rd quartile ranges. (**d**) *t*-SNE plot from **a** showing the annotation of each cell with naïve B cells (nB) and *ex vivo* differentiated activated B cells (actB) and ASC from Scharer *et al* [175]. (**e**) *t*-SNE plot from **a** showing the annotation of each cell with division sorted LPS-responding B cells from Barwick *et al* [174]. (**f**) Bar plot quantitating the number of cells from each cluster annotated to specific divisions in **e**. Data represent combined cells from two independent mice.

LPS-responding B cells were grouped into eight distinct clusters and visualized by t-distributed stochastic neighbor-embedded (*t*-SNE) projections (**Fig. 2-5a**). Hierarchical clustering of cells using the top 1,000 DEG between all clusters indicated that cells in cluster 5 were the most transcriptionally distinct (**Fig. 2-5b**). Strikingly, we observed variation between individual cells within each cluster, revealing a heterogeneity not previously appreciated.

To assign clusters to cell types, we assessed the expression of both single genes that define B cells, activated B cells (actB) and ASC [15], as well as global transcriptome signatures of each purified population [175]. B cell transcription factors, such as *Spib*, *Ciita*, and *Pax5*, were expressed in clusters 1-4 and 7-8 (**Fig. 2-5c, Supplementary Fig. 2-10**). ActB genes, such as *Zbtb32*, *Aicda*, and *Ezh2,* were expressed in clusters 2-4, 7, and 8. ASC genes, such as *Sdc1* (CD138), *Jchain*, and *Irf4*, were highly expressed in clusters 5 and 6. Using previously published RNA-seq datasets containing transcriptome profiles of $CD43^-$ naïve B cells (nB) and *ex vivo* LPS-responding actB and ASC [175], we assigned each cell to one of these three differentiation stages using a K-nearest neighbor (KNN) approach. Cluster 1 cells were classified as nB and those in clusters 2-4, 7, and 8 as actB (**Fig. 2-5d**). Cluster 5 and 6 cells were primarily classified as ASC with a subset of cluster 5 bearing hallmarks of actB. Importantly, the number of cells assigned to these clusters closely matched the frequency of $CD138^+$ ASC observed by flow cytometry (**Supplementary Fig. 2-10**).

To further annotate the clusters with respect to cell division, we compared the transcriptional state of each cell to gene expression data for LPS-responding B cells at divisions 0, 1, 3, 5, and 8- and 8+ [174] using KNN. This analysis reaffirmed that cells

assigned to cluster 1 represented those that were in the earliest stages of differentiation and cells assigned to clusters 5 and 6 represented B cells that have differentiated (**Fig. 2-5e-f**). Furthermore, we found that the transcriptome of cells assigned to actB aligned with gene expression data of LPS-responding B cells in divisions 3, 5 and 8-. These analyses indicate a continuum/progression of cellular differentiation from nB (cluster 1) through dividing actB (clusters 2-4, 7, and 8) to ASC (clusters 5 and 6), capturing the initial, intermediate, and end stages of B cell differentiation in response to LPS.

Pseudotime analysis defines divergent B cell differentiation trajectories

To construct potential differentiation trajectories and understand the progression between cellular states, we computationally ordered cells along pseudotime [209]. Strikingly, this analysis revealed two distinct branch points as cells proceeded along pseudotime and differentiated from nB to ASC (**Fig. 2-6a-b**). Analyzing the branching trajectory with cell division assignments revealed that the first branch point bifurcated actB into two groups, with one branch proceeding to $CD138^+$ ASC and the other remaining as B cells (**Fig. 2-6b**). We have termed these the "ASC-destined" and "non-ASC" branches, respectively. The ASC-destined branch includes clusters 5 and 6 and cells that are in division 8+ and possess all the hallmark features of ASC (**Fig. 2-6b**). The non-ASC branch terminates in cluster 7 and 8 and includes cells that have divided at least 5-8 times but have not differentiated further. To corroborate these observations using different host and stimuli, B cells were adoptively transferred to WT hosts and stimulated with both LPS and NP-Ficoll. At 72 hr, all responding cells were isolated and scRNA-seq was performed as above (**Supplementary Fig. 2-9**). For each dataset, a pseudotime trajectory was constructed and

each cell assigned both a cell-division and cell-type phenotype as with the μMT host data. This analysis revealed the presence of a branch point that separated actB into an ASC-destined and non-ASC trajectory (**Fig. 2-6c, Supplementary Fig. 2-10**).

To identify the properties of the different branches, gene set enrichment analysis (GSEA) [210] was performed on cell clusters just after the bifurcation point (clusters 3 and 7). This indicated that cells in the ASC-destined branch upregulated genes associated with MYC activation and oxidative phosphorylation (OXPHOS) (**Fig. 2-6d-f**), both of which are important for achieving the metabolic and catabolic requirements during plasma cell differentiation [80,211]. Examples within the ASC-destined trajectory include expression of *Srm*, *Dut*, *Idh3a*, and *Ldha*. Conversely, cells along the non-ASC branch displayed higher expression of genes, such as *Klf6* and *Ifngr1*, which were associated with an inflammatory response and were upregulated in cluster 7 and maintained in cluster 8.

A second branch point following $CD138^+$ ASC differentiation was identified in the μMT dataset within clusters 5 and 6 (**Fig. 2-6a-c**). GSEA between these clusters indicated that cells in cluster 6 were enriched for genes involved in endoplasmic reticulum (ER)-to-nucleus signaling and ER chaperones, co-chaperones and folding enzymes [212] (**Fig. 2-6g-h**). Examples of genes upregulated in cluster 6 included *Atf6*, *Hspa5*, and *Calr* (**Fig. 2-6i**). Although both clusters 5 and 6 have upregulated the ER stress response factor *Xbp1*, these data suggest that ASC in cluster 6 were under distinct ER stress.

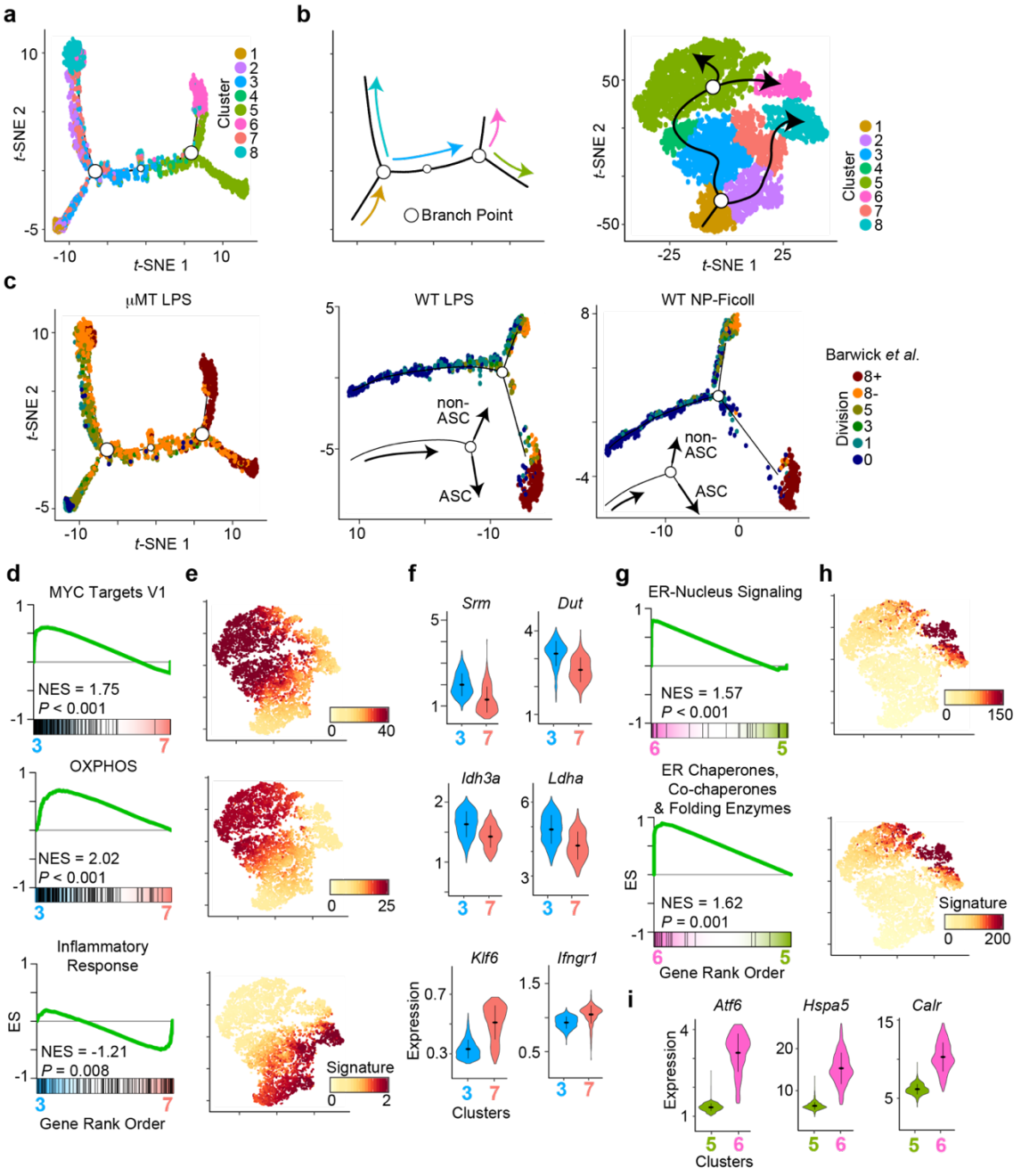

Figure 2-6. Pseudotime identifies divergent activated B cell differentiation trajectories. (**a**) *t*-SNE plot of pseudotime ordered cells from **Fig. 2-5a** showing the location of cells from each cluster. Open circles denote pseudotime branch points. (**b**) Schematic showing the pseudotime order of cells from **a** (left) and from the *t*-SNE plot from **Fig. 2-5a** (right). (**c**) Pseudotime *t*-SNE plot from **a** (left) or from scRNA-seq data on adoptively transferred cells responding to LPS (middle) or NP-Ficoll (right) in WT hosts showing cells annotated based on division sorted LPS-responding B cells from Barwick *et al.*[174] (see **Fig. 2-5e** and **Supplementary Fig. 2-9**). Circles denote pseudotime branch points. (**d**) GSEA of the indicated datasets comparing the transcriptional profile between cells in clusters 3 and 7. (**e**) *t*-SNE plot showing mean MAGIC expression levels for all

Leading Edge genes from the GSEA gene set in **d**. (**f**) Violin plots showing MAGIC expression levels for cells in clusters 3 and 7 for the indicated genes. Genes were chosen from the adjacent GSEA gene set from **d**. Within each violin plot, the dots represent mean MAGIC expression levels and lines represent 1st and 3rd quartile ranges. (**g**) GSEA of the indicated datasets comparing the transcriptional profile of cells in cluster 5 and 6. (**h**) *t*-SNE plot showing mean MAGIC expression levels for all Leading Edge genes from the adjacent GSEA gene set in **g**. The ER chaperones, co-chaperones, and folding enzymes gene set was described previously [212]. (**i**) Violin plots of select genes representative of gene sets in **g**. WT LPS and WT NP-Ficoll scRNA-seq data in **c** represent combined cells from two independent mice.

Multiple factors regulate the ASC-destined branch

To determine the transcription factors that might be guiding the first differentiation branch point, the SCENIC algorithm [213], which predicts transcription factor activity, was used to analyze cells in clusters 3 and 7 (**Fig. 2-7a**). Correlation of the fold change in expression of transcription factors versus the fold change in that factor's SCENIC score between clusters revealed a positive correlation between the data. Representing the non-ASC branch, cluster 7 cells were enriched for IRF9 and BACH2 expression and activities. Conversely, cluster 3 cells in the ASC-destined branch were enriched for KLF10, E2F1, and BATF activities. *Batf* was more highly expressed in clusters 3 and 4 compared to 7 and 8 and BATF target genes largely reflected this pattern of activity (**Fig. 2-7b-c**). Analysis of BATF target gene expression along pseudotime revealed that the majority were induced early and ultimately repressed and included *Aicda*, *Junb*, *Rela*, *Myc*, and *Batf* itself (**Fig. 2-7d**). This is consistent with evidence that BATF-deficient B cells proliferate but cannot class switch due to a failure to induce *Aicda* [214]. Further analysis of the BATF motifs identified by SCENIC above revealed that 35% were canonical AP-1 binding motifs whereas 65% were AP-1:IRF composite element (AICE) motifs that can be bound by AP-1 family member BATF and IRF4 [125] (**Fig. 2-7e**). This suggested that BATF:IRF4

complexes may be important in programming the ASC-destined branch. Our scRNA-seq data revealed that *Irf4* expression peaked in the ASC clusters (5 & 6); however, low expression levels of *Irf4* were observed in early differentiating clusters 3-4 and 7-8 (**Fig. 2-7f**). Consistent with these data, intracellular staining of B cells responding to LPS *in vivo* indicated that IRF4 was initially upregulated after division 1 and highly upregulated in division 8+ cells (**Fig. 2-7g**).

To explore the role of IRF4 in orchestrating B cell differentiation trajectories in more detail, we adoptively transferred CTV-labeled *Cd19*$^{Cre/+}$*Irf4*$^{fl/fl}$ (IRF4$^{-/-}$) B cells and performed scRNA-seq on all adoptively transferred cells at 72 hr post-LPS challenge. *t*-SNE projections revealed IRF4$^{-/-}$ B cells grouped into 6 distinct clusters, with the majority of the cells assigned to clusters 1 and 2 (**Fig. 2-7h**). Consistent with a failure to produce ASC [118], annotation of the IRF4$^{-/-}$ cells against the bulk RNA-seq data found no match to *ex vivo* or *in vivo* ASC (**Fig. 2-11**). The majority of IRF4$^{-/-}$ cells matched gene expression profiles of naïve and activated B cells that corresponded to those in divisions 1, 3, or 5. Pseudotime analysis revealed a more linear trajectory (**Fig. 2-7i, Supplementary Fig. 2-11**). KNN was used to assign each IRF4$^{-/-}$ cell to one of the eight WT scRNA-seq clusters. The majority of cells were assigned to the early clusters (1-3) as well as the two non-ASC branch clusters 7 and 8 (**Fig. 2-7j**), further indicating that the IRF4$^{-/-}$ cells failed to initiate the ASC-destined differentiation branch observed in WT B cells. Analysis of BATF signature in the IRF4$^{-/-}$cells found a lack of BATF activity (**Fig. 2-7k**). Additionally, IRF4$^{-/-}$ cells displayed little increases in OXPHOS gene expression that was characteristic of the ASC-destined branch (**Fig. 2-7l**). Conversely, IRF4$^{-/-}$ cells showed enrichment for Inflammatory Response genes that marked the non-ASC branch (**Fig. 2-7l**). Taken

together, these data suggest that IRF4 is necessary to establish the ASC-destined differentiation branch during the actB stage.

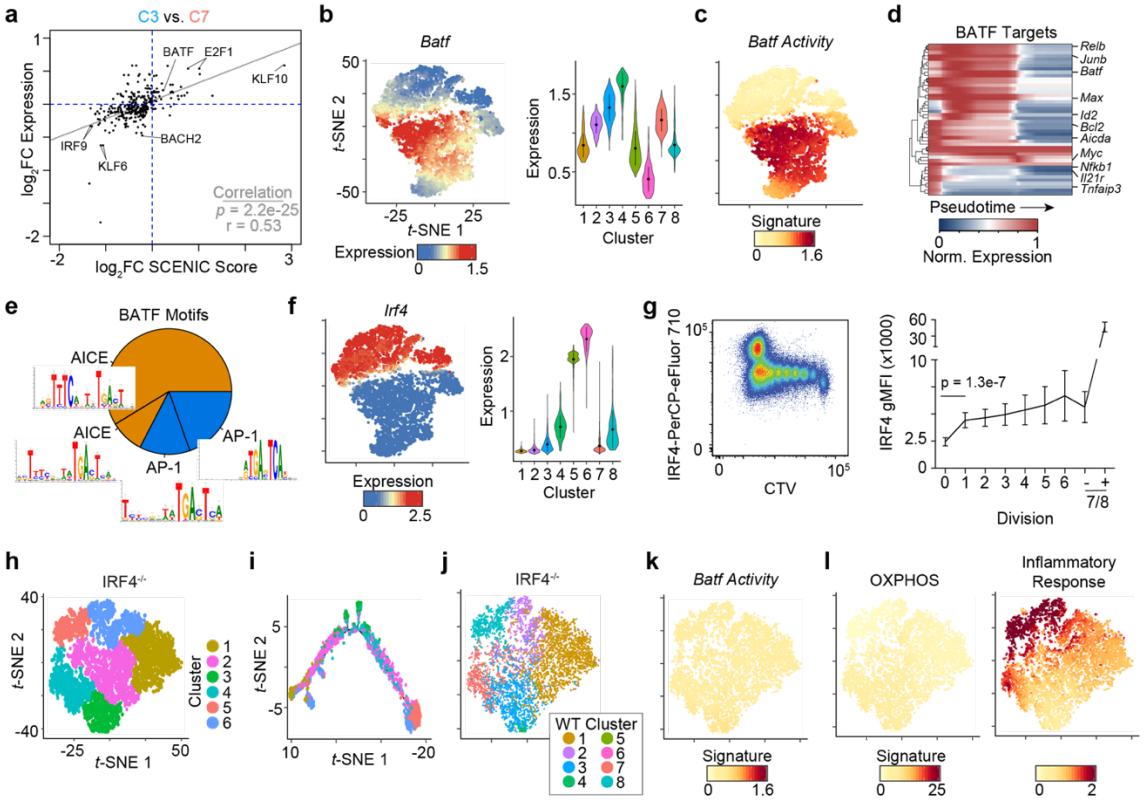

Figure 2-7. IRF4 is critical for establishing the ASC-destined branch transcriptional program.

(**a**) Scatter plot showing the expression $\log_2$ fold change ($\log_2$FC) versus the $\log_2$FC in SCENIC activity score between cluster 3 versus 7 for each transcription factor. Grey line represents linear regression with significance determined by one-way ANOVA. Pearson's r correlation is indicated. (**b**) *t*-SNE plot (left) from **Fig. 2-5a** and violin plot (right) for each cluster showing the MAGIC gene expression data for the indicated gene. For violin plots, dots represent mean and lines represent 1st and 3rd quartile ranges. (**c**) *t*-SNE plot showing mean MAGIC expression levels for BATF target genes determined by SCENIC. (**d**) Heatmap showing expression of 46 BATF target genes along pseudotime in WT cells. For each gene the mean MAGIC expression level is normalized to the maximal value. (**e**) Pie chart representing the percentage of BATF target genes containing either the canonical AP-1 or composite IRF:AP-1 (AICE) motif. (**f**) *t*-SNE plot (left) and violin plot (right) for each cluster showing the MAGIC gene expression data for the indicated gene. For violin plots, the dots represent mean and lines represent 1st and 3rd quartile ranges. (**g**) Representative flow cytometry (left) and geometric mean fluorescence intensity at each cell division (right) for intracellular staining of IRF4 levels versus CTV in LPS-responding B cells 72 hr after LPS inoculation. Division 7/8 cells are subdivided into CD138 negative

(-) and positive (+). Data represent mean ± SD and statistical significance between division 0 and 1 determined by two-tailed Student's *t*-test. Data represent two independent experiments of 9 mice. (**h**) *t*-SNE plot of 6,903 *Cd19*$^{Cre/+}$*Irf4*$^{fl/fl}$ (IRF4$^{-/-}$) cells responding to LPS showing the location of six distinct cell clusters. Data represent combined cells from two independent mice. (**i**) *t*-SNE plot of pseudotime ordered cells from **h** showing the location of cells from each cluster. (**j**) *t*-SNE plot from **h** showing the annotation of each cell with a WT cluster from **Fig. 2-5a**. (**k**) *t*-SNE plot from **h** showing mean MAGIC expression levels for BATF target genes as in **c**. (**l**) *t*-SNE plot from **h** showing mean MAGIC expression for Leading Edge genes from the indicated gene set (see **Fig. 2-6e**).

Loss of L-selectin expression marks B cells destined to become ASC

Given the divergent transcriptional programs of the ASC-destined and non-ASC branches, we sought to find markers that would allow separation of cells along either trajectory *in vivo*. L-selectin (CD62L) or *Sell* is a cell adhesion molecule that facilitates entry of lymphocytes into secondary lymphoid organs from the blood stream [215] and is expressed as part of the Inflammatory Response signature that marked the non-ASC branch. Analysis of *Sell* expression in WT cells revealed high levels within clusters 7 and 8 of the non-ASC branch with progressively decreasing levels in the ASC-destined branch (clusters 3-6) (**Fig. 2-8a-b**). Similarly, *Sell* expression decreased along the ASC-destined branch in cells responding to LPS and NP-Ficoll in WT hosts. Confirming the scRNA-seq data, flow cytometry revealed that CD62L was ultimately repressed in CD138^{+} ASC in all three systems (**Fig. 2-8c**). Analysis of CTV-labeled LPS- or NP-Ficoll-responding B cells showed a gradual bifurcation in CD62L surface expression as B cells divided, with cells appearing to both maintain and lose expression as they progressed through the divisions (**Fig. 2-8d**). These data suggest that CD62L could be used to separate B cells committed to either differentiation branch. To test this, we FACS isolated LPS-responding B cells from division 8 that were CD62L^{+}CD138^{-} (div8:non-ASC; cluster 8), CD62L^{-}CD138^{-} (div8:ASC-destined; cluster 4), and as a positive control, CD138^{+} ASC that were also

CD62L^{-} (clusters 5 and 6) (**Fig. 2-8e**). Furthermore, we isolated cells from divisions 5-6 CD62L^{+}CD138^{-} (div5-6:non-ASC; cluster 2) and CD62L^{-}CD138^{-} (div5-6:ASC-destined; cluster 3) representing early cells committed to each fate. Each group of cells were incubated in media without further stimulation and CD138^{+} ASC differentiation assessed by monitoring antibody secretion via ELISA over 48 hr. Regardless of division, ASC-destined cells secreted significantly more antibody compared to non-ASC cells in the same division across all time points assayed (**Fig. 2-8f**). Importantly, because the ASC-destined cells in div5-6 secreted IgM, this indicated the div8:non-ASC cells were provided sufficient time to differentiate. Thus, CD62L surface expression can be leveraged to separate actB cells that are destined to become ASC.

Finally, to determine if cells in division 8 on the non-ASC branch could be stimulated to differentiate, we sorted these cells, as well as div8:ASC-destined, and CD138+ ASCs. The cells were cultured for 16 hr in the presence of LPS, IL-2, and IL-5 to induce their *ex vivo* differentiation [216]. ASC formation was assessed by flow cytometry and antibody secretion was monitored by ELISA. Div8:ASC-destined cells readily differentiated into CD138^{+} cells whereas the div8:non-ASC cells produced ten-fold fewer CD138^{+} cells (**Fig. 2-8g-h**). Consistent with these findings, Div8:ASC-destined cells secreted significantly more IgM into the culture media compared to div8:non-ASC cells (**Fig. 2-8i**). Thus, div8:non-ASC cells do not readily differentiate upon re-stimulation. Taken together, at early stages of B cell differentiation, two distinct differentiation trajectories exist with only one leading to ASC.

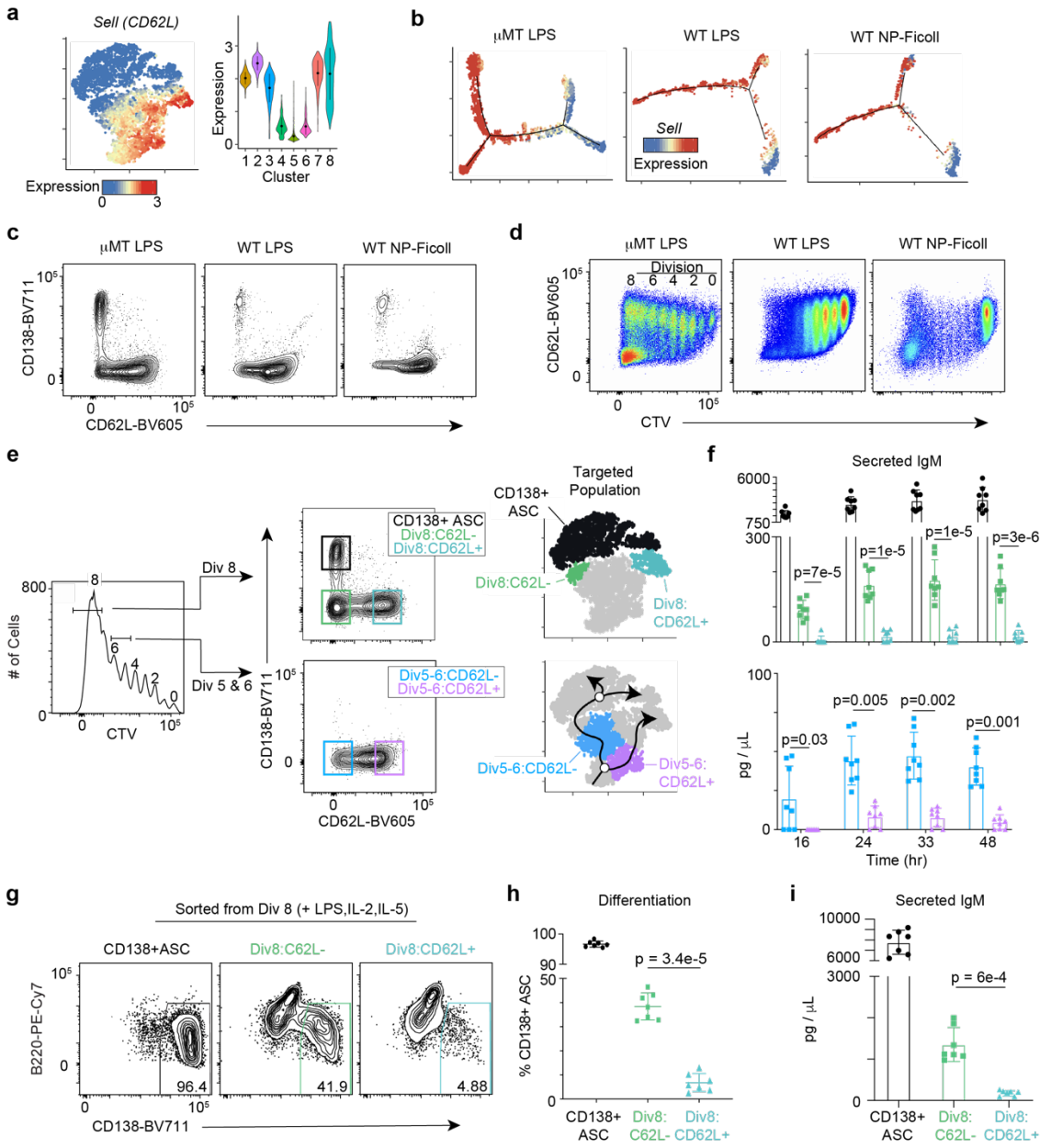

Figure 2-8. Loss of CD62L (L-selectin) delineates cells on the ASC-destined branch. (**a**) *t*-SNE plot (left) from **Fig. 2-5a** and violin plot (right) for each cluster showing the MAGIC gene expression data for *Sell* (CD62L) in WT cells. For violin plots, the dots represent mean and lines represent 1st and 3rd quartile ranges. (**b**) *Sell* expression projected along pseudotime for each scRNA-seq dataset (see **Fig. 2-6c**). (**c**) Representative flow cytometry plot of CD138 versus CD62L for adoptively transferred cells from μMT hosts challenged with 50 μg of LPS (left), WT hosts challenged with 50 μg of LPS (middle) or WT hosts challenged with 50 μg of NP-Ficoll (right). All plots are 72 hr after challenge. (**d**) Representative flow cytometry plot of CD62L versus CTV for each adoptive transfer setup described in **c**. The division number is indicated in the left panel. (**e**) Representative FACS strategy for isolating ASC in clusters 5 and 6 ($CD62L^{-}CD138^{+}$ cells), ASC-destined

cells in cluster 4 (div8:CD62L^{-}CD138^{-}), non-ASC destined cells in cluster 8 (div8:CD62L^{+}CD138^{-}), ASC-destined cells in cluster 3 (CD62L^{-}CD138^{-}), and non-ASC destined cells in cluster 2 (CD62L^{+}CD138^{-}). Cells were gated on division 5-6 or 8 and then separated by CD138 and CD62L expression 72 hr post-LPS challenge. (**f**) IgM titers in culture over time for the indicated samples from division 8 (top) and division 5-6 (bottom). (**g**) Representative flow cytometry plot of B220 versus CD138 expression after 16 hr of culture with LPS, IL-2, and IL-5 for the indicated samples. Percent of CD138^{+} ASC is indicated. (**h**) Percent of CD138^{+} cells and (**i**) IgM titers in culture for each sample. Statistical significance in **f**, **h**, **i** was determined by paired two-tailed Student's *t*-tests. Data in **f** represent two independent experiments with a total of 8 mice; data in **g-i** represent two independent experiments with a total of 7 mice.

IV. DISCUSSION

Using multiple model systems, this study has defined the *in vivo* relationship between cell division and cellular heterogeneity during B cell differentiation. B cells responding to T cell independent type I and II antigens in the absence of cell extrinsic signals required 8 cell divisions for CD138^{+} ASC differentiation. Strikingly, scRNA-seq of cells representing all stages of differentiation revealed a divergent actB program, with only a subset of B cells upregulating an IRF4-dependent transcriptional program that led to ASC formation. Cells along this ASC-destined branch downregulated CD62L and formed ten-fold more ASC in culture compared to B cells that followed the alternative non-ASC branch. Together, these data define an early cell fate-decision branch point for ASC formation that occurs early in differentiating and dividing activated B cells.

Comparing adoptive transfers using μMT, WT, or MYD88$^{-/-}$ mice as hosts and immunizing with LPS revealed that cell extrinsic effects in WT mice can impact the cell division kinetics of B cell differentiation. In contrast to μMT and MYD88$^{-/-}$ hosts, CD138^{+} ASC differentiation in WT hosts was detected in earlier divisions and indicate that in WT hosts, other LPS-responding cells, such as macrophages and dendritic cells [217], can influence B cell differentiation. While these cells are present in μMT hosts, the splenic

architecture is abnormal and may impact signals between cells [190]. When the B cell-specific stimulus NP-Ficoll was used, similar cell division/differentiation patterns were observed in both μMT and WT hosts. This indicates that the signaling downstream of toll-like receptor 4 signaling (via LPS) and B cell receptor signaling (via NP-Ficoll) both initiate a conserved differentiation program that includes the same cell division constraints. Despite the extrinsic effects observed in the WT hosts stimulated with LPS, the scRNA-seq data revealed a similar cell trajectory in each of the three differentiation models. This suggests that even if extrinsic effects modulate the cell division-differentiation relationship, the molecular reprogramming steps proceed along similar paths. Indeed, ASC-destined and non-ASC branches are observed for both stimuli with similar changes in gene expression, including increases in OXPHOS and MYC target genes along the ASC-destined branch. Thus in the absence of cell extrinsic modulation, *in vivo* B cell differentiation to T independent type I and II antigens is orchestrated in a manner that requires at least 8 cell divisions to fully attain the ASC program.

Our data support the quantal response model of B cell differentiation to LPS, where the concentration of LPS affects the proportion of cells responding but does not affect the rate of ASC formation within each division [180]. While we cannot rule out that at low doses there is selective activation of B cells that are specific for LPS, our data indicate this all-or-none response to a T cell-independent antigen also occurs *in vivo*. Lower doses of LPS *in vivo* impacted the overall magnitude of the B cell response, with fewer activated/dividing cells observed across the divisions. However, of the cells reaching division 8, the same percentage formed ASC. In contrast to the quantal response model, the kinetics of cell division and differentiation in response to a T cell-dependent antigen follow a distinct

graded response model *ex vivo,* which can be modulated by amounts of CD40L [180]. *In vivo*, T cell dependent responses are further complicated due to the complex dynamics of the germinal center reaction, cyclic reentry, and selection pressure for high affinity clones [218,219]. Using type I and type II T cell independent stimuli, our scRNA-seq data demonstrate that B cells progress down similar ASC differentiation paths in response to both BCR and TLR signals. Thus, these data confirm key aspects of *ex vivo* differentiation models to TI antigens and add new cell division parameters to help predict adaptive immune responses *in vivo*.

Here, transcriptional heterogeneity was observed both within cells at the same division and among cells at distinct differentiation stages. Despite the observed heterogeneity, a consistent percentage of responding B cells form ASC in an experimentally repeatable manner. Our data suggest that IRF4, in tandem with BATF at AICE DNA-binding elements, enforces early programming changes that drive a subset of B cells towards the ASC fate. The stochastic differentiation model predicts cell fate outcomes based on a probability distribution across the population of responding cells [220] and can be applied here to the bifurcation of ASC-destined versus non-ASC cells observed in the scRNA-seq data. In fact, the concentration of IRF4 is critically important for determining B cell fate [119,120,129]. Thus, the probability of inducing sufficient IRF4 expression to initiate the ASC-destined branch may be the same for each cell, with higher doses of LPS resulting in a greater number of cells being stimulated sufficiently to progress towards ASC.

One of the defining features of the ASC-destined branch was the loss of CD62L (L-selectin) expression. Thus, CD62L expression was used as a surface marker to

distinguish subsets of actB cells along divergent differentiation trajectories. CD62L is an adhesion molecule that mediates leukocyte migration to secondary lymphoid tissues, and shedding of CD62L allows leukocytes to be redirected to sites of infection [215]. In addition to its role as an adhesion molecule, CD62L also plays a role in triggering cell signaling events [221]. In our system, CD62L expression distinguished ASC-destined cells as early as division 5. In fact, the small number of ELISPOTs observed in division 8 $CD138^-$ cells may be due to cells that are continuing to differentiate during the *ex vivo* assay. The function of reduced CD62L could allow ASC-destined cells to remain in circulation where they could eventually home to the bone marrow for long-term survival. While the full role that CD62L plays in B cell biology is not fully understood, our data demonstrate that it is a useful marker to distinguish actB cells destined to differentiate to ASC.

Trajectory analysis of B cells differentiating to LPS in μMT hosts identified a second bifurcation event following differentiation that split differentiated ASC into two groups. Cells assigned to ASC clusters 5 and 6 displayed all the hallmarks of ASC, including high expression of *Xbp1*, a transcription factor required for initiating the unfolded protein response [102,222]. This indicates that cells in both clusters had initiated the ASC transcriptional program to counter ER stress. However, *Atf6*, an ER stress sensor was highly expressed in cluster 6. This suggests that these cells may be under distinct ER stress compared to ASC in cluster 5. Support for this concept comes from data showing that in response to LPS stimulation, targets of ATF6 in the I.29 micro(+) B cell line were upregulated later than other aspects of the unfolded protein response [94]. Although the same ASC bifurcation event was not observed from scRNA-seq when using WT hosts, this may be due to the timing in which the cells were harvested or limited by the numbers of ASCs

generated and sequenced. Differences in the ability to regulate ER stress may provide a means to select for ASC that can adapt to the stress of Ig production and secretion.

Together, these data provide insight into the heterogeneity and cell division kinetics of B cell differentiation *in vivo* and highlight an important IRF4-dependent bifurcation event that occurs early during actB reprogramming, with only a subset of B cells leading to ASC. This ASC-destined branch required an alignment of cellular proliferation and metabolic reprogramming events that enabled ASC formation and their ability to withstand the stress of high antibody production and secretion. The alternative non-ASC branch contained cells that were responding to inflammatory stimuli and may ultimately have a role in shaping immune responses. Ultimately, controlling which pathway cells follow could help in the therapeutic control of B cell mediated immunity.

V. SUPPORTING DATA

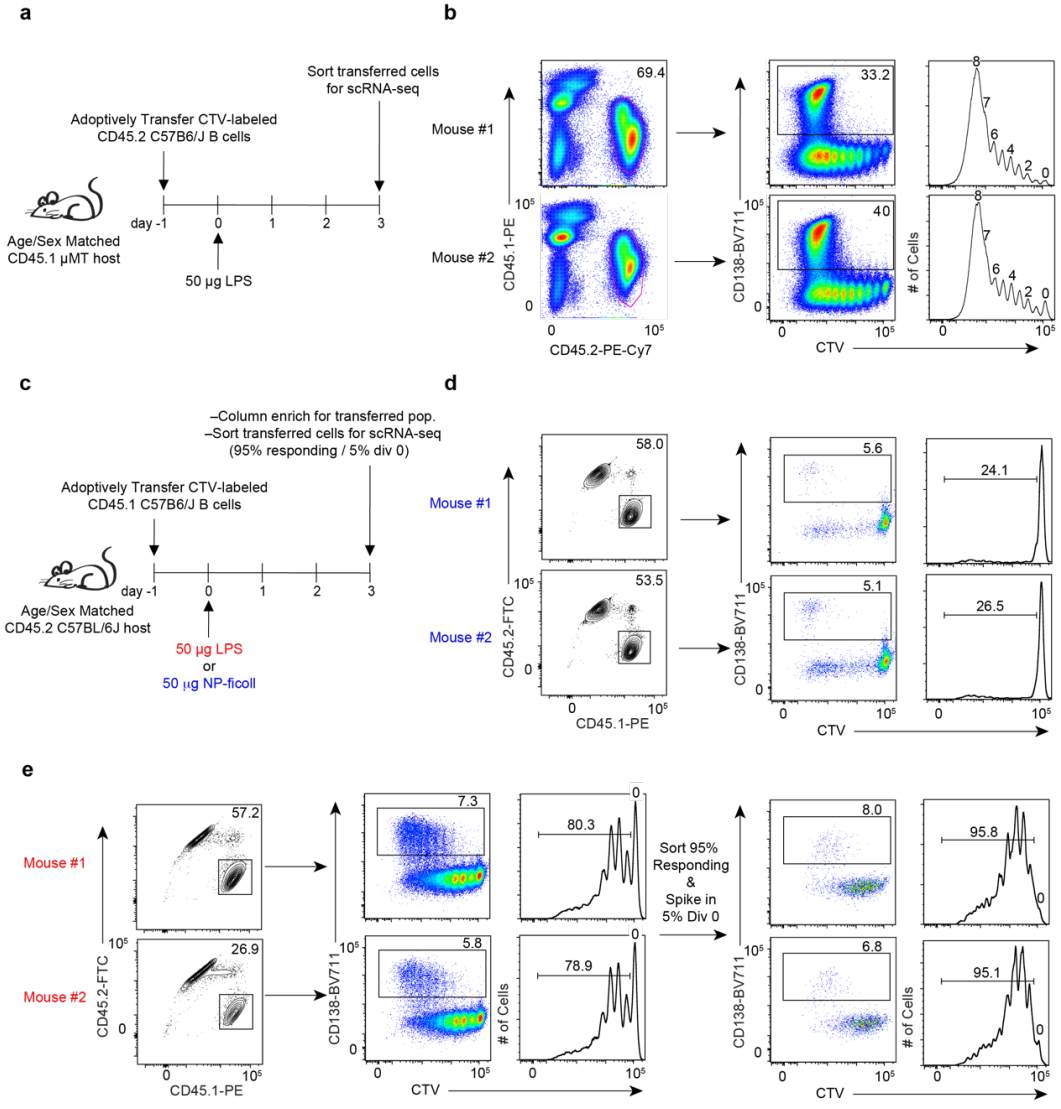

Figure 2-9. Summary of adoptive transfers used to generate scRNA-seq of LPS or NP-Ficoll responding wild-type B cells. (**a**) Schematic of experimental design for μMT hosts challenged with LPS. (**b**) Flow cytometry plot of CD45.1 versus CD45.2 with percentage of CD45.2$^+$ cells displayed (left), CD138 versus CTV with percentage of CD138$^+$ cells shown (middle), and CTV histograms with division numbers indicated (right) for each mouse used to generate scRNA-seq data (see **Fig. 2-5**). (**c**) Schematic of experimental design for WT hosts challenged with LPS or NP-Ficoll. (**d**) For NP-Ficoll, flow cytometry plot of CD45.2 versus CD45.1 with percentage of CD45.1$^+$ cells displayed (left), CD138 versus CTV with percentage of CD138$^+$ cells shown (middle), and CTV histograms with the frequency of cells that have responded indicated (right) for each mouse. A mixture of 95% responding cells and 5% division 0 cells were used to generate scRNA-seq data (final input not shown; see **e** for example). (**e**) For LPS, flow cytometry plot of CD45.2 versus CD45.1 with percentage of CD45.1$^+$ cells displayed (left), CD138 versus CTV with

percentage of CD138^{+} cells shown (middle-left), and CTV histograms with the frequency of responding cells indicated (middle-right) for each mouse. A mixture of 95% responding cells and 5% division 0 cells were used to generate scRNA-seq data; final input for scRNA-seq with the same gates/frequencies shown as the middle panel (right).

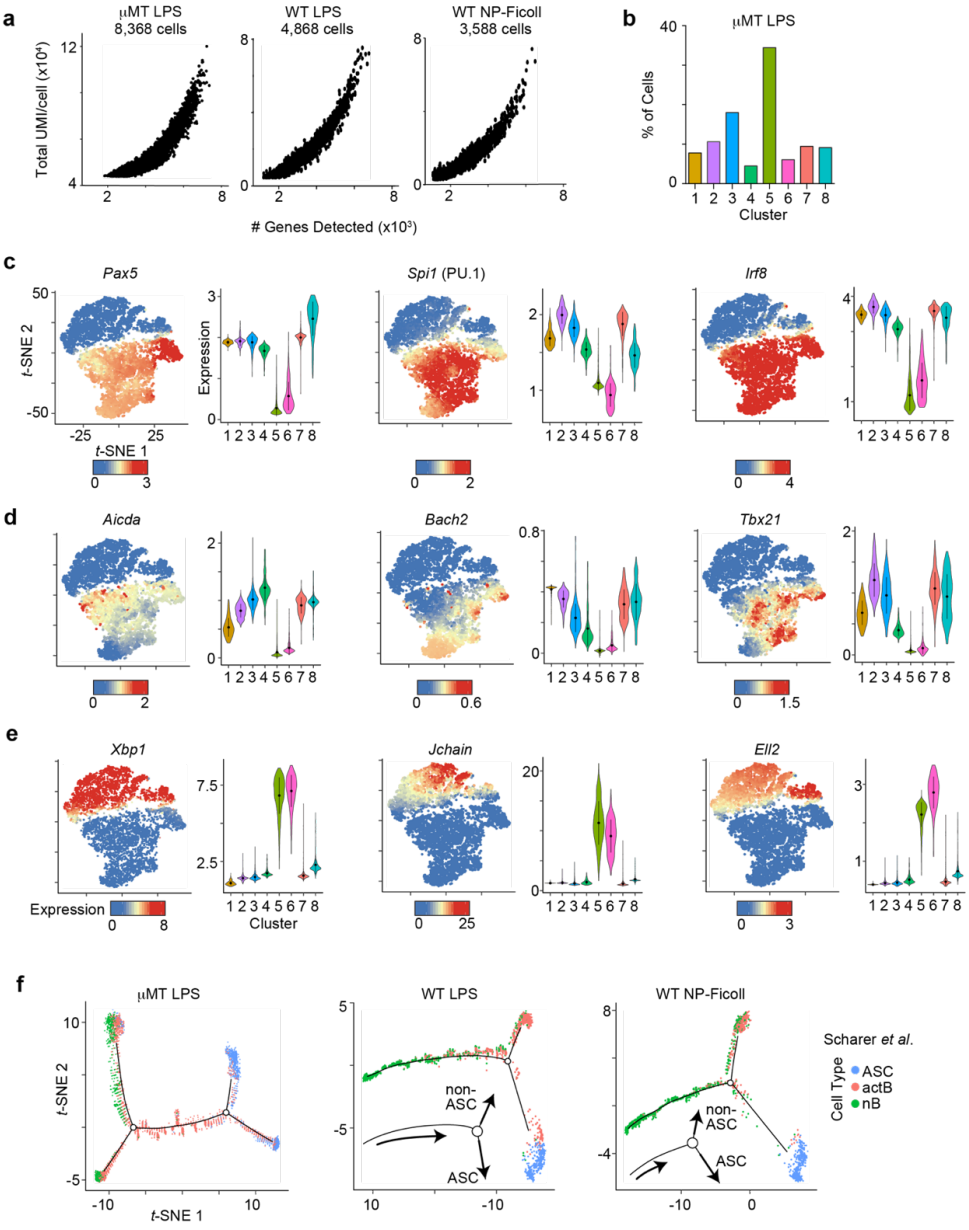

Figure 2-10. scRNA-seq of transferred CTV-labeled cells captures a continuum of responding B cells at all stages of differentiation.
(**a**) Scatterplot of unique molecular identifiers (UMI) versus number of genes detected per cell for each of the three scRNA-seq datasets. (**b**) Bar plot of the frequency of cells assigned to each cluster for the µMT LPS scRNA-seq dataset. *t*-SNE plot (left) from **Fig. 2-5a** and violin plots (right) for each cluster showing the MAGIC gene expression data for the

indicated genes representing (**c**) B cells, (**d**) activated B cells, and (**e**) ASC. For violin plots, the dots represent mean and lines represent 1st and 3rd quartile ranges. (**f**) Pseudotime *t*-SNE plot from μMT LPS (left), WT LPS (middle), or WT NP-Ficoll (right) showing cells annotated with naïve B cells (nB) and *ex vivo* differentiated activated B cells (actB) and ASC from Scharer *et al* [14]. Circles denote pseudotime branch points. See also **Fig. 2-6**.

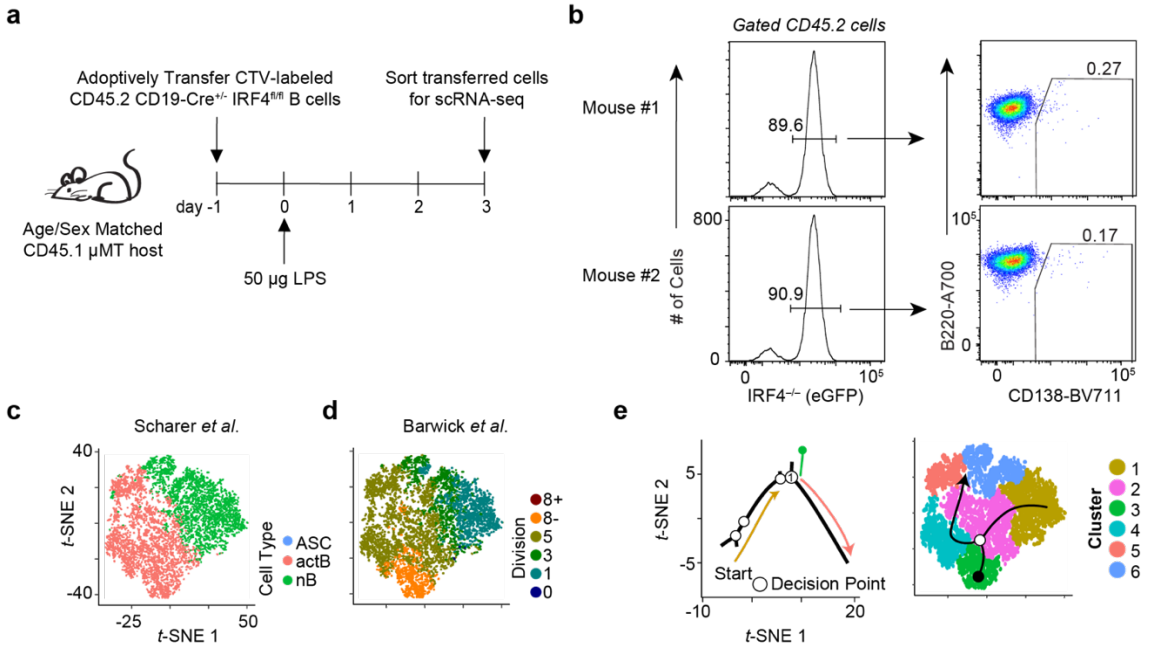

Figure 2-11. scRNA-seq of bulk transferred CTV-labeled IRF4-deficient B cells reveals a critical role for IRF4 in establishing the ASC-destined branch.

(**a**) Schematic of experimental design. (**b**) Flow cytometry plot of histograms of eGFP, which marks IRF4-null cells [40] (left) and B220 versus CD138 (right) are shown after previously gating CD45.2+ transferred cells for each mouse used to generate scRNA-seq data (see **Fig. 2-7h**). The percentage of eGFP (left) and CD138+ (right) cells are indicated. (**c**) *t*-SNE plot from **Fig. 2-7h** showing the annotation of each cell with naïve B cells (nB) and *ex vivo* differentiated activated B cells (actB) and ASC from Scharer *et al* [14]. (**d**) *t*-SNE plot from **Fig. 2-7h** showing the annotation of each cell with division sorted LPS-responding B cells from Barwick *et al* [16]. (**e**) Schematic showing the pseudotime order of cells from **Fig. 2-7i** (left) and from the *t*-SNE plot from **Fig. 2-7h** (right).

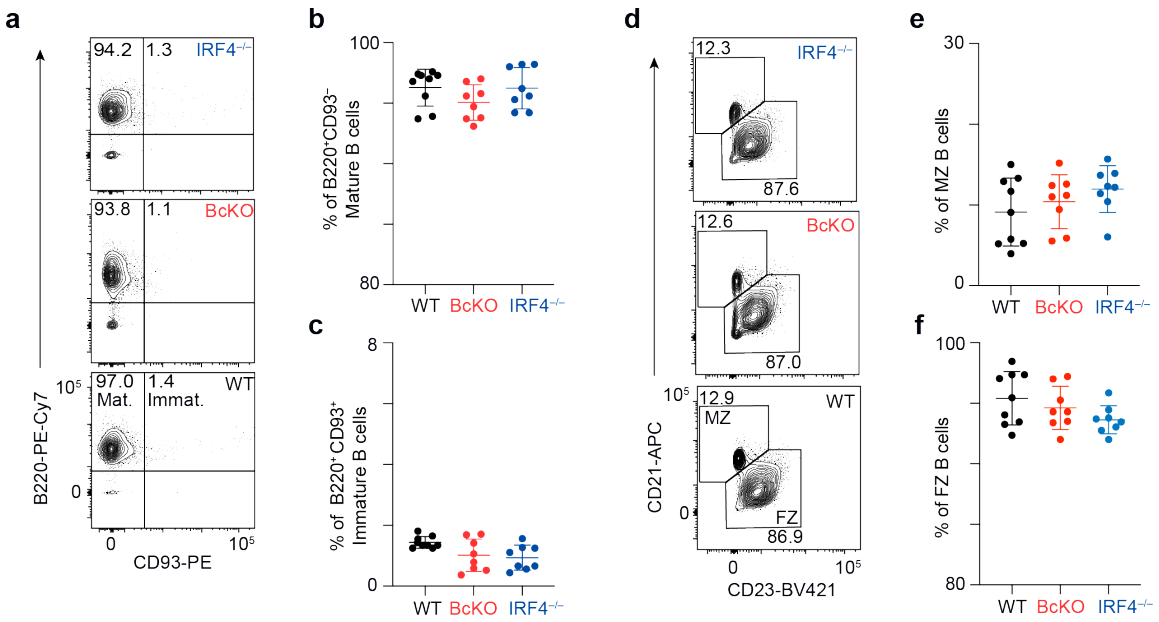

Figure 2-12. Equivalent CD43⁻ B cell populations were enriched from each mouse strain. (**a**) Representative flow cytometry plots of B220 versus CD93 following B cell isolation for IRF4$^{-/-}$ (top), BcKO (middle), and WT mice (bottom). Quadrant I shows the frequency of immature B cells (B220^{+}CD93^{+}), while quandrant II shows the frequency of mature B cells (B220^{+}CD93^{-}). Data summary of the frequency of mature (**b**) and immature (**c**) B cells for all replicates. (**d**) Representative flow cytometry plots of CD21 versus CD23 following B cell isolation for IRF4$^{-/-}$ (top), BcKO (middle), and WT mice (bottom). Frequency of marginal zone (MZ; CD21^{+}CD23^{-}) and follicular zone (FZ; CD21^{-}CD23^{+}) B cells are shown. Quantification of the frequency of MZ (**e**) and FZ (**f**) B cells for all replicates. Data in **b**, **c**, **e**, **f** represent mean ± SD. Data were derived from two independent experiments of 8 total IRF4$^{-/-}$ and BcKO mice and 9 total WT mice.

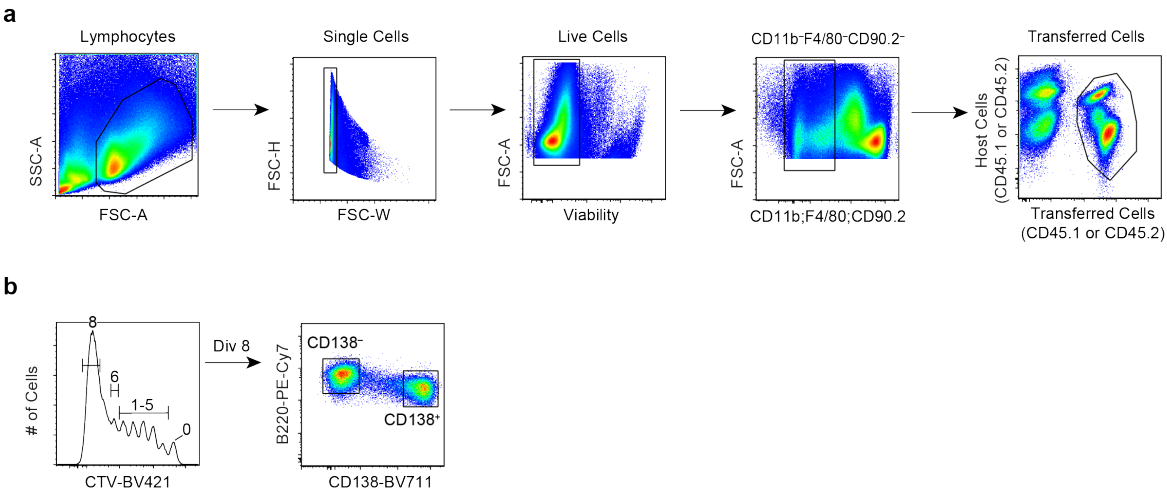

Figure 2-13. General gating strategies used for adoptive transfer analysis and cell sorting. (**a**) General gating strategy used to analyze all adoptively transferred cells with the purpose of each gate indicated at the top of each panel. Once live, single transferred cells were distinguished from host cells, other parameters, such as cell division and differentiation, could be assessed as in **Fig.2-2a-g**, **Fig. 2-3**, **Fig. 2-4a**, **Fig. 2-7g**, and **Fig. 2-8c,d**. These same gating strategies were applied before sorting transferred cells in **Fig. 2-5**, **Fig. 2-6**, and **Fig. 2-7** for single cell RNA-sequencing (detailed in **Supplementary Fig. 2-9** and **Supplementary Fig. 2-11**) or for sorting cells along the ASC-destined and non-ASC branch (detailed in **Fig. 2-8e-i**). (**b**) Gating strategy to sort responding B cells in discrete divisions for ELISPOTs presented on **Fig.2-2h,i**. Transferred cells were gated before examining cell division via CTV using the gating strategy outlined in **a**. Division 8 cells were sorted into distinct populations based on CD138 expression. The same strategy was used to sort Ctrl and BcKO cells presented in **Fig. 2-4** with the appropriate divisions gated.

Table 2-1. Comprehensive list of antibodies and stains.

Antibody	Conjugate	Clone	Company	Catalog Number	Dilution
B220	PE-Cy7	RA3-6B2	Biolegend	103222	1/400
B220	A700	RA3-6B2	Biolegend	103232	1/200
CD138	BV711	281-2	BD	563193	1/800
CD138	APC	281-2	Biolegend	558626	1/400
CD62L	BV605	MEL-14	Biolegend	104438	1/100
CD62L	PerCPCy5.5	MEL-14	Biolegend	104432	1/100
CD45.1	PE	A20	Biolegend	110708	1/100
CD45.1	APC	A20	Biolegend	110714	1/100
CD45.1	FITC	A20	Tonbo Biosciences	35-0453-U500	1/100
CD45.1	APC-Cy7	A20	Tonbo Biosciences	25-0453-U100	1/100
CD45.2	PE-Cy7	104	Biolegend	109830	1/100
CD45.2	PE	104	Tonbo Biosciences	50-0454-U100	1/100
CD45.2	FITC	104	Biolegend	109806	1/100
CD45.2	PerCPCy5.5	104	Tonbo Biosciences	65-0454-U100	1/100
CD45.2	APC	104	Biolegend	109814	1/100
CD11b	APC-Cy7	M1/70	Biolegend	101226	1/400
F4/80	APC-Cy7	BM8	Biolegend	123118	1/400
CD90.2	APC-Cy7	30-H12	Biolegend	105328	1/400
IRF4	PerCP-eFluor 710	3E4	ThermoFisher	46-9858-82	1/100
Goat anti-mouse Ig	Unlabeled	-	Southern Biotech	1010-01	1/200
Purified mouse IgM	Unlabeled	-	Southern Biotech	5300-01B	1/5000
Goat anti-mouse IgM	Horseradish Peroxidase	-	Southern Biotech	1021-05	1/1000
Goat anti-mouse Ig	Alkaline Phosphatase	-	Southern Biotech	1010-04	1/500
Stains	**Conjugate**	**Clone**	**Company**	**Catalog Number**	**Dilution**
CellTrace Violet	BV421	not applicable	Life Technologies	C34557	1/100
Zombie Yellow Fixable Viability Kit	BV570	not applicable	Biolegend	423104	1/400
Zombie NIR Fixable Viability Kit	APC-Cy7	not applicable	Biolegend	423106	1/400

VI. METHODS

Mice and adoptive transfers

C57BL/6J (JAX; 000664), CD45.1 (JAX; 002014), *Cd19*^{Cre} (JAX; 006785) [223], *Irf4*$^{fl/fl}$ (JAX; 009380) [118], *Prdm1*$^{fl/fl}$ (JAX; 008100) [224], MYD88$^{-/-}$ (JAX; 009088) [207], and CD45.2 μMT mice (JAX; 002288) [190] were purchased from The Jackson Laboratory and bred on

site. CD45.2 μMT were bred onto the CD45.1 background to obtain homozygous CD45.1 μMT mice. Mice used in experiments were between 8-12 weeks of age and were age/gender matched. For adoptive transfers/division assays, splenic $CD43^-$ B cells were isolated using the Miltenyi B cell Isolation Kit (Miltenyi; 130-090-862), which yielded equivalent proportions of B cells for all input populations in this study (**Fig. 2-12**). Isolated B cells were stained with CellTrace Violet (CTV) per the manufacturer's protocol, and $15x10^6$ CTV-labeled B cells were transferred to a disparate congenic μMT, $MYD88^{-/-}$, or wild-type mouse (CD45.1 or CD45.2) intravenously. At 24 hr post-transfer, mice were inoculated with the indicated dose of LPS (Enzo Life Sciences; ALX-581-008) or 50 μg NP-Ficoll (Biosearch Technologies; F-1420-10) intravenously in 100 μl. Animals were randomly placed in experimental groups, and independent replicates of 3 or more were used for all phenotyping experiments. Animals were housed by the Emory Division of Animal Resources and all procedures were approved by the Emory Institutional Animal Care and Use Committee.

Flow cytometry and cell sorting

For antibody staining, cells were resuspended at a concentration of $1x10^6$/100 μl in FACS buffer (1X PBS, 2mM EDTA, and 1% BSA), stained with Fc Block (BD; 553141) for 15 minutes, antibody-fluorophore conjugates for 30 minutes, and then washed with 10 volumes of FACS buffer. For flow cytometry analyses all cells were fixed using 1% paraformaldehyde. For enrichment of adoptively transferred CD45.2 or CD45.1 congenically marked cells, splenocytes were stained with CD45.2-PE or CD45.1-PE, respectively, followed by immunomagnetic enrichment using anti-PE beads (Miltenyi,

130-097-054). For analysis of adoptive transfers into WT hosts, all cells were enriched prior to flow cytometry analysis. For scRNA-seq experiments from μMT hosts, all transferred cells were FACS isolated. For scRNA-seq experiments from WT hosts, cells in division 1-8 and division 0 were FACS isolated separately and mixed to achieve a final ratio of 95% responding (dividing cells, division 1-8) and 5% non-responding (undivided, division 0) cells (**Fig. 2-9**). The following specific antibody-fluorochrome conjugates, with specific clones indicated in parentheses, and stains were used (**Table 2-1**): Tonbo Biosciences, Inc.: CD45.1-FITC (A20), CD45.1-APC-Cy7 (A20), CD45.2-PE (104), and CD45.2-PerCPCy5.5 (104); BioLegend, Inc.: B220-PE-Cy7 (RA3-6B2), B220-A700 (RA3-6B2), CD138-APC (281-2), CD62L-PerCy5.5 (MEL-14), CD62L-BV605 (MEL-14), CD45.1-PE (A20), CD45.1-APC (A20), CD45.2-PE-Cy7 (104), CD45.2-FITC (104), CD45.2-APC (104), CD11b-APC-Cy7 (M1/70), F4/80-APC-Cy7 (BM8), CD90.2-APC-Cy7 (30H12), Zombie Yellow Fixable Viability Kit (Cat. #423104), and Zombie NIR Fixable Viability Kit (Cat. #423106); BD Biosciences, Inc.: CD138-BV711 (281-2); ThermoFisher, Inc.: IRF4-PerCPeFluor710 (3E4); Life Technologies, Inc: CellTrace Violet (Cat. #C34557). For intracellular staining of IRF4, the FIX & PERM Cell Permeabilization Kit (ThermoFisher; GAS003) was used per the manufacturer's protocol. For all flow cytometry analysis, the following gating strategy was used (**Fig. 2-13**): lymphocytes based on SSC-A and FSC-A, single cells based on FSC-H and FSC-W, live cells based on exclusion of Zombie Yellow or Zombie NIR Fixable Viability Kit, and the markers $CD11b^{-}F4/80^{-}CD90.2^{-}$ to remove non-B cell lineage cells. All flow cytometry data were collected on a LSR II or LSRFortessa (BD Biosciences) and analyzed using FlowJo v9.9.5 or FlowJo v10.6.2. Cells sorting was performed at the Emory Flow

Cytometry Core or the Pediatrics and Winship Advanced Flow Cytometry Core using a FACSAria II (BD Biosciences).

ELISPOT

ELISPOT plates (Millipore; MAHAS4510) were coated with 1 μg of capture antibody (SouthernBiotech; 1030-01) for 12 hr, washed with PBS three times, and then blocked with B cell media (RPMI 1640 supplemented with 10% heat-inactivated FBS, 0.05 mM 2-BME, 1X nonessential amino acids, 1X penicillin/streptomycin, 10 mM HEPES, and 1 mM sodium pyruvate) for >1 hr. B cells were sorted directly into B cell media and resuspended to desired volume/cell numbers for plating. A 1:2 dilutions series was performed, and 70 μl of the diluted cells were added to each well and incubated (37°C, 5% CO_2) for 5 hr. Plates were then washed five times with PBS-T (1X PBS, 0.05% Tween-20) and secondary antibody (SouthernBiotech; Goat anti-mouse Ig, 1010-04) conjugated to alkaline phosphatase was diluted 1:500 in PBS and 100 μl added for 1 hr at room temperature. Plates were then washed five times in PBS-T and 5-Bromo-4-chloro-3-indolyl phosphate (BCIP) reagent (SouthernBiotech; 0302-01) was added to each well for 15 minutes to allow spots to develop. Finally, plates were washed four times in H_2O and allowed to dry completely before imaging. All samples and all dilutions were performed in technical duplicates. Spots were imaged using a ImmunoSpot S6 ULTIMATE Analyzer (Cellular Technology Limited) and quantified using ImmunoSpot software v5.0.9.21.

Ex vivo B cell differentiation

Cells were sorted and resuspended in B cell media containing 20 mg/ml *Escherichia coli* O111:B4 derived LPS (Sigma-Aldrich; L2630), 5 ng/ml IL-5 (eBioscience; 14-8051), and 20 ng/ml IL-2 (eBioscience; 14-8021) as previously described [216].

ELISA

Flat-bottomed ELISA plates (Sigma-Aldrich; M9410) were coated with goat anti-mouse Ig (Southern Biotechnology; 5300-05B) overnight at 4℃. Plates were then washed (1X PBS containing 0.05% Tween-20), blocked with 1% nonfat dry milk, and incubated with a series of diluted samples or purified mouse IgM (Southern Biotechnology; 5300-01B). Plates were then washed, incubated with 1:1000 diluted HRP-conjugated goat anti-mouse IgM (Southern Biotechnology; 1021-05), washed, and incubated with tetramethylbenzidine ELISA peroxidase substrate (Rockland; TMBE-1000) for 20 minutes at room temperature (50 µl/well). Fifty µl of 0.2 M sulfuric acid was applied to each well to quench the reaction. All incubations were performed for 1 hr at room temperature unless stated otherwise. Plates were read using a BioTek ELx800 Absorbance Microplate Reader.

Bulk RNA sequencing

For each sample, 1,000 cells were sorted into 300 µl of RLT buffer (Qiagen; 79216) containing 1% BME. RNA was extracted using the Quick-RNA Microprep kit (Zymo Research; R1050) and all purified RNA was used as input for the SMART-seq v4 cDNA synthesis kit (Takara; 634894) with 12 cycles of PCR amplification. 400 pg of cDNA was used as input for the NexteraXT kit (Illumina) using 12 cycles of PCR amplification. Final

libraries were quantitated by qPCR, size distributions determined by bioanalyzer, pooled at equimolar ratios, and sequenced at the New York University Genome Technology Center on a HiSeq3000 using a PE50 run.

Bulk RNA sequencing analysis

Raw sequencing reads were mapped to the mm9 genome using TopHat2 v2.0.13 [225] with the UCSC KnownGene reference transcriptome [226] and the ERCC spike-in RNA controls [227]. Duplicate reads were marked by PICARD v1.127 (http://broadinstitute.github.io/picard/) and removed from downstream analysis. Reads overlapping exons of each ENTREZ gene and the ERCC transcripts were summarized and normalized to fragments per kilobase per million (FPKM) using GenomicRanges v1.34 [228] and custom R v3.5.2 scripts. Genes with at least 3 reads per million in all samples for at least one group were considered detected and resulted in 10,532 expressed genes. All detected genes were used as input for edgeR v3.24.3 [208] and genes with an absolute $\log_2$ fold-change >1 and Benjamini-Hochberg FDR <0.05 were considered significantly differentially expressed. Principal component analysis was performed using vegan v2.5.5 and the indicated *z*-score normalized gene list. mRNA molecules per cell normalization was computed as previously described [174] with normalized mRNA content representing the sum total of all mRNA molecules in each sample.

Single cell RNA-sequencing and data processing

Single cell RNA-sequencing was performed using the 5' scRNA-seq platform (10X Genomics). For each sample an estimated 17,400 cells were used as input for GEM

generation and libraries prepared using the recommended protocol. Illumina bcl files were processed and mapped to the mm9 genome using CellRanger v2.1.1 and each biological replicate aggregated for downstream analysis using the 'aggr' function in CellRanger with the default parameters. Aggregated data were analyzed using Monocle2 v2.9.0 [209]. For *t*-SNE dimension reduction the following parameters were used: max_components = 2, norm_method = 'log', num_dim = 10, perplexity = 30. Assignment of cells to clusters was performed using the default rho and delta thresholds determined by the 'plot_rho_delta' function. To determine differentially expressed genes between clusters the 'differentialGeneTest' function with the 'fullModelFormulaStr' option was used. The top 1,000 differentially expressed genes ranked by FDR q value were used in the single cell trajectory analysis with the 'orderCells' function with default parameters and dimensional reduction performed using the 'DDRTree' function.

MAGIC transformation of UMI transcript counts

For MAGIC normalization [229] the Rmagic v1.3.0 R/Bioconductor package was used. The UMI gene expression matrix was exported from the Monocle CellDataSet object using the 'exprs' function. Genes that were expressed in less than 10 cells and cells with less than 1,000 total UMI were removed from the analysis. The data were normalized for library size and square root transformed and the resulting matrix was used as input for the 'magic' function using the "genes = all_genes" parameter.

SCENIC transcription factor activity prediction

The SCENIC v1.1.1 R/Bioconductor package [213] was used to predict transcription factor activity in each cell using the mm10 version of the cisTarget database (https://resources.aertslab.org/cistarget/). The UMI gene expression matrix was filtered using the 'geneFiltering' function with the parameters minCountsPerGene = 10 and minSamples=9 and the resulting matrix $\log_2$ transformed. Next, all subsequent steps of Genie3 and SCENIC were run with the default parameters. The resulting output file 'regulonTargetsInfo.tsv' file was used to identify transcription factor target genes. The correlation of SCENIC activity score and expression was calculated using the 'cor' function with the pearson method in R.

KNN classification of single-cells with bulk RNA-seq data

K-nearest neighbor classification was performed using the FNN v1.1.2.1 R package. The UMI gene expression matrix was merged with reads per million normalized bulk RNA-seq data sets using gene symbol as unique identifiers. The combined data was quantile normalized using 'normalize.quantiles' function in the preprocessCore v1.40.0 package. Next, to assign bulk RNA-seq to single-cells, the 'knn' function was run using the bulk RNA-seq samples as a training set, single cells as the testing set, and the K was set to the number of replicates in bulk the RNA-seq experiments. The resulting cell assignments were appended to the pData table associated with the Monocle CellDataSet object. For assignment of IRF4$^{-/-}$ cells to WT scRNA-seq clusters the UMI matrices containing each cell were merged using the gene symbol and quantile normalized. The 'knn' function was run using the WT cells as the training set, the IRF4$^{-/-}$ cells as the testing set, and the K was

set to 11. The IRF4$^{-/-}$ cells were then annotated with the WT cluster of the cell they were assigned.

scRNA-seq data display

For all data display, the MAGIC [229] transformed gene expression data was used. For Gene Set Enrichment Analysis (GSEA) [210] between clusters, all detected genes were ranked by multiplying the *P*-value derived from the Monocle 'differentialGeneTest' function by the sign of the fold change (i.e., positive or negative) between the two clusters. The resulting list was used in a GSEA PreRanked analysis. All indicated gene sets were derived from the Molecular Signatures Database (MSigDB) [210] except the "ER chaperones, co-chaperones, and folding enzymes" gene set, which was previously described [212]. For gene set activity plots, the mean expression cubed of all leading edge genes was computed and visualized as a projection on the *t*-SNE plot. For BATF transcription factor activity, the mean expression cubed of all target genes predicted by SCENIC was computed and visualized as above. All other data display was performed using custom R/Bioconductor scripts that are available upon request.

Statistics

All statistical analyses were performed with GraphPad Prism v6.0c or v8.4.1, Microsoft Excel v14.5.7 or v16.36, and R/Bioconductor v3.5.2. The exact statistical test, number of tails, group size, and number of experimental repeats for each figure is detailed in the legend. P-values or where indicated multiple hypothesis testing corrected P-values < 0.05

were considered significant. For differential gene expression a combination of fold-change and false-discovery rate corrected P-values were used to determine significance.

Chapter 3. An IRF4-MYC-mTORC1 integrated pathway controls cell growth and the proliferative capacity of activated B cells during B cell differentiation *in vivo*

Dillon G. Patterson*, Anna K. Kania*, Madeline J. Price*, James R. Rose*, Christopher D. Scharer* and Jeremy M. Boss*†

*Department of Microbiology and Immunology, and the Emory Vaccine Center, Emory University School of Medicine, Atlanta, GA 30322, USA

†Correspondence: jmboss@emory.edu

Author Contributions

D.G.P. designed and performed experiments, analyzed the data, and wrote the manuscript. A.K.K., M.J.P., and J.R.R. performed experiments. C.D.S. designed experiments. J.M.B. designed the experiments and wrote the manuscript. All authors participated in editing the manuscript.

This manuscript was submitted to *The Journal of Immunology*. Dillon G. Patterson, Anna K. Kania, Madeline J. Price, James R. Rose, Christopher D. Scharer, and Jeremy M. Boss. 2021. An IRF4-MYC-mTORC1 integrated pathway controls cell growth and the proliferative capacity of activated B cells during B cell differentiation *in vivo*.

I. ABSTRACT

Cell division is an essential component of B cell differentiation to antibody-secreting plasma cells, with critical reprogramming occurring during the initial stages of B cell activation. However, a complete understanding of the factors that coordinate early reprogramming events *in vivo* remain to be determined. In this study, we examined the initial reprogramming by IRF4 in activated B cells using an adoptive transfer system and mice with a B cell-specific deletion of IRF4. IRF4-deficient B cells responding to influenza, NP-Ficoll and LPS divided, but stalled during the proliferative response. Gene expression profiling of IRF4-deficient B cells at discrete divisions revealed IRF4 was critical for inducing MYC target genes, oxidative phosphorylation, and glycolysis. Moreover, IRF4-deficient B cells maintained an inflammatory gene expression signature. Complementary chromatin accessibility analyses established a hierarchy of IRF4 activity and identified networks of dysregulated transcription factor families in IRF4-deficient B cells, including E-box binding bHLH family members. Indeed, B cells lacking IRF4 failed to fully induce *Myc* after stimulation and displayed aberrant cell cycle distribution. Furthermore, IRF4-deficient B cells showed reduced mTORC1 activity and failed to initiate the B cell-activation unfolded protein response and grow in cell size. *Myc* overexpression in IRF4-deficient was sufficient to overcome the cell growth defect. Together, these data reveal an IRF4-MYC-mTORC1 relationship critical for controlling cell growth and the proliferative response during B cell differentiation.

II. INTRODUCTION

A key component of the adaptive immune response is the generation of antibody by antibody-secreting plasma cells (ASC). Upon antigen encounter, quiescent naïve B cells become activated, rapidly proliferate, and a subset differentiate to ASC. One essential component of B cell differentiation to ASC is cell division [170,172,179,182]. Culturing purified B cells and blocking cell division prevents the generation of ASC [170]. However, the number of cell divisions does not exclusively determine ASC formation. This has led to a stochastic model of differentiation that describes population-level immune responses and accounts for heterogeneity in cell fates among responding cells, such as whether they will continue to divide, die, or differentiate [179,183,184,202]. One molecular determinant that contributes to such heterogeneity is the expression levels of MYC [68,172,181,230-232]. MYC levels are influenced by immune stimulation and serve as a division-independent timer to control the proliferative capacity of responding cells [68,172,180]. IRF4 is another factor that contributes to heterogeneity at the population level [118-120,176]. During the initial stages of B cell activation, high IRF4 expression biases cells towards the ASC fate [120,176]. Notably, initial IRF4 expression levels are influenced by the intensity of immune stimulation, and $IRF4^{hi}$ cells are among the first to divide [128]. Indeed, proliferation is reduced in IRF4-deficient B cells stimulated *ex vivo* [118,119,152]; however, the impact of IRF4 on *in vivo* B cell proliferation is unknown. Furthermore, the timing, scope, and mechanism by which IRF4 contributes to control the proliferative response remains undefined.

Cell division is tightly linked to ASC formation, with transcriptional and epigenetic reprogramming [195,200,201,203] occurring as the cells divide [74,80,174,176]. As such, each cellular division represents a distinct stage during B cell differentiation, with ASC formation

occurring after at least eight cell divisions [174-176]. Cell extrinsic signals can impact the specific division in which differentiation occurs, but the molecular programming events leading to ASC remain the same [176]. Many essential ASC programming events [14] are initiated during the early stages of B cell activation and are progressively reinforced in subsequent divisions [80,174,175]. For example, ASC formation requires a metabolic shift from glycolysis to oxidative phosphorylation (OXPHOS), and the OXPHOS program is increasingly established across cell divisions [80]. Additionally, ASC differentiation requires activation of the unfolded protein response (UPR), an essential stress response needed during increased protein production [233,234]. While canonically considered to be induced in newly formed ASC, recent work indicates that activated B cells (actB) upregulate an array of UPR-affiliated genes. This process is controlled by mTORC1 prior to antibody production and before XBP1 activity [105], a known regulator of UPR in ASC [102,222]. Moreover, single-cell RNA-sequencing (scRNA-seq) of actB uncovered an IRF4-dependent bifurcation event that committed a portion of actB to ASC during the early stages of B cell activation [176]. Thus, while recent work has highlighted critical early reprogramming events in actB, the timing and extent to which the above factors, and others, remains to be fully understood and integrated.

In this study, we aimed to understand the IRF4-dependent division-coupled reprogramming events that occur during the initial stages of B cell differentiation. Using an *in vivo* model of B cell differentiation [174], we found that IRF4-deficient B cells begin to divide normally but stall during the proliferative response. To assess the timing and scope of IRF4-dependent reprogramming, IRF4-sufficient and -deficient B cells at discrete divisions were sorted for RNA-seq and the assay for transposase accessible chromatin-

sequencing (ATAC-seq) [197,198]. RNA-sequencing revealed that early upregulation of gene sets critical for ASC formation were dependent on IRF4. These included MYC target genes and genes important for OXPHOS. Indeed, IRF4-deficient B cells failed to fully upregulate *Myc* and displayed altered cell cycle distribution. The activity of mTORC1 was also reduced, resulting in an inability of IRF4-deficient B cells to undergo cell growth and initiate the UPR [105]. ATAC-seq identified hundreds of differentially accessible regions (DAR) and established a hierarchy of IRF4 activity, with AP-1:IRF (AICE motifs) active during early divisions and ETS:IRF (EICE) motifs active in later divisions. Together, these data create a road map defining the role of IRF4 during the earliest stages of B cell differentiation *in vivo* and reveal a critical role for IRF4 in controlling cell growth and maintaining the proliferative response.

III. RESULTS

IRF4-deficient B cells responding to LPS in vivo stall during the proliferative response

Cell division is one of the earliest events following B cell activation, however a complete understanding of factors that control or maintain the proliferative response remain to be determined. Recent work identified an IRF4-dependent bifurcation event in the earliest stages of B cell activation [176]. Cells along the IRF4-dependent branch upregulated gene sets critical for proliferation, indicating IRF4 may be important for controlling the proliferative response *in vivo*. To explore if IRF4 impacted cell proliferation during B cell differentiation, an *in vivo* adoptive transfer model was applied [174]. Here, splenic naïve B cells from CD45.2^{+}*Cd19*$^{+/+}$*Irf4*$^{fl/fl}$ (Ctrl) or CD45.2^{+}*Cd19*$^{Cre/+}$*Irf4*$^{fl/fl}$ (IRF4cKO) mice were isolated, labeled with CellTrace Violet (CTV), and transferred to CD45.1^{+} μMT hosts.

After 1 day, host mice were challenged with the type I T cell independent antigen LPS and cell division and differentiation were determined via CD138 expression [135,191] in a time course covering three days (**Fig. 3-1A**). At 24 h, no division was observed for Ctrl and IRF4cKO cells, indicating a similar delay before initiating the proliferative response (**Fig. 3-1B**). At 48 h, both Ctrl and IRF4cKO cells began to divide, and the majority of responding cells were observed in divisions 2-4. A modest difference in IRF4cKO B cells in divisions 0-1 was observed at this time point (**Fig. 3-1B-C**). At 60 h, Ctrl were distributed in all cell divisions (0-8), with a subset differentiating after reaching or exceeding division 8. Comparatively, IRF4cKO cells accumulated in divisions 2-4, with few cells observed in divisions 5 and 6 (**Fig. 3-1B-C**). Strikingly, while more than half of Ctrl cells accumulated in division 8 at 72 h, the cell division pattern for cells from IRF4cKO largely remained the same as their 60 h time point, indicating the IRF4cKO cells stalled during the proliferative response (**Fig. 3-1B-C**). Indeed, the mean division number (MDN) [235] for Ctrl cells increased by ~2 divisions from 60 to 72 h, while the MDN for IRF4cKO cells was unchanged (**Fig. 3-1D**). This proliferative defect was also reflected in reduced frequency of IRF4cKO cells detected in host spleens at 72 h (**Fig. 3-1E-F**). Importantly, staining for the pro-apoptotic marker annexin V revealed no differences in apoptosis or necrosis at 72 h *in vivo* (**Supplemental Fig. 3-8**). Furthermore, no differences in homeostatic proliferation were observed in mice that received Ctrl or IRF4cKO B cells but no LPS (**Fig. 3-1B**). It is also important to note that the vast majority of the splenic cells transferred divided at least once to LPS stimulation, indicating that nearly all B cells and not just a subset were responding *in vivo*. Proliferation defects were also observed when

C57BL/6J mice were used as hosts (**Supplemental Fig. 3-9**). These data indicate IRF4 controls the proliferative capacity of B cells in response to LPS immune challenge.

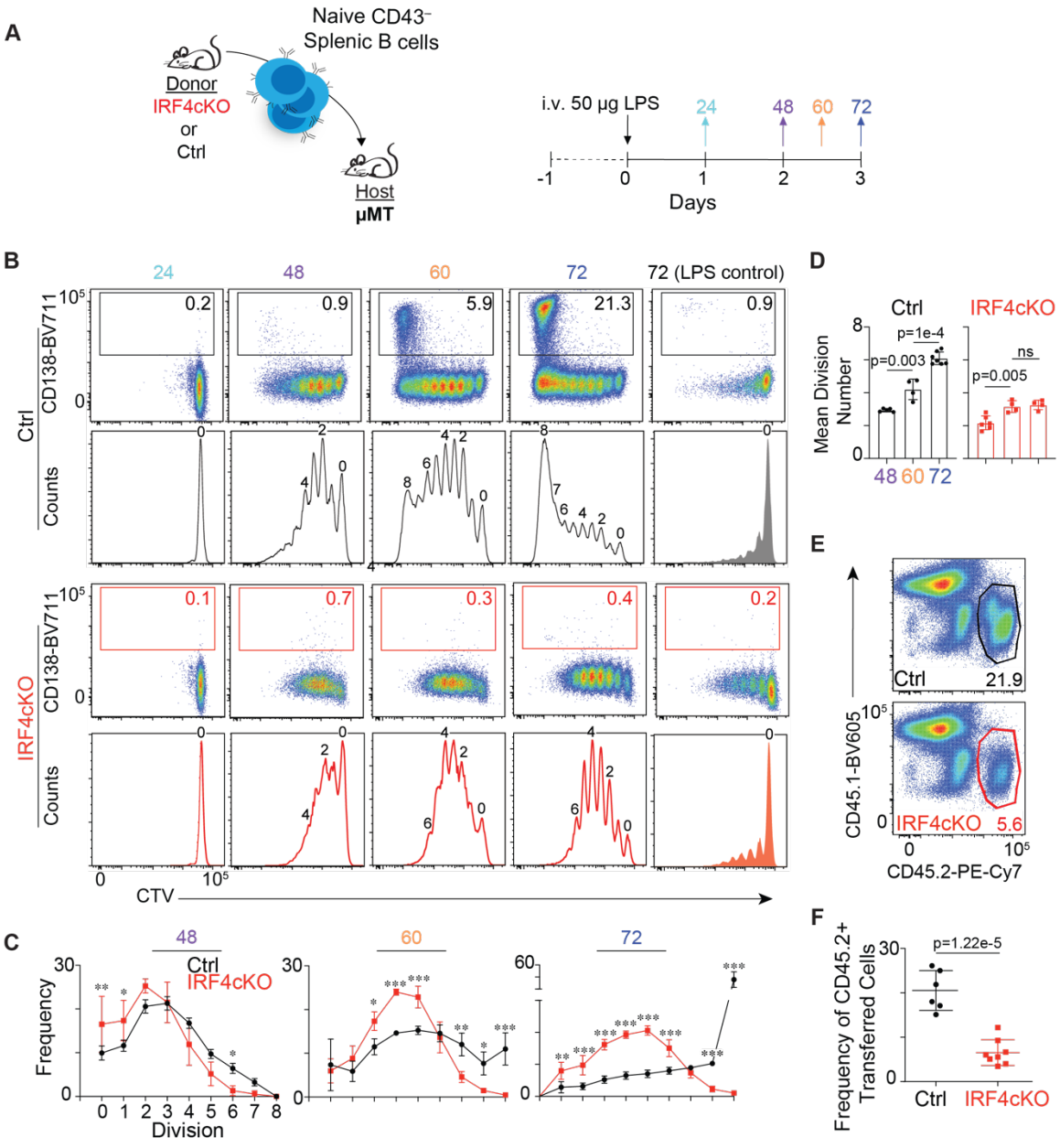

Figure 3-1. IRF4-deficient B cells stall during the proliferative response to LPS. (A) Schematic of experimental design. Ctrl (CD45.2^{+}*Cd19*$^{+/+}$*Irf4*$^{fl/fl}$) or IRF4cKO (CD45.2^{+}*Cd19*$^{Cre/+}$*Irf4*$^{fl/fl}$) splenic B cells were CTV-labeled and adoptively transferred into µMT (CD45.1+) mice, as described in the methods. At 24 h post transfer, mice were inoculated with LPS i.v. At the indicated time points, spleens were harvested and analyzed. **(B)** Flow cytometry histograms displaying cell division and ASC differentiation (CD138^{+}). The frequency of CD138+ cells are shown. **(C)** Frequency of transferred (CD45.2^{+}) cells

at discrete divisions for 48, 60, and 72 h. **(D)** Mean division number of all responding cells at each time point. (**E)** Ctrl (top) and IRF4cKO (bottom) representative flow cytometry plots of CD45.1 versus CD45.2 with gates drawn and frequencies shown for the transferred population. **(F)** Quantification of the frequency of CD45.2 transferred cells from **E**. All data are representative of at least two independent experiments using at least 3 mice per group. Data in **C**, **D**, and **F** represent mean ± SD. Statistical significance in **C** was determined by a two-way ANOVA with Sidak's multiple comparisons test. Statistical significance in **D** was determined by a paired two-tailed Student's *t* test, while statistical significance in **F** was determined by determined by a two-tailed Student's *t* test. * $p < 0.05$, ** $p < 0.01$, *** $p < 0.001$.

IRF4-deficient B cells exhibit a proliferation defect to T-independent and -dependent antigens

To determine whether IRF4 controls the proliferative response to other stimuli, adoptive transfers were performed followed by challenge with the type II T-independent antigen 4-hydroxy-3-nitrophenylacetyl (NP)-Ficoll or the T-dependent antigen influenza A/HK-X31 (X31). Five days post-NP-Ficoll and six day after X31 challenge, host mice were sacrificed, and cell division and differentiation were assessed by flow cytometry (**Fig. 3-2A**). Because NP-Ficoll and X31 stimulate antigen-specific B cells that represent a small portion of the population, the majority of Ctrl and IRF4cKO cells remained undivided for both stimulation conditions (**Fig. 3-2B**). For NP-Ficoll, Ctrl cells were distributed in all cell divisions 1-8, and a subset of cells that reached or surpassed division 8 differentiated (**Fig. 3-2B-C**). Similar results were observed following X31 challenge and independent of whether the transferred cells were recovered in the mediastinal lymph node or the spleen (**Fig. 3-2B-D**). Interestingly, CD138+ ASC were observed at division eight for all three antigen conditions for Ctrl cells. Comparatively, cells from IRF4cKO were mainly distributed in the first few divisions for both stimulation conditions, with very few IRF4cKO B cells detected after division 4 and almost none reaching division 8 and forming

ASC (**Fig. 3-2B-D**). Taken together, these data indicate IRF4 plays a critical role in controlling the proliferative response to type II T independent and early T dependent antigen responses.

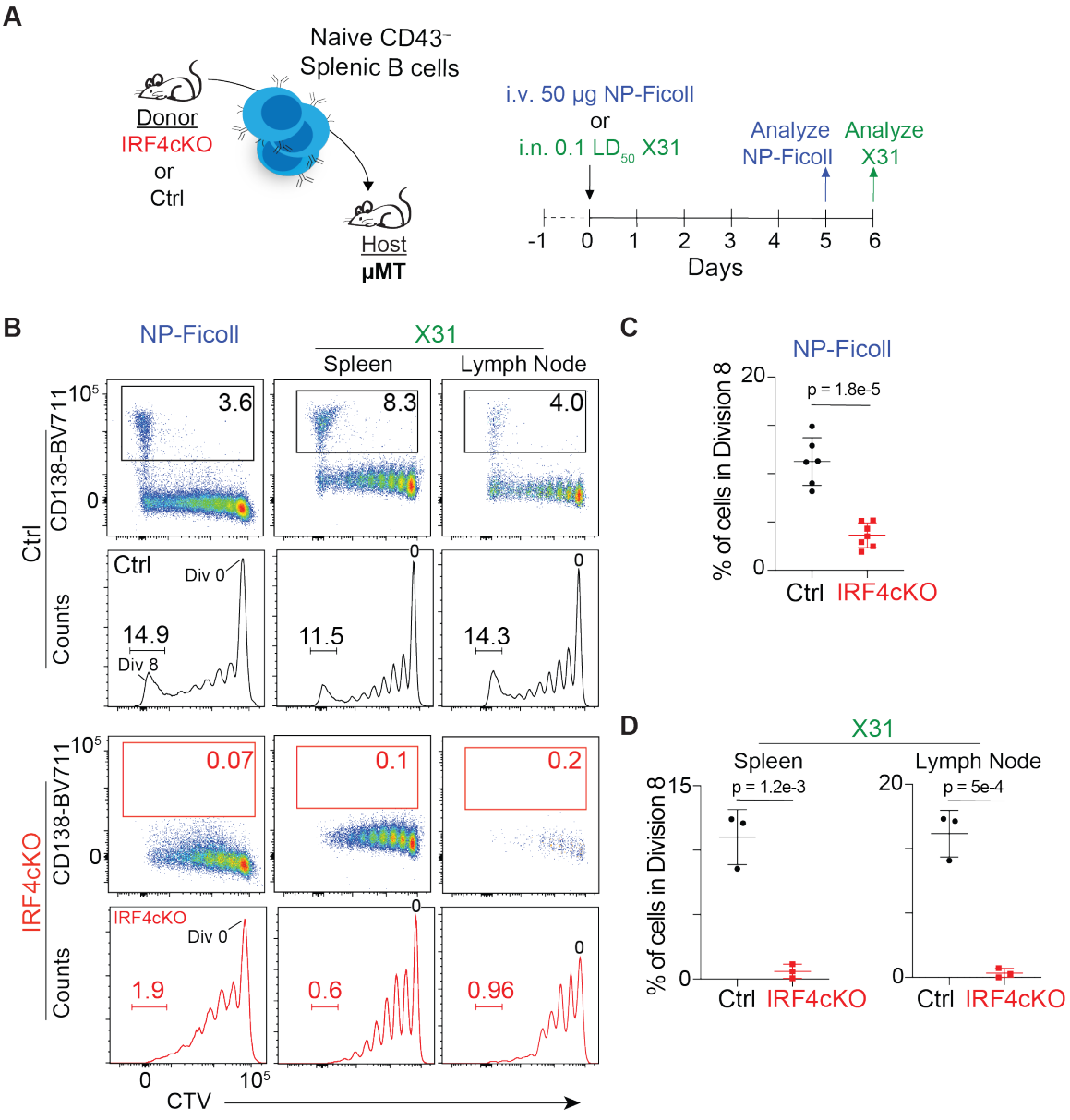

Figure 3-2. IRF4-deficient B cells exhibit a proliferation defect in response to T-independent and T-dependent antigens. (**A**) Schematic of experimental design. Ctrl and IRF4cKO B cells were prepared and adoptively transferred as in Fig 1 and the methods section. Here, animals were stimulated with either NP-Ficoll or infected with influenza strain X31 as described in the methods. Spleens from NP-Ficoll inoculated animals were

harvested at d5; and for influenza, both spleens and the draining mediastinal lymph nodes were isolated at d6 post-challenge. **(B)** Representative flow cytometry plots of CD138 versus CTV or CTV histograms for Ctrl and IRF4cKO. The frequency of $CD138^+$ (top) and division 8 (bottom) cells are shown. Frequency of division 8 cells for Ctrl and IRF4cKO from **B** following NP-Ficoll (**C**) or influenza X31 (**D**) challenge. All data are representative of two independent experiments using at least 3 mice per group. Data in **C** and **D** represent mean ± SD with statistical significance determined by a two-tailed Student's *t* test.

IRF4-deficient B cells display altered cell cycle distribution

To better understand the proliferative defect observed above, the role that IRF4 played with respect to cell cycle was investigated. CTV-labeled Ctrl and IRF4-deficient B cells were adoptively transferred into μMT mice and recovered 72 h post-LPS stimulation. Cells were stained with Ki-67 and 7AAD to distinguish the frequency of cells in each phase of the cell cycle at discrete divisions [236] and analyzed by flow cytometry. These data revealed that in the final detectable divisions, IRF4cKO cells accumulated in G_0/G_1 with a corresponding decrease in cells found in the G_2/M (**Fig. 3-3A-B**). This was in stark contrast to Ctrl cells, which revealed more cells in S and G2/M at the same divisions. This indicates that the cell cycle was significantly perturbed in B cells from IRF4cKO in these final divisions (**Fig. 3-3A-B**). To better understand the proliferative defect observed in IRF4cKO cells *in vivo*, the frequency of actively proliferating cells by BrdU incorporation was examined after IRF4cKO cells had stalled. Appreciably, a lower frequency of $BrdU^+$ IRF4cKO compared to Ctrl cells were observed (**Fig. 3-3C-D**). BrdU+ IRF4cKO cells were also distributed proportionally to the total population. In contrast, BrdU+ Ctrl cells were largely distributed in division 8 (**Fig. 3-3C**). Thus, IRF4 is critical for cell cycle control and maintaining the proliferative response.

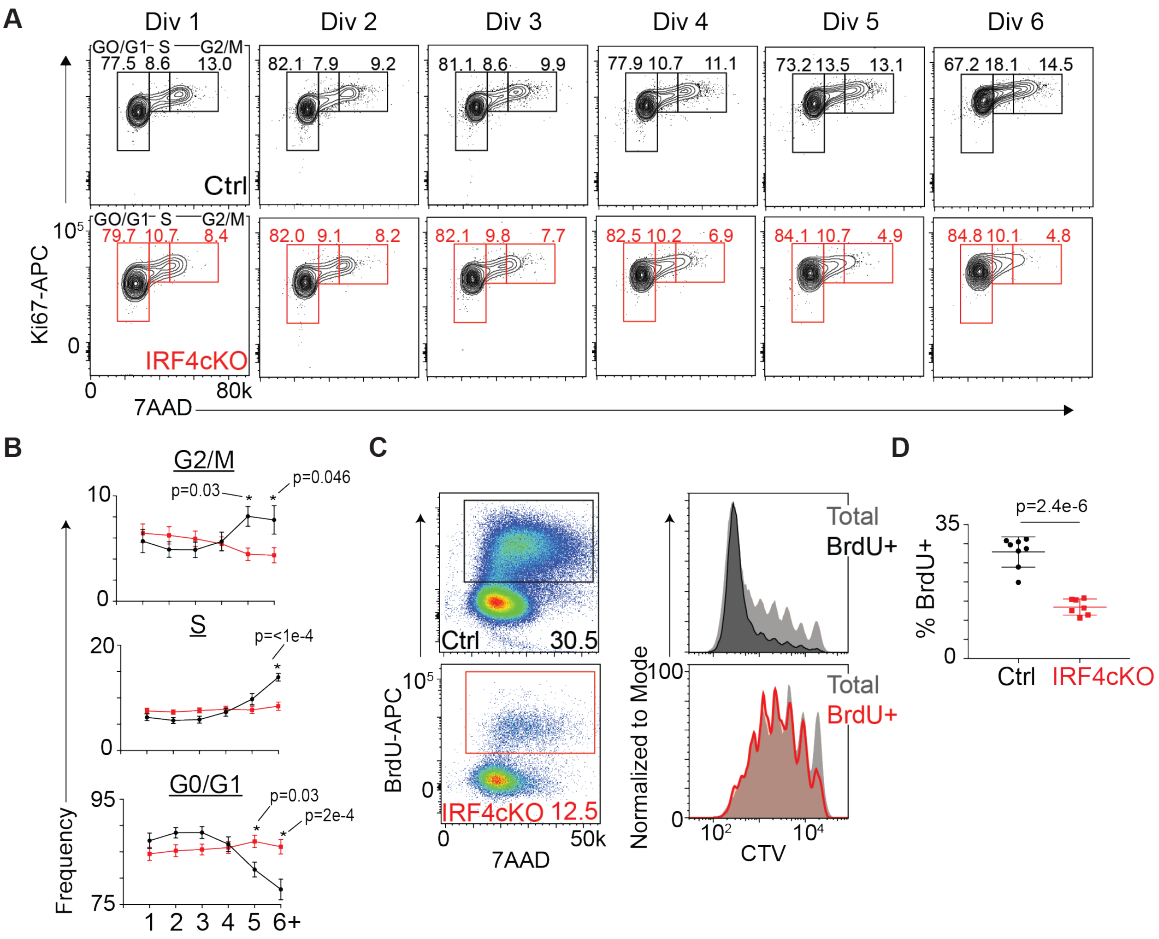

Figure 3-3. IRF4-deficient B cells display altered cell cycle distribution. **(A)** Ctrl (black) and IRF4cKO (red) B cells were prepared, adoptively transferred, and inoculated with LPS as in Fig 1. At 72 h, mice were sacrificed and the spleens harvested. Cells were stained with Ki67 and 7AAD and representative flow cytometry plots at the indicated divisions are shown. Flow cytometry gates indicating G0/G1, S, and G2/M phase of the cell cycle are shown with the frequency of cells for each. **(B)** Quantification of the data from **A** displaying the frequency of cells found in each phase of the cell cycle at each division. **(C)** Following the above adoptive transfer scheme described in **A**, mice were injected with BrdU 1 h prior to sacrifice to assess active S phase of the cell cycle. Representative flow cytometry plot of BrdU versus 7AAD (left) and CTV histograms (right) of the total transferred population (grey) overlaid with the $BrdU^+$ cells to visualize the distribution of actively proliferating cells. **(D)** Quantification of the data from **C** displaying the frequency of $BrdU^+$ cells. All data are representative of at least two independent experiments using at least 3 mice per genotype. Data in **B** and **D** represent mean ± SD. Statistical significance in **D** was determined by a two-tailed Student's *t* test. Statistical significance in **B** was determined by a two-way ANOVA with Sidak's multiple comparisons test. P-values are shown at points of significance.

Cell division-coupled IRF4-dependent transcriptional reprogramming

B cell differentiation to ASC requires considerable transcriptional rewiring that consists of progressive cell division-based reprogramming events [174]. To determine the impact of IRF4 on this process, Ctrl and IRF4cKO cells were sorted from divisions 0, 1, 3, 4, 5, and 6 as determined by CTV dilution (**Fig. 3-4A**) and subjected to RNA-seq analyses. Comparing gene expression profiles for Ctrl and IRF4cKO cells in the same division revealed hundreds of differentially expressed genes (DEG) that increased or decreased expression in IRF4-deficient B cells, indicating IRF4 functions to repress and activate gene expression programs, even in the earliest stages of actB reprogramming (**Fig. 3-4B**). This activity is consistent with previous work, demonstrating that a significant increase in IRF4 levels occurrs after the first cell division [128,176]. After successive divisions, IRF4cKO B cells became progressively transcriptionally divergent compared to Ctrl cells (**Fig. 3-4B**). Hierarchical clustering of samples reflected this divergency with Ctrl and IRF4cKO samples in divisions 0 and 1 clustering by gene expression and divisions 3 - 6 clustering by IRF4 status (**Fig. 3-4C**). T-distributed stochastic neighbor-embedded (t-SNE) projections of gene expression data from all samples indicated major cell division-dependent transcriptional reprogramming events that were dependent on IRF4 and predominately in divisions 3 - 6. (**Fig. 3-4D**). Collectively, IRF4cKO are transcriptionally distinct by division 3 and continue to diverge through subsequent divisions. Thus, cell division-based IRF4-dependent reprogramming occurs during the initial stages of B cell differentiation.

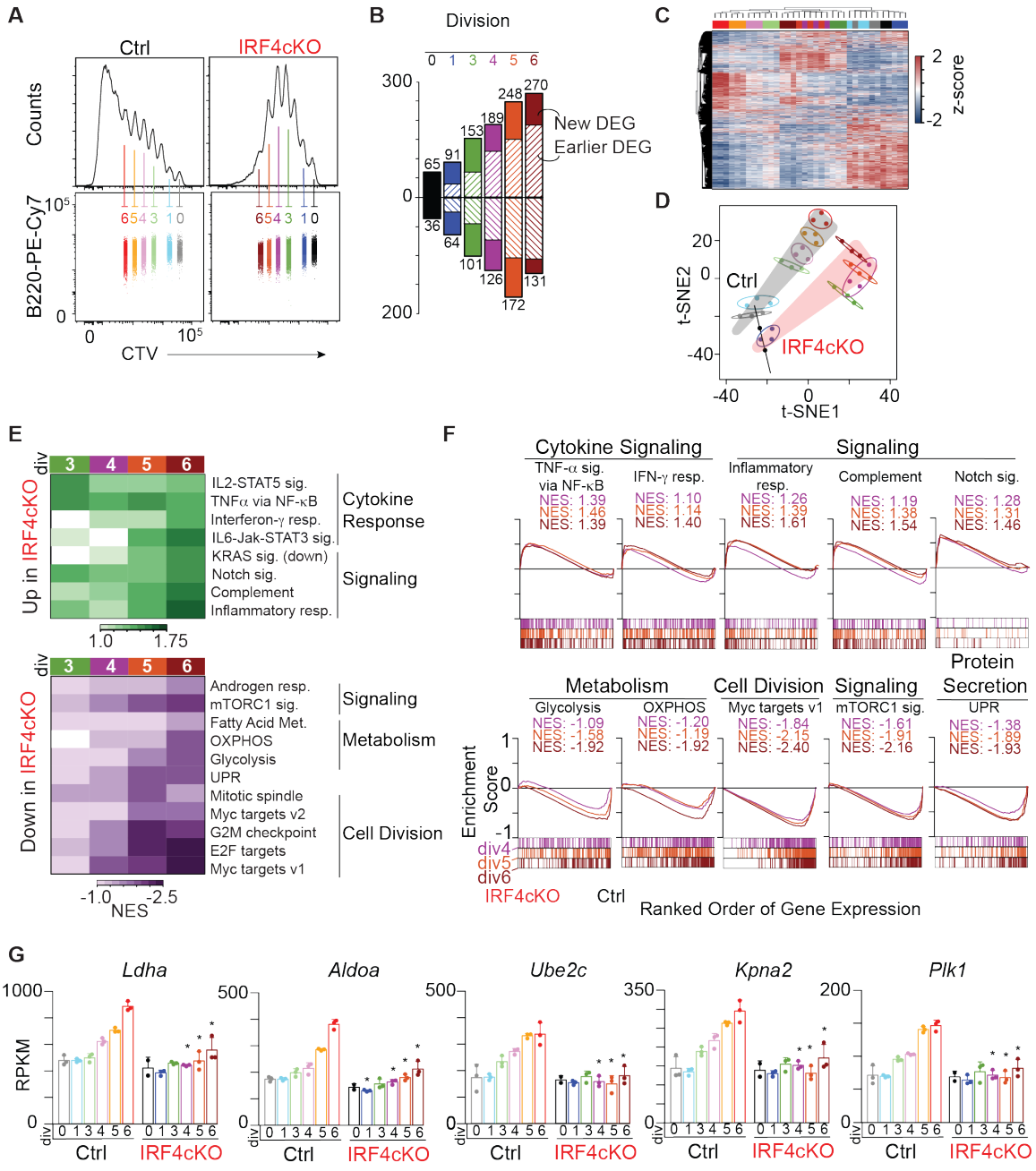

Figure 3-4. IRF4-deficient B cells fail to upregulate metabolic and proliferative gene expression programs during B cell differentiation. (A) Ctrl and IRF4cKO B cells were prepared, adoptively transferred, and inoculated with LPS as in Fig 1 and harvested at 72 h. Cells at the indicated divisions were sorted and subjected to RNA-seq as described in methods. Representative flow cytometry plots of B220 and CTV histograms and projections of the sorted populations are shown and labeled by division number. **(B)** Bar plot quantifying the number of differentially expressed genes (DEG) at each division that increase (top) or decrease (bottom) expression in IRF4cKO cells compared to Ctrl. Solid bars indicate the proportion of genes that represent a new DEG appearing in that division while striped bars indicate the proportion of genes that were a DEG in an earlier division.

(C) Hierarchical clustering of the expression of 10,404 genes detected from **A**. **(D)** t-SNE projections of RNA-seq data from control samples (highlighted in grey) and IRF4cKO samples (highlighted in red). **(E)** Heat map of normalized enrichment scores (NES) calculated by gene set enrichment analysis (GSEA) [210] for pathways upregulated and downregulated in IRF4cKO. **(F)** GSEA examples for the indicated gene sets for IRF4cKO up and down DEG from divisions 4, 5, and 6. NES values are indicated for each division. **(G)** Bar plot displaying reads per kilobase million (RPKM) values for the indicated genes at all sequenced divisions for Ctrl and IRF4cKO cells. Asterisks above IRF4cKO division data indicate significance (FDR < 0.001) when compared to the corresponding Ctrl division. Data were derived from 3 independent adoptive transfers for Ctrl and IRF4cKO. One division 0 IRF4cKO sample was excluded due to a high frequency of duplicate reads.

To determine the transcriptional programs dependent on IRF4, gene set enrichment analysis (GSEA) [210] was performed for DEG that increased or decreased expression in IRF4cKO cells in divisions 3 - 6. IRF4cKO B cells progressively failed to induce gene sets important for cell division, metabolism, and signaling (**Fig. 3-4E-F**). This consisted of genes critical for glycolysis and OXPHOS, which are critical metabolic programs for actB and ASC, respectively [80,211] (**Fig. 3-4E-F**). Enzymes that failed to be induced and are critical for glycolytic metabolism included *Ldha* [237] and *Aldoa* [238] (**Fig. 3-4G**). Additionally, mTORC1 signaling and MYC target genes failed to be induced in IRF4cKO cells, and included genes that promote cell proliferation such as *Ube2c* [239], *Kpna2* [240], and *Plk1* [241,242] (**Fig. 3-4G**). Notably, the cell cycle was significantly perturbed in IRF4cKO cells in the divisions in which MYC target genes were the most dysregulated (**Fig. 3-3A-B**). These data are consistent with reports that reduction of *Myc* impacts G1-S transition of the cell cycle [243-245]. Genes sets that failed to be repressed consisted of those involved in cytokine and cell signaling, such as the inflammatory response, and reflect previous reports that IRF4-deficient B cells progress down a reprogramming path whose gene expression program reflects cells responding to inflammatory stimuli [176]. Collectively, these data

suggest that early metabolic and proliferative programs essential for cell growth and division are dependent on IRF4.

ATAC-sequencing reveals a hierarchy of IRF4 activity

To identify regions that change chromatin accessibility during B cell differentiation upon deletion of *Irf4,* paired ATAC-seq [246] data derived from the above divisions was analyzed to reveal IRF4-specific regulatory activities and IRF4-dependent transcription factor networks that impact B cell differentiation. Comparison of Ctrl and IRF4cKO cells in discrete divisions identified hundreds of differentially accessible regions (DAR), with a progressive increase in DAR occurring after the first cell division and more than 700 DAR by divisions 5 and 6 (**Fig. 3-5A**). These differences were also reflected in t-SNE spatial projections (**Fig. 3-5B**), and indicated that similar to RNA-seq, chromatin accessibility differences occurred predominately in divisions 3 - 6 (**Fig. 3-5A-B**). Collectively, these data support the notion that IRF4-dependent reprogramming occurs progressively beginning during the initial stages of B cell differentiation and that the chromatin landscape of IRF4cKO B cells is markedly distinct by division 3.

To gain a better understanding of the transcription factor networks dependent on IRF4, the top 10 enriched DNA sequence motifs in division 6 DAR were determined and matched to known putative transcription factor binding motifs using HOMER [247]. Because enrichment p-values are dependent on the number of DAR, each transcription factor motif was rank normalized based on significance at each division, and the change in rank score across the divisions plotted, revealing how motif accessibility was altered across the divisions. Motifs enriched in regions that decreased accessibility in IRF4cKO cells (down

DAR) included known IRF4 DNA binding motifs [119,120,128,129], such as the core IRF motif (GAAA), AP-1-IRF composite element (AICE) [125], and ETS-IRF composite element (EICE) [122,123] (**Fig. 3-5C**). Interestingly, this revealed a hierarchy among heterodimeric IRF4 binding sites [109], with AICE more highly ranked in early divisions and EICE motifs more highly ranked in later divisions. DAR in proximity of *Itm2c* and *Gpcpd1* reflected this hierarchy of activity (**Fig. 3-5D**). These data support the kinetic control of IRF4 activity [128,175], as well as previous work implicating the timing of IRF4 in conjunction with the AP-1 transcription factor BATF in early cell fate decisions during B cell differentiation [176]. Other transcription factors enriched in down DAR in the final divisions included RUNX and E-box binding bHLH family members (**Fig. 3-5C**).

Among regions that increased accessibility in IRF4cKO (up DAR), TBOX family members were more highly ranked in early divisions compared to subsequent divisions (**Fig. 3-5C**). Notably, the TBOX family member TBET supports ASC formation through repression of the inflammatory gene expression program [248], which was progressively upregulated in IRF4cKO cells (**Fig. 3-4E-F**). RUNX and ETS family members were most highly ranked in the final divisions, suggesting that these transcription factors are playing roles at both regions gaining and losing accessibility as the cells differentiate (**Fig. 3-5C**). Collectively, these data demonstrate the timing of IRF4-dependent reprogramming, establish a hierarchy of IRF4 activity that occurs at early and late cell divisions, and identify transcription factor networks dependent on IRF4.

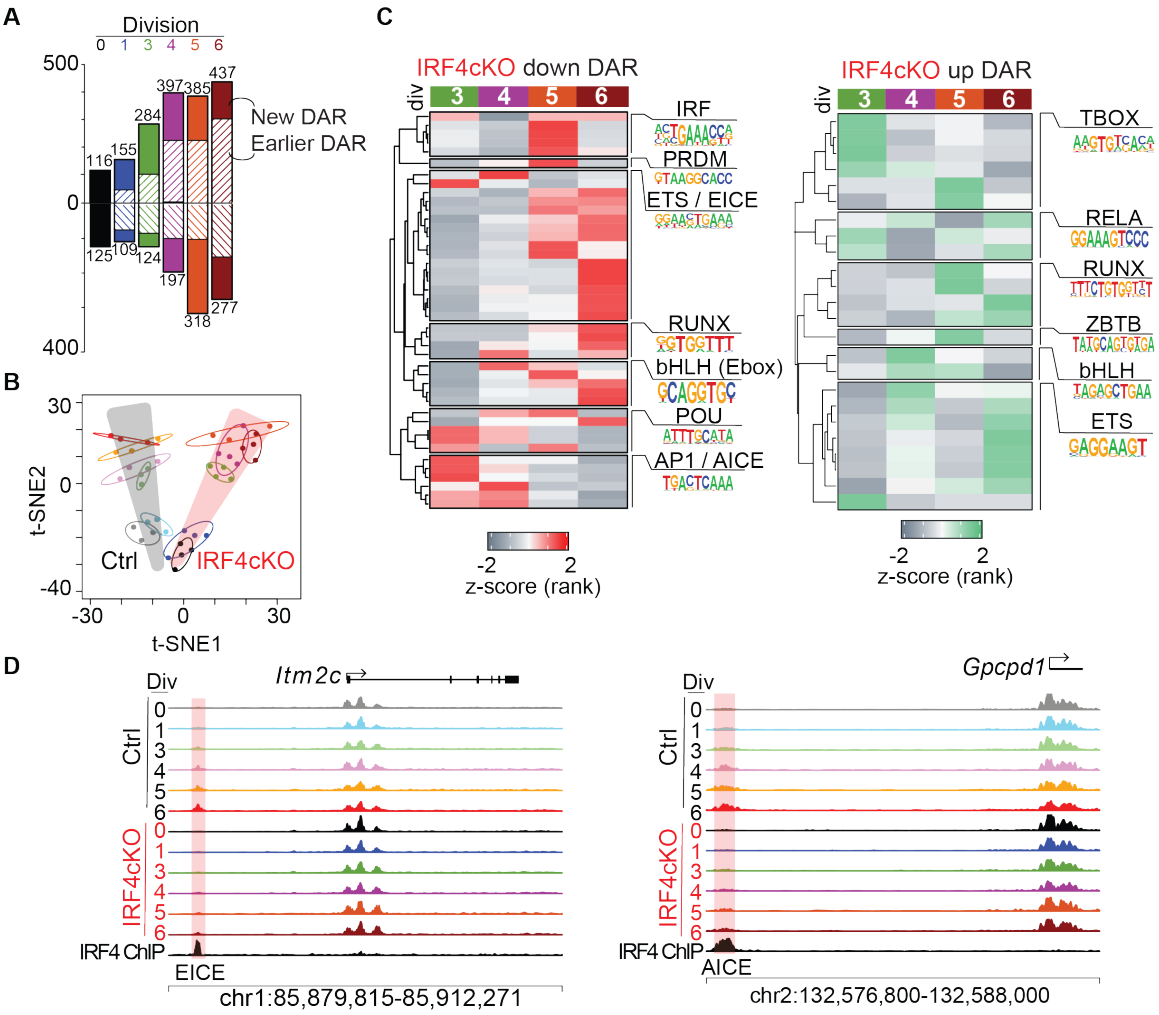

Figure 3-5. IRF4-deficient B cells display progressively altered chromatin accessibility profiles after subsequent divisions. ATAC-seq was performed on the sorted cell populations described in Figure 4. **(A)** Bar plot quantifying the number of differentially accessible regions (DAR) at each division that increase or decrease in IRF4cKO compared to Ctrl. Solid bars indicate the proportion of DAR that are new to that division, while striped bars indicate the proportion of regions that were a DAR in an earlier division. **(B)** t-SNE plots of 8,005 accessible loci from Ctrl samples (highlighted in grey) and IRF4cKO samples (highlighted in red). **(C)** Heatmap of HOMER [247] rank scores (by division) for the top 10 transcription factor motifs and related family members identified in IRF4cKO division 6 DAR. TF family names and a representative motif are displayed in their respective group. **(D)** ATAC accessibility profile for the indicated regions at DAR with an EICE (left) and AICE (right) motif. DAR regions are highlighted in red. IRF4 ChIP-seq from Minnich et al [138] was included in the IRF4 track. ATAC-seq data were derived from 3 independent adoptive transfers for Ctrl and 4 independent adoptive transfer for IRF4cKO. One division 5 IRF4cKO sample was excluded due to low coverage.

IRF4-deficient B cells fail to upregulate MYC

Recent work described MYC as a cell division timer during lymphocyte differentiation, with division cessation occurring when MYC levels fell below a critical threshold [181]. We reasoned that *Myc* may be dysregulated in IRF4-deficient B cells because IRF4cKO cells: 1) stalled during the proliferative response to LPS (**Fig. 3-1**); 2) accumulated in G_0/G_1 phase of the cell cycle (**Fig. 3-3A-B**); 3) progressively failed to induce MYC target genes (**Fig. 3-4E-F**); and 4) E-box binding bHLH family members were enriched in down DAR in divisions where MYC target genes were the most dysregulated (**Fig. 3-5C**). In fact, IRF4cKO cells were progressively enriched for genes dysregulated in MYC-deficient B cells stimulated with LPS and IL4 [232], further supporting the notion that MYC programming is altered in IRF4cKO cells (**Fig. 3-6A**). To determine if *Myc* failed to be induced in IRF4-deficient B cells, Ctrl and IRF4cKO cells were cultured *ex vivo* with LPS, IL2, and IL5 to initiate the pathway to ASC [216], and expression was analyzed by RT-qPCR before and 24 h after stimulation. While no differences in *Myc* levels were detected prior to stimulation, a significant reduction was observed at 24 h (**Fig. 3-6B**). Similar observations were detected by intracellular staining of MYC, which confirmed that while MYC levels were increased over naïve B cells, IRF4cKO cells failed to upregulate MYC to the same level as Ctrl cells (**Fig. 3-6C-D**). These data are consistent with previous reports following PMA/IO treatment of IRF4-deficient and -sufficient B cells [169]. The observed differences in MYC expression are likely caused by transcription of *Myc* and not due to alterations in MYC protein stability [249] (**Supplemental Fig. 3-10**).

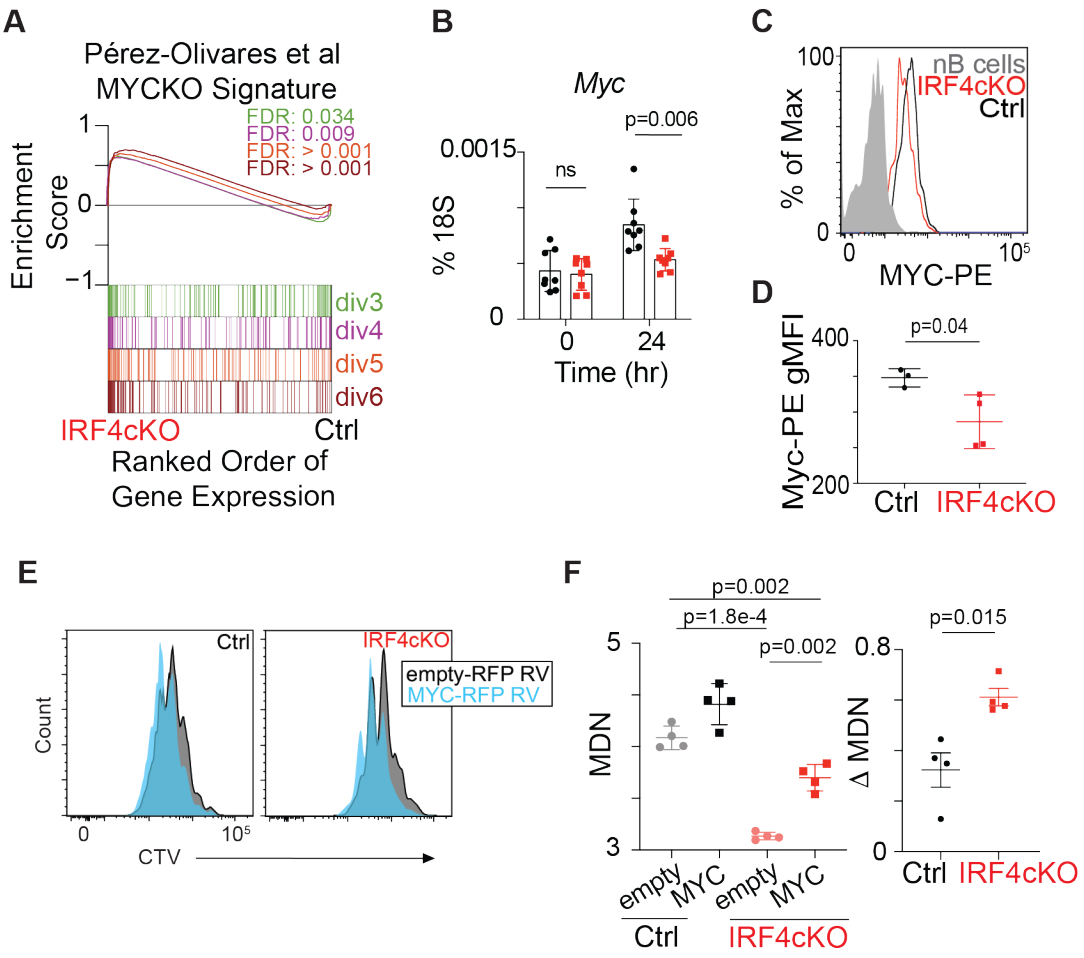

Figure 3-6. IRF4-deficient B cells fail to fully upregulate MYC. (A) GSEA using the top differentially expressed genes dysregulated in MYC-deficient B cells stimulated with LPS and IL-4 for 72 h [232]. FDR values are displayed for each division as indicated by color. Splenic B cells from Ctrl and IRF4cKO mice were isolated and treated with LPS, IL2, and IL5 *ex vivo* as described in methods. **(B)** Quantitative RT-PCR expression of *Myc* relative to 18S rRNA expression before (0 h) or 24 h after stimulation. **(C)** Representative intracellular staining of MYC for naïve untreated B cells (nB) and 24 h stimulated Ctrl and IRF4cKO cells (top). **(D)** Geometric mean fluorescence intensity (gMFI) quantified for the stimulated samples for **C**. **(E)** Representative CTV histograms of Ctrl (left) and IRF4cKO (right) transduced with empty-RFP retrovirus (black) or MYC-RFP expressing retrovirus (blue). **(F)** (Left) Quantification of the mean division number (MDN) for Ctrl and IRF4cKO cells transduced with empty-RFP retrovirus or MYC-RFP retrovirus from **E**. (Right) Quantification of the change in MDN after MYC overexpression in Ctrl and IRF4cKO cells from **E**. All data are representative of at least two independent experiments using at least 3 mice per genotype. Data in **B**, **D**, and **F** represent mean ± SD. Statistical significance in **B** and **D** was determined by a two-tailed Student's *t* test. Statistical significance in **F** when comparing IRF4cKO samples was determined by a paired two-tailed Student's *t* test, while significance between Ctrl and IRF4cKO samples was calculated by a two-tailed Student's *t* test.

To explore whether MYC overexpression could rescue the cell division defect of IRF4-deficient B cells, Ctrl and IRF4cKO cells were again cultured *ex vivo* with LPS, IL2, and IL5 and transduced with retrovirus expressing MYC-RFP or control RFP. Overexpression of *Myc* significantly improved the proliferation capacity of cells, and this improvement was greater for B cells from IRF4cKO than Ctrl (**Fig. 3-6E-F**). However, while IRF4cKO cells exhibited a greater proliferative gain upon MYC overexpression compared to Ctrl cells, full cell division capacity was not restored, as Ctrl B cells transduced with control RFP still displayed greater proliferative capacity. Collectively, these data suggest that IRF4cKO B cells fail to fine-tune the levels of *Myc* during the initial stages of B cell activation, which impact the overall cell division pattern and are consistent with the observation that IRF4cKO B cells begin to divide normally but stall in the middle of the proliferative response (**Fig. 3-1**). However, *Myc* overexpression alone does not fully restore the division capacity of IRF4cKO B cells, indicating additional deficiencies are contributing to the proliferative defect.

IRF4-deficient B cells exhibit reduced mTORC1 activity and are unable to initiate the UPR

Activation of the mammalian target of rapamycin (mTOR) is essential for promoting biosynthetic processes necessary for cell growth and division [250]. Importantly, ablation of mTORC1 activity impacted the proliferative effects of MYC overexpression in murine tumor cells [251], indicating there is significant crosstalk between the two signaling cascades [252-255]. Recent work indicated mTORC1 coordinates an early B cell-activation unfolded protein response (UPR), in which a subset of UPR-affiliated genes are upregulated

independent of XBP1 [105], a known driver of the UPR [101,102]. Interestingly, while Ctrl B cells gradually upregulated the B cell-activation UPR as early as division 3, IRF4cKO cells failed to initiate the program to the same levels (**Fig. 3-7A-B**). Indeed, genes associated with mTORC1 signaling progressively failed to be induced in IRF4cKO B cells (**Fig. 3-4E-F**). Collectively, these data implied that mTORC1 activation may be dysregulated in IRF4-deficient B cells. To test for mTORC1 activity, Ctrl and IRF4cKO cells were cultured *ex vivo* with LPS, IL2, and IL5 for 48 h, and intracellular staining for phosphorylation of the canonical mTORC1 substrate S6 (pS6) was performed. Strikingly, while the majority of B cells from Ctrl exhibited high amounts of pS6, most IRF4cKO cells contained pS6 levels similar to cultures where mTORC1 activity was blocked following treatment with rapamycin (**Fig. 3-7C-D**). Consistently, proliferating IRF4cKO cells also failed to increase in cell size compared to Ctrl B cells at 48 h post-LPS *in vivo* (**Fig. 3-7E-F**). Intriguingly, this reduction in cell size was rescued via overexpression of *Myc* in IRF4cKO cells cultured *ex vivo* (**Fig. 3-7G**). Thus, IRF4cKO B cells exhibit a defect in mTORC1 activity that impacts the ability of cells to increase in cell size that is overcome with *Myc* overexpression. Thus, these data support the role of mTORC1 in upregulating an early B cell-activation UPR, assign the cell division in which this process occurs, and implicate IRF4 in this process.

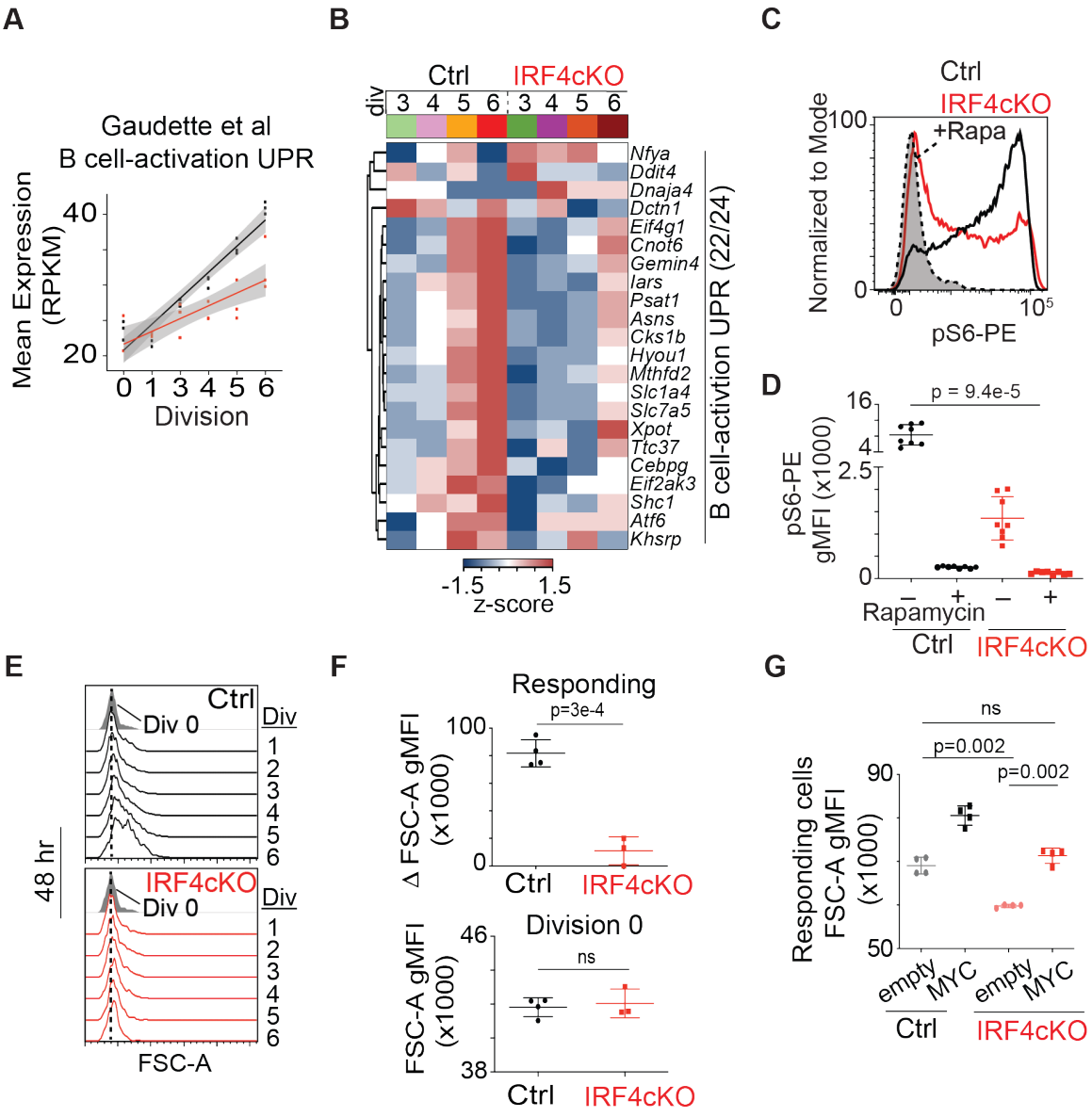

Figure 3-7. IRF4-deficient B cells exhibit reduced mTORC1 activity and fail to initiate the B cell-activation UPR. (A) RNA-seq (described in Fig 4) average RPKM of all detected genes (22/24) in the B cell-activation UPR gene set [105]. **(B)** Heatmap of *z* score-normalized gene expression data for all detected genes from **A** for the indicated divisions. **(C)** Representative flow cytometry histograms displaying intracellular phosphorylated S6 (pS6) protein staining for Ctrl or IRF4cKO activated B cells cultured *ex vivo* with LPS, IL2, and IL5 for 48 h. Grey histogram is representative of Ctrl cultures treated with rapamycin to block mTORC1 activity 2 h before harvest. **(D)** Quantification of geometric mean fluorescence intensity (gMFI) for pS6 from **C**. **(E)** Histograms displaying cell size distribution via forward scatter area (FSC-A) at divisions 0 - 6 48 h post-LPS inoculation of adoptive transfer host mice, as described in Fig 1. Grey histogram represents cell size at division 0, with the dashed line drawn from the summit to better visualize changes in cell size across the divisions. Cell divisions are indicated to the right of each trace. **(F)**

Quantification of data from **E** indicating cell size at division 0 (bottom) and the average change in cell size among responding cells (top). **(G)** Quantification of cell size via forward scatter area (FSC-A) for all responding cells in Ctrl and IRF4cKO transduced with empty-RFP retrovirus or MYC-RFP expressing retrovirus. All data are representative of at least two independent experiments using at least 3 mice per genotype. Data in **D**, **F**, and **G** represent mean ± SD. Statistical significance in **D** and **F** was determined by a two-tailed Student's *t* test. Statistical significance in **G** when comparing IRF4cKO samples was determined by a paired two-tailed Student's *t* test, while significance between Ctrl and IRF4cKO samples was calculated by a two-tailed Student's *t* test.

DISCUSSION

This study establishes the timing and extent of IRF4-dependent reprogramming instructed in the initial stages of B cell differentiation *in vivo* and ascribe a role for IRF4 in controlling cell growth and proliferation. Using multiple antigen model systems, IRF4-deficient B cells divided initially, but stalled during the proliferative response. Characterization of the proliferative defect revealed fewer actively dividing cells and abnormal cell cycle distribution. B cells lacking IRF4 maintained an inflammatory gene signature but failed to induce critical actB and ASC gene expression programs, including metabolic pathways (glycolysis and OXPHOS), MYC target genes, and mTORC1 signaling. Reduced *Myc* expression and mTORC1 activity contributed to the cell division and growth defect following stimulation. Additionally, IRF4-deficient B cells failed to induce the B cell-activation UPR, which relies on mTORC1 [105]. Thus, we define the cell division-coupled IRF4-dependent reprogramming events that occur in the initial stages of B cell activation and identify an IRF4-MYC-mTORC1 relationship that impacts cell growth and proliferation.

The role of MYC as a division-independent timer to regulate lymphocyte proliferation has been described [172,181]. In this model, the combination and strength of

stimuli determine the amount of MYC initially generated. This serves as a timer to regulate the overall number of cell divisions, or a cell's division destiny, with division cessation occurring when MYC levels fall below a critical level [181]. Analyzing the cell division kinetics of IRF4-deficient B cells responding to LPS revealed they can initiate cell division appropriately but stall in the middle of the proliferative response. Applying the MYC dilution model, IRF4-deficient B cells fall below the MYC threshold sooner, which caused the observed stalling. Indeed, IRF4-deficient B cells displayed reduced MYC levels 24 h after stimulation. Interestingly, MYC expression is not dependent on cell division [181], but we found progressive dysregulation of MYC target genes in IRF4-deficient B cells, implying that other factors reinforce MYC programming throughout the cell divisions. Importantly, both *Irf4* expression and *Myc* induction levels are dependent on the strength of signaling [181], irrespective of whether the stimulus is from BCR [128] or TLR [256]. Furthermore, IRF4 binding to the *Myc* promoter has been reported [169,257]. While no differences in chromatin accessibility were observed in IRF4-deficient B cells at known regulatory elements of *Myc* [258], this is likely due to the timing in which the samples were collected or compensatory effects of IRF8 [116,117], which often binds to the same sites. Collectively, these data support the concept that IRF4 serves as a rheostat in B cells to regulate the overall proliferative response by fine-tuning initial *Myc* expression levels. Indeed, a similar role for IRF4 has been noted in CD8 T cells in which IRF4 serves as a molecular rheostat of TCR affinity. Similar to our observations, IRF4-deficient CD8 T cells can initiate proliferation but fail to maintain clonal expansion [259], suggesting IRF4 may play a similar role in controlling the proliferative response in T cells.

Differentiating actB undergo an IRF4-dependent bifurcation event that commits a portion of actB to an ASC fate [176]. Additionally, differentiating actB utilize mTORC1 to anticipate antibody synthesis by upregulating UPR-affiliated genes [105]. We demonstrate that IRF4-deficient B cells display reduced mTORC1 activity and fail to initiate the B cell-activation UPR. Thus, actB anticipation of antibody synthesis and secretion is a component of ASC fate commitment and programmed during the initial stages of B cell activation. Our gene expression data indicate that this process occurs as early as division 3 during B cell differentiation, with reduced expression of UPR-affiliated genes in IRF4-deficient B cells. Interestingly, the interplay between mTORC1 and IRF4 has been noted, with mTOR inhibition negatively impacting IRF4 expression [260-262]. Here, IRF4 also impacts mTORC1 activity, suggesting the existence of a positive IRF4-mTORC1 feedback loop that impacts actB reprogramming. MYC is central to this regulatory network, as MYC overexpression in IRF4-deficient B cells restores cell growth. mTOR may impact IRF4 transcription by effecting downstream transcription factors or by directly impacting IRF4 protein translation or stability [263].

Occupancy of IRF4 at composite motifs is dependent on its concentration and availability of binding partners [119]. IRF4 levels are increased as the cells divide and ultimately sustained at high levels in ASC [128,176]. In contrast, IRF8 levels are decreased as B cells differentiate, allowing for IRF4 to more readily partner with transcription factors and establish the IRF4-dependent gene expression program [116]. In IRF4cKO cells, differentiating cells showed changes in accessibility surrounding composite motifs. Previously, ATAC-seq data in wild-type differentiating B cells suggested that EICE motifs were most accessible in early dividing actB and that AICE sites became increasingly

accessible as IRF4 levels increased during the division-coupled differentiation process [175]. In the absence of IRF4, this program is altered. In regions that decreased accessibility, AICE motifs were the most affected motifs in early divisions (divisions 3 and 4), while EICE motifs were most highly ranked at later divisions (divisions 5 and 6). Although both motifs are affected at all divisions, this analysis pinpoints specific divisions and differentiation stages where IRF4 cooperates with AP-1 or ETS factors to establish differentiation programs, suggesting a hierarchy of IRF4 activity. Consistent with these data, single-cell analysis of LPS responding B cells showed that IRF4 was required for BATF (an AP-1 family member) targets as early as division 3, suggesting that IRF4 may be BATF's partner in AICEs at the early stages of B cell differentiation to ASC [176]. Furthermore, IRF4 binding at AICE motifs largely occurs at newly established accessible regions [120]. Taken together, these data indicate that these reprogramming steps occur at divisions 3 and 4.

The cell division requirement needed for ASC formation *in vivo* following LPS [174-176] and NP-ficoll [176] stimulation has been described. We observed similar cell division requirements for adoptive transfers using Ctrl B cells and add that ASC formation occurs after cells reach or exceed division 8 following stimulation with the T-dependent antigen influenza X31. As this analysis was performed at day 6 following infection, it is unlikely that the generation of ASC at this time point involve a full germinal center reaction. However, antigen-specific ASC can be observed at this time point [157]. These data suggest that the timing of division-coupled reprogramming events needed for ASC differentiation are similar for T-independent antigens and the early differentiation process that occurs with T-dependent antigens. Studying the cell division requirement of T-dependent ASC

formation at later time points is complicated by the dynamics and selection pressures of the germinal center reaction and increased cell divisions [53,218].

Together, these data indicate IRF4 coordinates cell growth and the proliferative response during B cell differentiation. We demonstrate that part of the mechanism involves regulation of *Myc* and mTORC1 activity. Indeed, the relationship between MYC and mTORC1 has been noted, with mTORC1 controlling MYC translation [264] and MYC-driven tumorigenesis dependent on mTORC1 [251,254]. Both factors converge to control protein production and cell growth. MYC controls the expression of translation initiation factors needed for increased protein synthesis [253] and mTOR controls their activity [265]. Here, IRF4cKO cells displayed reduced mTORC1 activity and were unable to increase in cell size as they divided. However, the deficiency in cell growth was overcome by overexpression of *Myc,* suggesting that this aspect of MYC/mTOR relationship is dependent on *Myc* expression. RNA-seq analyses showed IRF4-deficient B cells failed to induce MYC target genes and mTORC1 signaling by division 3, and these gene sets became progressively dysregulated as the cells divided. Thus, reprogramming events needed for continued cell growth and proliferation occur during the initial cell divisions during B cell differentiation and are coordinated by IRF4, MYC, and mTORC1.

SUPPORTING DATA

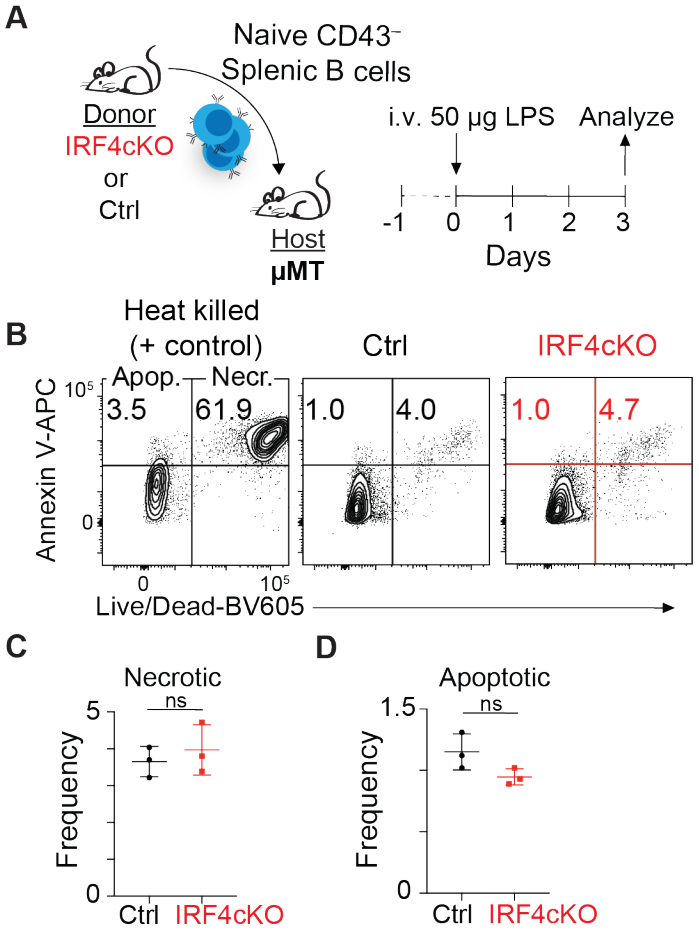

Figure 3-8. IRF4-deficient and -sufficient B cells exhibit similar frequencies of apoptosis *in vivo*. (A) Schematic of experimental design. Ctrl or IRF4cKO cells were transferred into µMT hosts. After 24 h, host mice were challenged with 50 mg LPS and apoptosis was assessed 72 h post-LPS inoculation. **(B)** Representative flow cytometry plots of Annexin V versus Live/Dead viability dye for Ctrl (middle) or IRF4cKO (right). Heat killed control samples were prepared to faithfully gate apoptotic (Apop.) and necrotic (Necr.) cells (left). **(C** and **D)** Frequency of necrotic (C) and apoptotic cells (D) from **B**. Data are representative of two independent experiments using 3 mice per genotype. Statistical significance in **C** and **D** was determined by a two-tailed Student's *t* test.

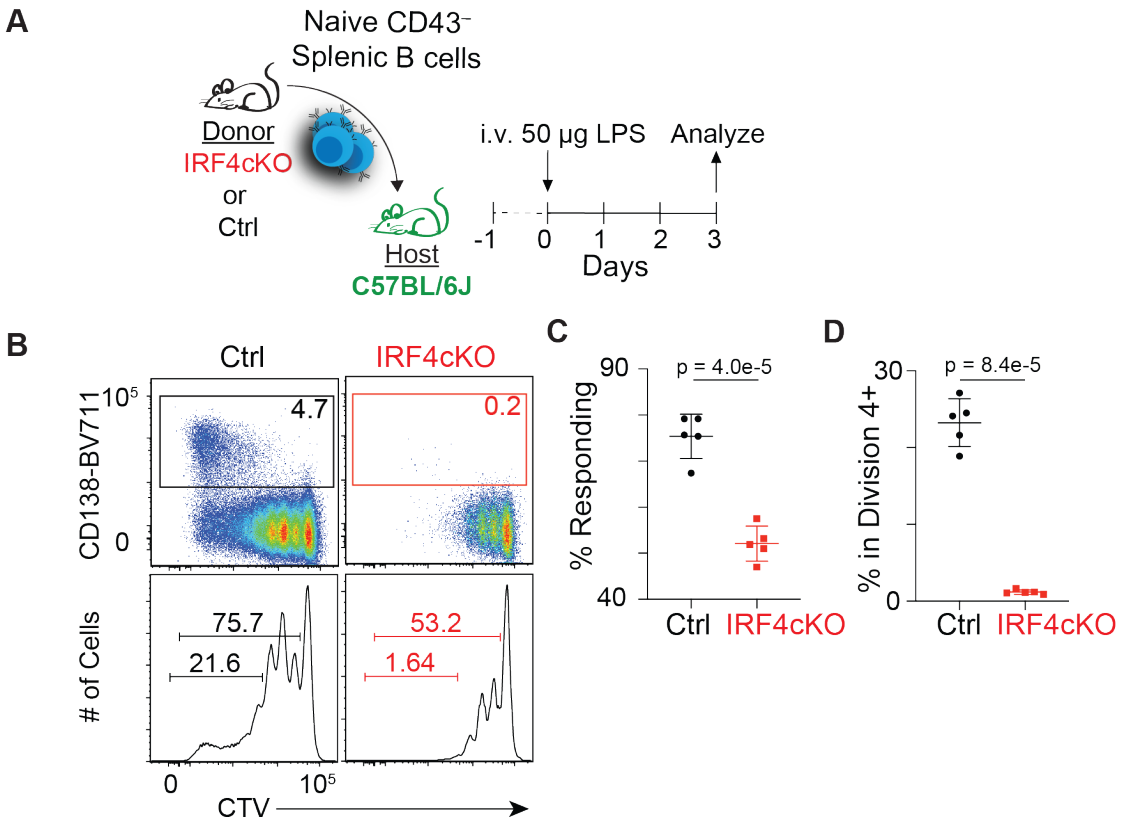

Figure 3-9. IRF4-deficient B cells exhibit a proliferation defect when transferred to C57BL/6J animals. (A) Schematic of experimental design. CTV-labeled Ctrl or IRF4cKO cells were transferred into CD45.1 C57BL/6J hosts. After 24 h, host mice were challenged with 50 mg LPS. Cell division and differentiation were assessed 72 h post-LPS inoculation. **(B)** Representative flow cytometry plots of CD138 versus CTV (top) and CTV histograms (bottom). Frequency of CD138+ ASC are indicated (top), and the frequency of all responding cells, as well as the frequency of cells in divisions 4+ are displayed (bottom). (**C** and **D**) Frequency of all responding cells (C) and cells in division 4+ (D) from **B**. Data are representative of two independent experiments using 3 mice per genotype. Statistical significance in **C** and **D** was determined by a two-tailed Student's *t* test.

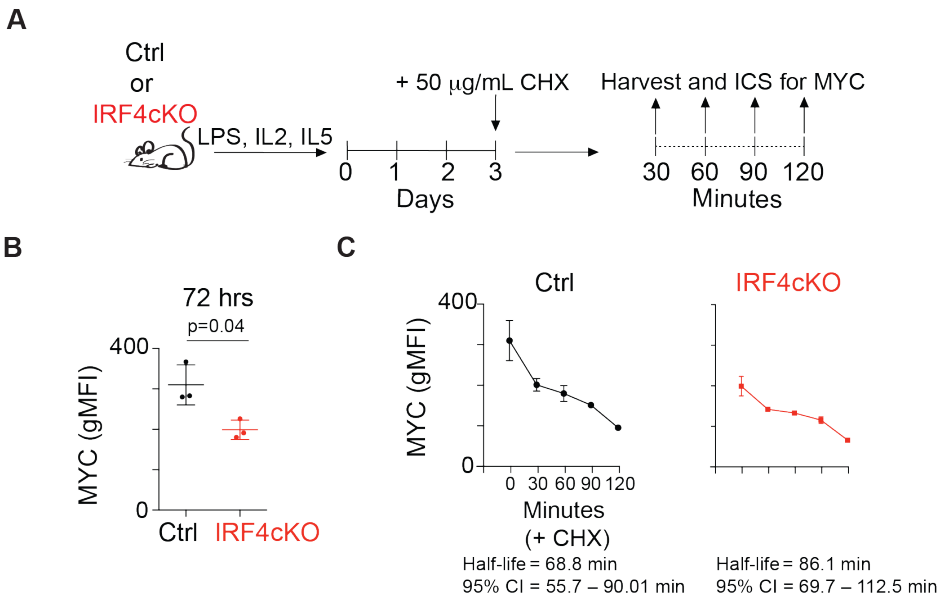

Figure 3-10. MYC protein stability is similar between IRF4-deficient and -sufficient B cells. (A) Schematic of experimental design. Ctrl and IRF4cKO were cultured for 3 days. At 72 h, 50 mg/ml cycloheximide (CHX) was added, and intracellular staining of MYC was performed at the time course shown. **(B)** MYC geometric mean fluorescence intensity (gMFI) at 72 h. **(C)** MYC protein decay curves displayed as gMFI at the indicated time points after CHX treatment. Half-life and 95% confidence intervals (CI) are shown below and were estimated by fitting exponential decay curves. Data are representative of two independent experiments using 3 mice per genotype. Statistical significance in **B** was determined by a two-tailed Student's *t* test.

Table 3-1. List of antibodies and stains.

Antibody and Stains	Conjugate	Clone	Company	Catalog Number	Dilution
B220	PE-Cy7	RA3-6B2	Biolegend	103222	1/400
B220	A700	RA3-6B2	Biolegend	103232	1/200
BrdU	APC	Bu20a	Biolegend	339808	1/10
c-MYC	PE	D84C12	Cell Signaling	14819	1/33
c-MYC	Alexa Fluor 647	D84C12	Cell Signaling	13871	1/33
CD11b	APC-Cy7	M1/70	Biolegend	101226	1/400
CD138	BV711	281-2	BD	563193	1/800
CD138	APC	281-2	Biolegend	558626	1/400
CD45.1	FITC	A20	Tonbo Biosciences	35-0453-U500	1/100
CD45.1	PE	A20	Biolegend	110708	1/100
CD45.1	APC	A20	Biolegend	110714	1/100
CD45.1	APC-Cy7	A20	Tonbo Biosciences	25-0453-U100	1/100
CD45.2	PE-Cy7	104	Biolegend	109830	1/100
CD45.2	PerCP-Cy5.5	104	Tonbo Biosciences	65-0454-U100	1/100
CD45.2	PE	104	Tonbo Biosciences	50-0454-U100	1/100
CD45.2	APC	104	Biolegend	109814	1/100
CD90.2	APC-Cy7	30-H12	Biolegend	105328	1/400
F4/80	APC-Cy7	BM8	Biolegend	123118	1/400
Fas	PerCP-Cy5.5	SA367H8	Biolegend	152610	1/400
GL7	eFluor 660	GL7	Fisher Scientific	50-112-9500	1/400
GL7	PerCP-Cy5.5	GL7	Biolegend	144610	1/400
GL7	PE-Cy7	GL7	Biolegend	144620	1/400
Ki67	APC	16A8	Biolegend	652406	1/10
pS6	PE	D57.2.2E	Cell Signaling	5316	1/100
Rabbit mAb IgG XP Isotype	Alexa Fluor 647	DA1E	Cell Signaling	2985	equal
Rabbit mAb IgG XP Isotype	PE	DA1E	Cell Signaling	5742	equal
Zombie Yellow Fixable Viability Kit	-	-	Biolegend	423104	1/400
Zombie NIR Fixable Viability Kit	-	-	Biolegend	423106	1/400
CellTrace Violet	-	-	Life Technologies	C34557	1/100
7AAD	-	-	Biolegend	76332	1/5

METHODS

Mice and adoptive transfers

Cd19^{Cre} (JAX; 006785) [223] and *Irf4*$^{fl/fl}$ (JAX; 000664) [118] mice were purchased from The Jackson Laboratory and bred to generate *Cd19*$^{Cre/+}$*Irf4*$^{fl/fl}$. CD45.2 μMT (JAX; 008100) [190] were bred onto the CD45.1 background to obtain CD45.1 μMT mice [176]. All experimental animals were between 7 - 12 weeks of age and genders were equally represented. For adoptive transfers, naïve splenic CD43^{-} B cells were magnetically isolated using the B cell isolation kit (Miltenyi Biotec, Inc.; 130-090-862) and LS columns (Miltenyi Biotec, Inc.; 130-042-40). Isolated B cells were stained with CellTrace Violet (CTV) (Life Technologies; C34557) per the manufacturer's protocol and resuspended in sterile PBS (Corning; 21-040-CV) before transferring 15x10^{6} B cells into a disparate congenic μMT host. At 24 h post-transfer, host mice were challenged intravenously with 50 μg LPS (Enzo Life Sciences; ALX-581-008), intranasally with 0.1 LD_{50} influenza A/HK-X31 (X31), or intravenously with 50 μg NP-Ficoll (Biosearch Technologies; F-1420-10). For influenza infections, mice were anesthetized with vaporized isoflurane (Patterson Veterinary; 07-893-1389) before X31 administration. Experimental mice were euthanized via carbon dioxide asphyxiation in accordance with AVMA guidelines. All procedures were approved by the Emory Institutional Animal Care and Use Committee.

Flow cytometry and sorting

Cells were resuspended at 1x10^{6} / 100 μl in FACS buffer (1X PBS, 1% BSA, and 2 mM EDTA), stained with Fc Block (BD; 553141) and antibody-fluorophore conjugates for 15

and 30 m, respectively, and then washed with 1 ml of FACS. For adoptive transfers when NP-Ficoll or X31 was used, CD45.2 transferred cells were enriched prior to antibody staining using anti-CD45.2-APC or anti-CD45.2-PE followed by magnetic enrichment using anti-APC (Miltenyi; 130-090-855) or anti-PE (Miltenyi; 130-097-054) microbeads. The following antibody-fluorophore conjugates and stains were used (**Table 3-1**): B220-PE-Cy7 (Biolegend; 103222), B220-A700 (Biolegend; 103232), BrdU-APC (Biolegend; 339808), c-MYC-PE (Cell Signaling; 14819), c-MYC-Alexa Fluor 647 (Cell Signaling; 13871), CD11b-APC-Cy7 (Biolegend; 101226), CD138-BV711 (BD; 563193), CD138-APC (Biolegend; 558626), CD45.1-FITC (Tonbo Biosciences; 35-0453-U500), CD45.1-PE (Biolegend; 110708), CD45.1-APC (Biolegend; 110714), CD45.1-APC-Cy7 (Tonbo Biosciences; 25-0453-U100), CD45.2-PE-Cy7 (Biolegend; 109830), CD45.2-PerCP-Cy5.5 (Tonbo Biosciences; 65-0454-U100), CD45.2-PE (Tonbo Biosciences; 50-0454-U100), CD45.2-APC (Biolegend; 109814), CD90.2-APC-Cy7 (Biolegend; 105328), F4/80-APC-Cy7 (Biolegend; 123118), Fas-PerCP-Cy5.5 (Biolegend; 152610), GL7-eFluor 660 (Fisher Scientific; 50-112-9500), GL7-PerCP-Cy5.5 (Biolegend; 144610), GL7-PE-Cy7 (Biolegend; 144620), Ki67-APC (Biolegend; 652406), pS6-PE (Cell Signaling; 5316), Rabbit mAb IgG XP Isotype-Alexa Fluor 647 (Cell Signaling; 2985), Rabbit mAb IgG XP Isotype-PE (Cell Signaling; 5742), Zombie Yellow Fixable Viability Kit (Biolegend; 423104), Zombie NIR Fixable Viability Kit (Biolegend; 423106), CellTrace Violet (Life Technologies; C34557), and 7AAD (Biolegend; 76332). For all flow cytometry analyses involving adoptive transfers, the following general gating strategy was used: lymphocytes were gated based on SSC-A / FSC-A, single cells by FSC-H / FSC-W or FSC-H / FSC-A, live cells based on exclusion of Zombie Yellow or Zombie NIR

Fixable Viability Kit, and the markers CD11b, F4/80, and CD90.2 to remove non-B cells. All flow cytometry were performed on an LSR II, LSRFortessa, or LSR FACSymphony (BD) and analyzed using FlowJo v9.9.5, v10.5.3, or v10.6.2. Cell sorting was performed at the Emory Flow Cytometry Core using a FACSAria II (BD) and BD FACSDiva software v8.0.

Cell cycle analysis and intracellular staining

In some adoptive transfers, hosts were injected with 800 µg BrdU (Biolegend; 423401) intravenously 1 h prior to euthanasia. Staining of BrdU, Ki67, and 7AAD was achieved using the Phase-Flow BrdU Cell Proliferation Kit (Biolegend; 370704), substituting anti-BrdU for anti-Ki67 when desired. Intracellular pS6 staining was accomplished following BD's two-step protocol using BD Phosflow Fix Buffer I (BD; 557870) and BD Phosflow Perm Buffer III (BD; 558050). As a negative control for intracellular pS6, cultured cells were treated with 200 nM of rapamycin (Sigma-Aldrich; R8781) for 2 h prior to staining. Intracellular staining of MYC was performed using the FIX & PERM Cell Permeabilization Kit (ThermoFisher; GAS003) per the manufacturer's protocol.

Ex vivo B cell differentiation

Isolated B cells were cultured at a concentration of 0.5 x 10^6 cells/ml in B cell media (RPMI 1640 supplemented with 1X nonessential amino acids, 1X penicillin/streptomycin, 10 mM HEPES, 1 mM sodium pyruvate, 10% heat-inactivated FBS, and 0.05 mM 2-ME) containing 20 mg/ml *Escherichia coli* O111:B4 derived LPS (Sigma-Aldrich; L2630), 5 ng/ml IL-5 (Biolegend; 581504), and 20 ng/ml IL-2 (Biolegend; 575406) as previously

described [216]. Additional LPS (10 µg/ml), IL-5 (2.5 ng/ml), and IL-2 (10 ng/ml) were added to the cultures every 24 h for the duration of the time course.

Retroviral production and transduction

Retrovirus was prepared as previously described [266]. Briefly, Platinum-E cells were transfected at 70-80% confluency on 10 cm plates with 4 µg pCL-Eco [267] and 6 µg of either pMSCV-pBabeMCS-IRES-RFP (Addgene; 33337) or pMSCV-Myc-IRES-RFP (Addgene; 35395) [268] using 40 µl TransIT-293 (Mirus; MIR2700). Cell media (antibiotic-free DMEM supplemented with 10% heat-inactivated FBS) was replaced with High-BSA cell media (DMEM supplemented with 10% heat-inactivated FBS and 1g/100ml BSA) 18 h after transfection. Retrovirus was harvested 24 and 48 h later, filtered through a 0.45 µm membrane, and concentrated using 5x PEG-it viral precipitation solution (System Biosciences; LV825A-1). Transduction of B cells was performed 12-24 h after stimulation via spinfection at 800 g for 1 h.

Quantitative RT-PCR

One million cells were resuspended in 600 µl of RLT Buffer (Qiagen; 79216) containing 1% 2-BME and snap frozen in a dry ice – ethanol bath for RNA isolation. Lysates were thawed, subjected to QIAshredder homogenization (Qiagen; 79656), and then total RNA isolation using the RNeasy Mini Ki (Qiagen; 74104). RNA was reverse transcribed using SuperScript II Reverse Transcriptase (Invitrogen; 18064014). cDNA was diluted 1 µg / 100 µl and qPCR was performed on a CFX96 Instrument (Bio-Rad) using SYBR Green incorporation. Primers used included: 18S-forward 5'-GTAACCCGTTGAACCCCATT-

3’ 18S-reverse 5’-CCATCCAATCGGTAGTAGCCG-3’, MYC-forward 5’-CGATTCCACGGCCTTCTC-3’, and MYC-reverse 5’-TCTTCCTCATCTTCTTGCTCTTC-3’. All primers were purchased from Integrated DNA Technologies.

RNA-sequencing and data analysis

For all samples, 1,000 cells were sorted into 300 µl of RLT buffer (Qiagen; 79216) containing 1% 2-ME and snap frozen in a dry ice – ethanol bath. RNA isolation was achieved using the Quick-RNA Microprep kit (Zymo Research; R1050). Isolated RNA was used as input for the SMART-seq v4 cDNA synthesis kit (Takara; 634894), and 400 pg of cDNA was used as input for the NexteraXT kit (Illumina). Final libraries were quantified by qPCR and bioanalyzer traces, pooled at equimolar ratios, and sequenced at the New York University Genome Technology Center on a HiSeq 4000.

Raw sequencing data were mapped to the mm10 genome using STAR v.2.5.3 [269]. Duplicate reads were identified and removed using PICARD (http://broadinstitute.github.io/picard/). The Bioconductor package edgeR v3.24.3 [208] was employed to determine differentially expressed genes (DEG), which were defined as having an absolute $\log_2$ fold-change of ≥ 1 and a false discovery rate (FDR) of ≤ 0.05. All detected transcripts were ranked by multiplying the sign of fold change (+/–) by $-\log_{10}$ of the p-value, and gene set enrichment analysis (GSEA) [210] was performed on this ranked gene list. All t-SNE projections were generated using ‘Rtsne’ v 0.15 (https://github.com/jkrijthe/Rtsne). Clustering and heatmap analysis were achieved using ‘heatmap3’ (https://github.com/cdschar/heatmap).

ATAC-sequencing and data analysis

For each sample, 10,000 cells were sorted into FACS buffer and the assay for transposase-accessible chromatin sequencing (ATAC-seq) was performed. Tn5 preparation and library generation was previously described [201]. Briefly, cells were centrifuged at 500 g for 10 min at 4 °C. The supernatant was removed and cells were resuspended in 25 µl of Tn5 tagmentation reaction (2.5 µl Tn5, 12.5 µl 2X tagmentation buffer (20 mM TAPS-NaOH pH 8.1, 10 mM MgCl2, 20% DMF), 2.5 µl 1% Tween-20, 2.5 µl 0.2% digitonin, and 5 µl of molecular grade water). Resuspended samples were incubated at 37°C for 1 h. Cells were then lysed by adding 25 µl lysis buffer (300 mM NaCl, 100 mM EDTA, 0.6% SDS, and 2 µl 10 mg/ml proteinase K) and incubated for 30 min at 40°C. Transposed DNA was isolated using AMPure XP SPRI beads (A63880) by adding 0.7x volumes to remove high molecular weight DNA and then 1.2x volumes to positively select for low molecular weight DNA. Tagmented DNA was eluted in 15 µl EB buffer (Qiagen; 19086) and amplified using Nextera indexing primers (Illumina) and KAPA HiFi polymerase (Roche; KK2601). Final libraries were sequenced at the New York University Genome Technology Center on a HiSeq 4000.

Raw sequencing data were mapped to the mm10 genome using Bowtie v1.1.1 [270]. Peaks were called using MAC2 v 2.1.0 [271] and annotated to the nearest gene using HOMER v4.8.2 [247]. Reads per peak million normalization was performed for all samples as previously described [198]. The Bioconductor package edgeR v3.24.3 [208] was used to determine differentially accessible regions (DAR), which were defined as having an absolute $\log_2$ fold-change of ≥ 1 and a FDR of ≤ 0.05. Motif analysis was performed using

the HOMER program findMotifsGenome.pl (*de novo* results). For plotting the rank value of transcription factors, enriched transcription factor motifs were ranked according to their p-value and normalized by the total number of enriched motifs found for a given sample. Resulting values were z-score normalized and motifs binned according to their DNA binding domain family.

Statistics

All statistical analyses were achieved by using R/Bioconductor v3.5.2, Microsoft Excel v16.36 or v16.48, and GraphPad Prism v6.0c, v8.4.1, or 8.4.3. P values of less than 0.05 were considered significant. For RNA- and ATAC-seq significance, a combination of FDR and fold-change was used to designate DEG and DAR.

Data availability

All sequencing data generated in this study have been deposited in NCBI Gene Expression Omnibus (https://www.ncbi.nlm.nih.gov/geo/) under accession code GSE173437 (GSE173435 for ATAC-seq and GSE173436 for RNA-seq).

Chapter 4. Work in progress

Dillon G. Patterson, Christopher D. Scharer, Sakeenah L. Hicks, and Jeremy M. Boss

*Department of Microbiology and Immunology, and the Emory Vaccine Center, Emory University School of Medicine, Atlanta, GA 30322, USA

Author Contributions

D.G.P. designed, performed experiments, analyzed, and interpreted the data. S.L.H. generated sequencing libraries. C.D.S. and J.M.B designed the experiment, analyzed, and interpreted the data.

Chapter Notes

This authorship order is irrelevant and only serves to describe those who generated, analyzed, and interpreted the preliminary data described below.

In chapter 2, we described a bifurcation event that occurred during the initial stages of B cell differentiation with cells progressing down either an antibody-secreting cell (ASC)-destined or a non-ASC branch. ASC-destined activated B cells (actB) downregulated CD62L (L-selectin), while non-ASC cells maintained CD62L expression. We leveraged the differences in CD62L expression to distinguish and isolate cells on each branch. ActB that progressed down the ASC-destined branch upregulated gene sets necessary for ASC differentiation, including oxidative phosphorylation and MYC-target genes. Indeed, ASC-destined cells, whether restimulated or not, more readily differentiated to ASC compared to cells along the non-ASC branch. ActB progressing down the non-ASC branch maintained an inflammatory gene signature, but their cell fate was not determined.

To investigate the non-ASC branch, we used an adoptive transfer approach using either μMT or wild-type mice as hosts and LPS or NP-ficoll as the immune challenge (**Figure 4-1A**). After three days, actB on each differentiation trajectory in division 8 were sorted based on CD62L and CD138 expression for RNA-sequencing (**Figure 4-1B-C**). In Chapter 2, we demonstrated that the ASC-destined trajectory was dependent on IRF4, with IRF4-deficient B cells only progressing down the non-ASC branch. Consistent with these data, gene sets that progressively failed to be induced in non-ASC cells mirrored those that were dysregulated in IRF4-deficient B cells, described in Chapter 3 (**Figure 4-1D**). These included failure to upregulate the unfolded protein response, oxidative phosphorylation, MYC target genes, and mTORC1 signaling pathways (**Figure 4-1D**). Similar observations were seen for gene sets that failed to be repressed in IRF4-deficient B cells, such as those involving cytokine signaling and the inflammatory response (**Figure 4-1D**).

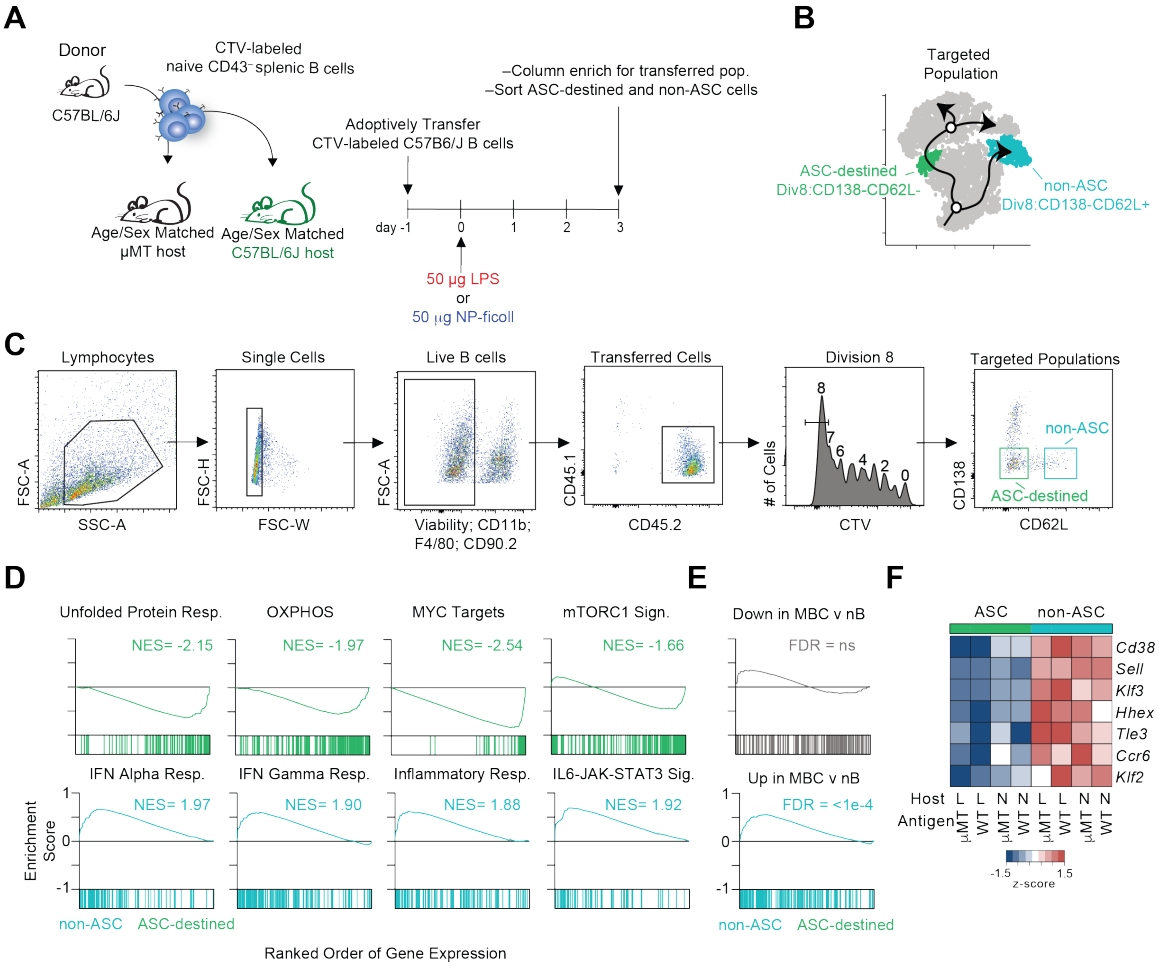

Figure 4-1. Activated B cells along the non-ASC differentiation trajectory resemble pre-memory B cells. (**A**) Schematic of experimental design. Briefly, splenic naive B cells were isolated, labeled with CellTrace Violet (CTV), and transferred into a disparate µMT or C57BL/6J host. After 24 hr, hosts were challenged with 50 µg LPS or NP-ficoll. On day 3 post-challenge, transferred B cells were recovered from host spleens and ASC-destined and non-ASC cells were isolated via FACS for RNA-sequencing. (**B**) from Chapter 2, t-SNE projections of single cell data overlaid with differentiation trajectories indicating the targeted sorted populations. (**C**) Schematic for sorting the targeted populations described in **B**. (**D**) Gene set enrichment analysis (GSEA)[210] for the indicated gene sets for pathways upregulated and downregulated in non-ASC cells. (**E**) GSEA using genes that are downregulated (top graph) or upregulated (bottom graph) in MBC compared to naive B cells [272]. (**F**) Heatmap of canonical pre-memory B cell genes from all ASC-destined and non-ASC samples. Data in **C**-**E** are derived from experiments with µMT hosts challenged with LPS, but similar results are obtained in all host–stimulus combinations. L, LPS; N, NP-ficoll,; WT, wild-type. All data were derived from 2-3 replicates per group.

Strikingly, while ASC-destined cells progressed towards ASC, non-ASC actB exhibited a partial memory B cell (MBC) transcriptional signature (**Figure 1-E**). Genes upregulated in MBC were enriched in non-ASC cells; however, genes normally downregulated in MBC were not enriched in either population (**Figure 4-1E**). These data suggest that non-ASC actB are progressing down a differentiation trajectory leading to MBC formation. However, the complete MBC transcriptional program has not been established, or alternatively, the observed MBC program is unique to T-cell independent antigens (**Figure 4-1E**). Indeed, precursor memory (pre-memory) B cells have been described [273-276] that transcriptionally resemble MBC, and non-ASC actB expressed canonical pre-memory B cell markers independent of host and stimuli (**Figure 4-1F**). Thus, non-ASC cells in division 8 transcriptionally resemble pre-memory B cells, and the same differentiation trajectories exist for two different T cell independent antigens.

These data are consistent with previous reports that deletion of IRF4 in germinal center B cells impacts ASC formation but does not perturb the early MBC pool, which may explain why IRF4-deficient B cells progress down the non-ASC trajectory. Given these data, it may be suitable to rename the non-ASC branch the MBC-destined branch. While this study is in its infancy, these data suggest that cell fate outcomes, such as ASC and MBC differentiation, are programmed during the initial stages of B cell differentiation (**Figure 4-2**). Further work is needed to better understand additional factors that instruct such cell fate decisions. Moreover, additional efforts are needed to evaluate whether the non-ASC pre-memory cells acquire the transcriptional and phenotypic characteristics of mature MBC. The knowledge gained from such studies may help influence desired immune outcomes, which would have considerable therapeutic potential.

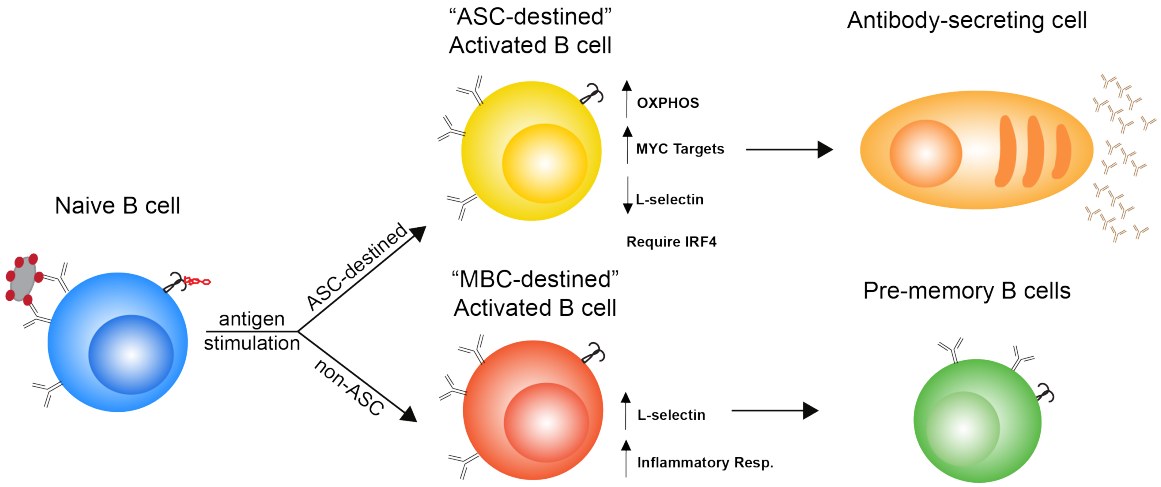

Figure 4-2. Graphical representation of the bifurcating trajectories during B cell differentiation *in vivo*. Upon antigen encounter with T cell independent type I (LPS) or II antigens (NP-ficoll), naive B cells become activated and bifurcate into ASC-destined and non-ASC trajectories. ASC-destined activated B cells upregulate gene sets critical for ASC differentiation, require IRF4, and can be distinguished by loss of L-selectin expression. Activated B cells progressing down the non-ASC trajectory appear to be memory B cell (MBC)-destined. MBC-destined actB maintain CD62L expression, express gene expression programs indicating they are responding to inflammatory stimuli, and upregulate genes previously described to characterize MBC.

Chapter 5. Discussion

Dillon G. Patterson

[1]Department of Microbiology and Immunology, and the Emory Vaccine Center, Emory University School of Medicine, Atlanta, GA 30322, USA

B cell differentiation to an antibody-secreting plasma cell (ASC) is the cornerstone of humoral immunity. This process requires substantial reprogramming to ultimately repress the naive B cell (nB) program and replace it with one conducive to ASC physiology and function [14,15]. Dysregulation during B cell differentiation can lead to hematological malignancies, autoimmunity, and short-lived or ineffective antibody responses [277]. Thus, a complete understanding of the molecular reprogramming events that occur throughout B cell differentiation is necessary to understand how these diseases arise, which may lead to novel preventative or curative therapeutic strategies. The work presented in this thesis helps to address this gap in knowledge in several ways. First, we described a novel bifurcation event during the initial stages of B cell differentiation. Some activated B cells (actB) followed a differentiation branch leading to ASC formation (termed the ASC-destined branch), and preliminary analyses suggested cells following the alternative branch are differentiating to memory B cells (MBC). Second, we designated IRF4 as one critical mediator necessary for initiation of the ASC-destined branch. Third, we detailed the IRF4-dependent division-coupled reprogramming events that occur during the initial stages of B cell differentiation. These data indicated that IRF4-deficient B cells were transcriptionally and epigenetically distinct by division 3, pinpointing the cell division in which IRF4 reprogramming is needed. Fourth, we demonstrated that part of the IRF4-dependent reprogramming of actB involves control of cell growth and proliferation through a MYC-mTORC1 network. Collectively, these data ascribe a novel role for IRF4 in controlling actB cell fate during the initial stages of B cell differentiation.

While the data presented in this thesis improves our understanding of the molecular reprogramming events leading to ASC formation, it also leads to several new questions.

We consistently demonstrated that B cell differentiation to lipopolysaccharide (LPS) required a minimum of 8 cell divisions when adoptively transferring B cells into B cell-deficient μMT mice [190]. However, one intriguing observation when examining B cell differentiation in wild-type (WT) hosts was that ASC were found as early as division 4. The requirement for 8 cell divisions was restored when host cells were prevented from responding to LPS by using MYD88-/- mice [207] as hosts. These data indicated that cell extrinsic factors secreted by LPS-responding cells in WT mice could influence the division in which ASC differentiation occurred. However, the signal(s) or cellular source(s) responsible was not determined. Cytokines that enhance differentiation of actB include IL-2, IL-10, IL-21, and TNF-α [278–280]. Monocytes, granulocytes, and B cells are major responders to LPS and can be a cellular source for cytokine-mediated regulation of ASC differentiation [279,281,282]. While μMT mice contain monocytes and granulocytes, their splenic architecture is perturbed, which may impact the signals received between cells [190]. Regardless, examining B cell differentiation in μMT mice revealed each cellular division represented a distinct stage during B cell differentiation [80,174,176,195,283]. This lends the following questions: Is reprogramming complete for ASC that form prior to division 8 in WT hosts? If so, how can reprogramming be uncoupled from cell division, and what cell extrinsic factors influence these events? Single-cell RNA-sequencing of responding cells in WT and μMT hosts indicated similar differentiation branch points occur, so it is possible the ASC-destined cell fate decisions may be happening in an earlier division in WT mice. Elucidating these differences will improve our understanding of factors that influence differentiation. Furthermore, comparing responding cells in discrete divisions in WT hosts

with comparable divisions from µMT hosts will allow us to determine which components are truly coupled to cell division compared to those influenced by extrinsic factors.

Independent of which host was used during adoptive transfers, an IRF4-dependent bifurcation event in actB was observed, with only a subset of cells proceeding along a differentiation branch to an ASC. We predicted the bifurcation event to occur around divisions 3-5 in µMT hosts, and our sequencing data using IRF4-deficient B cells in discrete divisions corroborated this prediction. However, what is unclear is how only a subset of cells initiate the IRF4-dependent program because we observed that all responding cells upregulated IRF4. Of note, there was some variability in IRF4 expression on a per cell basis, which ultimately could impact cell fate outcomes. Indeed, graded expression of IRF4 [119,120,128,129] and competition with IRF8 [116,117] can regulate cell fate outcomes. Thus, initial ratios of IRF4-to-IRF8 may explain why cells follow the ASC-destined or non-ASC branch (**Figure 5-1**).

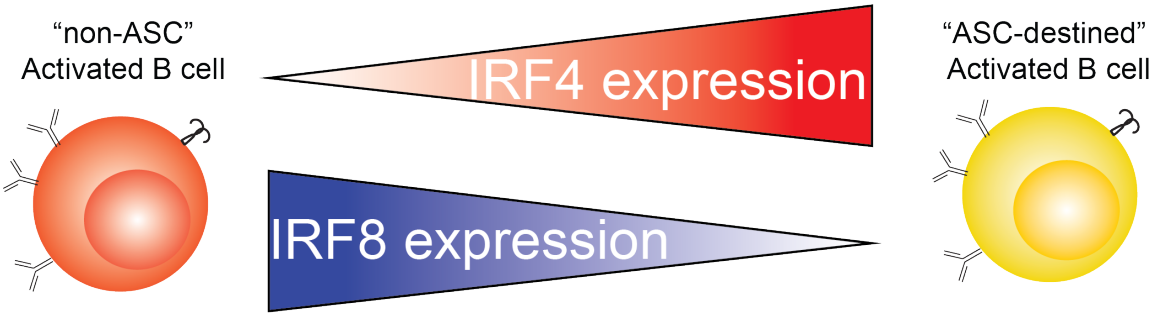

Figure 5-1. Graphical model describing how the ratio of IRF4 to IRF8 levels may shape cell fate outcomes. Following antigen encounter, stochastic differences in IRF4 and IRF8 levels may shape whether cells follow the ASC-destined or non-ASC differentiation branch. $IRF4^{high}IRF8^{low}$ cells are likely to follow the ASC-destined branch, whereas $IRF4^{low}IRF8^{high}$ cells may proceed down the non-ASC branch. IRF4 and IRF8 expression is depicted as shaded red and blue colors, respectively, with dark colors representing higher expression.

Similar roles for IRF4 and IRF8 have been described for regulation of ASC versus germinal center cell (GC) formation [116]. Part of the mechanism involves competition for ETS / AP1 binding partners and distinct genomic binding sites for IRF4 and IRF8 [116]. This mutual antagonism between factors helps to coordinate different cell fate outcomes, and a similar mechanism may be at play in our system. An alternative explanation could be that naive B cells are a heterogenous pool of cells, with a subset pre-destined to differentiate. While possible, this hypothesis is less likely because actB were observed on two differentiation paths in later cells divisions rather than at the onset of activation. As a final explanation, stochastic expression of ETS / AP1 binding partners may also occur, which would influence IRF4 activity. These hypotheses are not mutually exclusive, and several may ultimately contribute to shape the overall immune response.

In addition to the differentiation branchpoint observed in actB, a second bifurcation event was observed among differentiated ASC. Cells along both ASC paths displayed the hallmarks of ASC, including expression of *Syndecan-1* (CD138) [135,191], *Blimp1* [131], *Ell2* [138,139], and *Xbp1* [100-102]. *Xbp1*, described in detail in Chapter 1, is typically considered to be the master transcription factor regulating the unfolded protein response observed in ASC [102]. While *Xbp1* is expressed at high levels in cells on both ASC paths, the endoplasmic reticulum stress sensor *Atf6* [91,234] is uniquely expressed in ASC on only one branch. This implied that a subset of ASC were under distinct ER stress. One explanation for this observation could be that some ASC are unable to adapt to the stress of increased immunoglobulin production triggering the expression of other conserved signal transduction pathways, such as *Atf6*. This suggests that only a subset of ASC are capable of efficiently handling ER stress. This hypothesis assumes that all ASC express similar

rates of antibody. However, another explanation could be that a subset of ASC are capable of secreting higher levels of antibody, and this is reflected in increased ER stress due to increased immunoglobulin production. In either case, understanding the differences observed between the differentiated subsets would aid in our understanding of how ASC can most efficiently and effectively secrete high levels of antibody.

While our analyses have centered around the differentiation of naive B cells, MBC generated in a primary immune response have similar differentiation outcomes upon antigen reencounter. MBC, however, respond much faster and with greater magnitude than naive B cells [284-286]. In fact, MBC are epigenetically primed to differentiate to ASC, including exhibiting increased accessibility in genomic regions near hallmark ASC genes like *Blimp1* and *Irf4* [286]. Thus, extending our analyses to determine whether MBC respond with similar differentiation branch points may reveal earlier cell fate decisions for MBC. It is also known that MBC are a heterogenous population of cells, with some favoring ASC differentiation and others prone to renew the MBC pool [287]. Therefore, we may also uncover additional differentiation trajectories and factors controlling such cell fate decisions that are currently unknown.

Our analyses have centered around using T cell independent antigens to study B cell immune responses. It is also compelling to extend this analysis to T cell dependent antigens that develop additional differentiated cell types, including GC B cells, short-lived ASC, long-lived antibody-secreting plasma cells (LLPC), and MBC [53]. Each of these cell types are likely to progress down distinct differentiation trajectories, which would allow factors controlling their formation to be uncovered. Trajectory analysis relies on gradual changes in gene expression that occur over the course of differentiation to computationally

infer the order of cells [288]. Thus, to capture the transcriptional profiles of cells at all stages of differentiation, a detailed time course is needed to understand the timing of GC, ASC, MBC, and LLPC formation. Based on when the cells emerged, these data would infer the timing in which samples should be collected for single cell RNA-sequencing, which could then be combined and collapsed into one trajectory analysis. Including *bona fide* naive B cell, MBC, and bone marrow-derived mature LLPC may be necessary to improve the analysis because each would serve as anchors denoting the beginning and end stages of differentiation. These data would also include a time component; thus, one could infer when trajectories emerged. Such an analysis has been performed to model murine gut endoderm develop, which allowed the precise ordering of differentiated cell types [289].

In chapter 3, we identified IRF4 as a critical mediator of cell growth and proliferation. Part of the mechanism involved failure of IRF4-deficient B cells to upregulate *Myc* to the same levels as control B cells, which would ultimately result in reduced division capacity [68,181]. Consistently, IRF4-deficient B cells began dividing appropriately, but stalled during the proliferative response. We observed differences in *Myc* expression at 24 hours, prior to the first cell division, suggesting IRF4 fine-tunes the cell division capacity of responding B cells by controlling the initial amount of *Myc.* We speculate IRF4 directly regulates *Myc* expression in activated B cells through binding of known regulatory elements of *Myc.* Indeed, IRF4 has been shown to bind the *Myc* promoter in human multiple myeloma [169] and T cell lymphoma cell lines [257], although there is no evidence this occurs in murine cells when examining canonical IRF4 sequence motifs and IRF4 ChIP-seq data [138]. Instead, we hypothesize IRF4 fine-tunes the expression of *Myc* in murine B cells by binding to known enhancer elements [258] (**Figure 5-2**).

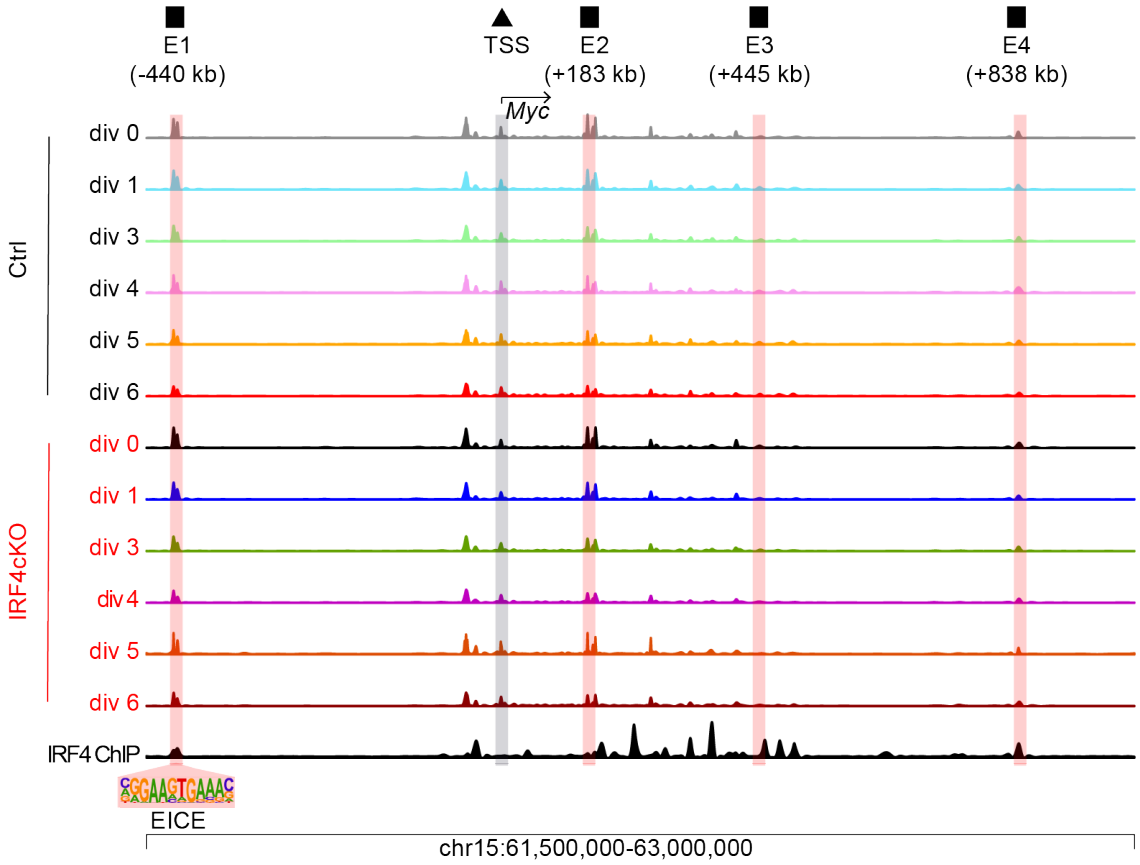

Figure 5-2. Regulatory landscape of murine *Myc*. Assay for transposase accessible chromatin-sequencing (ATAC-seq) data generated in Chapter 3. Briefly, Ctrl ($CD45.2^{+}Cd19^{+/+}Irf4^{fl/fl}$) or IRF4cKO ($CD45.2^{+}Cd19^{Cre/+}Irf4^{fl/fl}$) naive splenic B cells were CTV-labeled and adoptively transferred into μMT (CD45.1+) mice. At 24 hours post-transfer, mice were inoculated with LPS intravenously. At 72 hr post-LPS, Ctrl and IRF4cKO cells were sorted in discrete divisions for ATAC-seq. ATAC accessibility profiles for each division surrounding the murine *Myc* regulatory region are displayed. Known enhancers (E1-4) of *Myc* [258] and the transcription start site (TSS) are indicated at the top and highlighted in the gene tracks. The distance of each enhancer region from the TSS is also noted. The bottom track is previously published IRF4 ChIP-seq [138]. Motif analysis using HOMER [247] identified an ETS:IRF composite elements (EICE) [121-124] in enhancer element 1 (E1), which is displayed below the IRF4 ChIP track.

Four *Myc* enhancers have been identified in murine B cells [258]. Of these enhancer elements, IRF4 ChIP-seq generated in murine activated B cells [138] suggests IRF4 may bind two (E1 and E4) sites. Indeed, an ETS:IRF composite elements (EICE) [121-124] is observed for one

of the enhancer sites (E1) (**Figure 5-2**). While no differences in chromatin accessibility were observed in B cells with or without IRF4, this is likely due to the timing in which the samples were collected or compensatory effects of IRF8 [116,117]. Collectively, these data support the hypothesis that IRF4 may serve as a rheostat to regulate the proliferative response during B cell differentiation.

Given the data outlined above and current knowledge of the GC reaction, these data imply that IRF4 likely functions as a rheostat in GC B cells to control enhanced proliferation of high-affinity GC B cells. As detailed in Chapter 1, light zone GC B cells of varying affinities capture, process, and present antigen to T follicular helper (Tfh) cells [60]. Tfh cells select for high affinity GC B cells because of their ability to capture and present more antigen [61-64], and the signals received from Tfh cells are directly proportional to the amount of antigen captured [65,66]. These enhanced signals lead to increased proliferation in the dark zone such that with each iterative cycle, clones of increasing high affinity dominate the GC response [60]. One critical component in this signaling process involves engagement of CD40. In fact, lack of CD40 or it's ligand (CD40L), or blocking their interaction via antibodies during the GC reaction, results in a loss of GC B cells [290-293]. Importantly, CD40 and BCR signals independently induce *Irf4* expression [128,165]. Likewise, both signals are critical for induction of *Myc* and mTORC1 in GC B cells [294]. MYC expression in light-zone B cells is proportion to Tfh cell help, which determines the cell division capacity of dark zone GC B cells [68]. Induction of mTORC1 permits cell cycle entry of light zone GC B cells [294] and enables GC B cells to sustain extensive cell division in the dark zone [295]. Collectively, these studies suggest that a similar IRF4-MYC-mTORC1 integrated network described in this thesis may be controlling the proliferative response

during a GC reaction. If this is indeed the case, *Irf4* expression levels must be tightly coordinated following signals from Tfh cells because high levels of IRF4 bias light zone GZ B cells to an ASC fate over GC cyclic reentry [296].

In summary, this work uncovered novel aspects of B cell differentiation and focused on the role of IRF4 in controlling cell fate outcomes during the initial stages of B cell activation, including cell proliferation, cell growth, and ASC formation. We discovered that responding activated B cells are progressing down two distinct differentiation trajectories during the initial stages of B cell activation, with one branch leading to ASC (termed the ASC-destined branch) and another leading to cells displaying a pre-memory B cell transcriptional signature (originally termed the non-ASC branch). We demonstrated IRF4 as one factor essential for establishing the ASC-destined program, which was launched by division 3. A part of the IRF4-dependent reprogramming involved control of cell growth and the proliferative capacity of responding B cells. Part of the mechanism involved regulation of MYC and mTORC1 activity, and this occurred during the initial cell divisions during B cell differentiation. Collectively, these data indicate that B cell fates are instructed during the initial stages of B cell activation, which may therapeutically beneficial if exploited to modulate immune responses to a desired outcome.

References

1. Bloch H. Edward Jenner (1749-1823). The history and effects of smallpox, inoculation, and vaccination. *Am J Dis Child*. 1993;147(7):772-774.

2. Riedel S. Edward Jenner and the history of smallpox and vaccination. *Proc (Bayl Univ Med Cent)*. 2005;18(1):21-25.

3. Smith KA. Louis pasteur, the father of immunology? *Front Immunol*. 2012;3:68.

4. Kitasato EvBaS. The mechanism of immunity in animals to diphteria and tetanus. *Deutscbe Medizhiscbe Wocbenschift*. 1890;16:1113-1114.

5. Schenck HP. The plasma cell theory of antibody formation; its importance in the interpretation of the physiology of the lymphoid structures of Waldeyer's ring. *Ann Otol Rhinol Laryngol*. 1955;64(1):109-118.

6. Bjorneboe M, Gormsen H, Lundquist F. Further experimental studies on the role of the plasma cells as antibody producers. *J Immunol*. 1947;55(2):121-129.

7. Fagraeus A. Plasma cellular reaction and its relation to the formation of antibodies in vitro. *Nature*. 1947;159(4041):499.

8. Cooper MD, Peterson RD, Good RA. Delineation of the Thymic and Bursal Lymphoid Systems in the Chicken. *Nature*. 1965;205:143-146.

9. Dent PB, Good RA. Absence of antibody production in the bursa of Fabricius. *Nature*. 1965;207(996):491-493.

10. Kemenes F, Pethes G. Further Evidence for the Role of the Bursa of Fabricius in Antibody Production in Chickens. *Z Immunitats Allergieforsch*. 1963;125:446-458.

11. Mueller AP, Wolfe HR, Meyer RK, Aspinall RL. Further studies on the role of the bursa of Fabricius in antibody production. *J Immunol*. 1962;88:354-360.

12. Martin F, Chan AC. Pathogenic roles of B cells in human autoimmunity; insights from the clinic. *Immunity*. 2004;20(5):517-527.

13. Nussenzweig MC, Alt FW. Antibody diversity: one enzyme to rule them all. *Nat Med*. 2004;10(12):1304-1305.

14. Nutt SL, Hodgkin PD, Tarlinton DM, Corcoran LM. The generation of antibody-secreting plasma cells. *Nat Rev Immunol*. 2015;15(3):160-171.

15. Nutt SL, Taubenheim N, Hasbold J, Corcoran LM, Hodgkin PD. The genetic network controlling plasma cell differentiation. *Semin Immunol*. 2011;23(5):341-349.

16. Loffert D, Schaal S, Ehlich A, et al. Early B-cell development in the mouse: insights from mutations introduced by gene targeting. *Immunol Rev*. 1994;137:135-153.

17. Busslinger M. Transcriptional control of early B cell development. *Annu Rev Immunol*. 2004;22:55-79.

18. Kondo M, Weissman IL, Akashi K. Identification of clonogenic common lymphoid progenitors in mouse bone marrow. *Cell*. 1997;91(5):661-672.

19. Kondo M. Lymphoid and myeloid lineage commitment in multipotent hematopoietic progenitors. *Immunol Rev*. 2010;238(1):37-46.

20. Akashi K, Traver D, Miyamoto T, Weissman IL. A clonogenic common myeloid progenitor that gives rise to all myeloid lineages. *Nature*. 2000;404(6774):193-197.

21. Adolfsson J, Borge OJ, Bryder D, et al. Upregulation of Flt3 expression within the bone marrow Lin(-)Sca1(+)c-kit(+) stem cell compartment is accompanied by loss of self-renewal capacity. *Immunity*. 2001;15(4):659-669.

22. Mackarehtschian K, Hardin JD, Moore KA, Boast S, Goff SP, Lemischka IR. Targeted disruption of the flk2/flt3 gene leads to deficiencies in primitive hematopoietic progenitors. *Immunity*. 1995;3(1):147-161.

23. McKenna HJ, Stocking KL, Miller RE, et al. Mice lacking flt3 ligand have deficient hematopoiesis affecting hematopoietic progenitor cells, dendritic cells, and natural killer cells. *Blood*. 2000;95(11):3489-3497.

24. Sitnicka E, Bryder D, Theilgaard-Monch K, Buza-Vidas N, Adolfsson J, Jacobsen SE. Key role of flt3 ligand in regulation of the common lymphoid progenitor but not in maintenance of the hematopoietic stem cell pool. *Immunity*. 2002;17(4):463-472.

25. Bain G, Maandag EC, Izon DJ, et al. E2A proteins are required for proper B cell development and initiation of immunoglobulin gene rearrangements. *Cell*. 1994;79(5):885-892.

26. Zhuang Y, Soriano P, Weintraub H. The helix-loop-helix gene E2A is required for B cell formation. *Cell*. 1994;79(5):875-884.

27. Hagman J, Belanger C, Travis A, Turck CW, Grosschedl R. Cloning and functional characterization of early B-cell factor, a regulator of lymphocyte-specific gene expression. *Genes Dev*. 1993;7(5):760-773.

28. Georgopoulos K. Haematopoietic cell-fate decisions, chromatin regulation and ikaros. *Nat Rev Immunol*. 2002;2(3):162-174.

29. Wang JH, Nichogiannopoulou A, Wu L, et al. Selective defects in the development of the fetal and adult lymphoid system in mice with an Ikaros null mutation. *Immunity*. 1996;5(6):537-549.

30. Scott EW, Simon MC, Anastasi J, Singh H. Requirement of transcription factor PU.1 in the development of multiple hematopoietic lineages. *Science*. 1994;265(5178):1573-1577.

31. DeKoter RP, Singh H. Regulation of B lymphocyte and macrophage development by graded expression of PU.1. *Science*. 2000;288(5470):1439-1441.

32. Cobaleda C, Schebesta A, Delogu A, Busslinger M. Pax5: the guardian of B cell identity and function. *Nat Immunol*. 2007;8(5):463-470.

33. Nutt SL, Heavey B, Rolink AG, Busslinger M. Commitment to the B-lymphoid lineage depends on the transcription factor Pax5. *Nature*. 1999;401(6753):556-562.

34. Romanow WJ, Langerak AW, Goebel P, et al. E2A and EBF act in synergy with the V(D)J recombinase to generate a diverse immunoglobulin repertoire in nonlymphoid cells. *Mol Cell*. 2000;5(2):343-353.

35. Alt FW, Yancopoulos GD, Blackwell TK, et al. Ordered rearrangement of immunoglobulin heavy chain variable region segments. *EMBO J*. 1984;3(6):1209-1219.

36. Jung D, Giallourakis C, Mostoslavsky R, Alt FW. Mechanism and control of V(D)J recombination at the immunoglobulin heavy chain locus. *Annu Rev Immunol*. 2006;24:541-570.

37. Sakaguchi N, Melchers F. Lambda 5, a new light-chain-related locus selectively expressed in pre-B lymphocytes. *Nature*. 1986;324(6097):579-582.

38. Vettermann C, Herrmann K, Jack HM. Powered by pairing: the surrogate light chain amplifies immunoglobulin heavy chain signaling and pre-selects the antibody repertoire. *Semin Immunol*. 2006;18(1):44-55.

39. Kraus M, Alimzhanov MB, Rajewsky N, Rajewsky K. Survival of resting mature B lymphocytes depends on BCR signaling via the Igalpha/beta heterodimer. *Cell*. 2004;117(6):787-800.

40. Herzog S, Reth M, Jumaa H. Regulation of B-cell proliferation and differentiation by pre-B-cell receptor signalling. *Nat Rev Immunol*. 2009;9(3):195-205.

41. Melchers F, ten Boekel E, Seidl T, et al. Repertoire selection by pre-B-cell receptors and B-cell receptors, and genetic control of B-cell development from immature to mature B cells. *Immunol Rev*. 2000;175:33-46.

42. Hartley SB, Crosbie J, Brink R, Kantor AB, Basten A, Goodnow CC. Elimination from peripheral lymphoid tissues of self-reactive B lymphocytes recognizing membrane-bound antigens. *Nature*. 1991;353(6346):765-769.

43. Nemazee DA, Burki K. Clonal deletion of B lymphocytes in a transgenic mouse bearing anti-MHC class I antibody genes. *Nature*. 1989;337(6207):562-566.

44. Macallan DC, Wallace DL, Zhang Y, et al. B-cell kinetics in humans: rapid turnover of peripheral blood memory cells. *Blood*. 2005;105(9):3633-3640.

45. Sprent J, Basten A. Circulating T and B lymphocytes of the mouse. II. Lifespan. *Cell Immunol*. 1973;7(1):40-59.

46. Greiff V, Miho E, Menzel U, Reddy ST. Bioinformatic and Statistical Analysis of Adaptive Immune Repertoires. *Trends Immunol*. 2015;36(11):738-749.

47. Allman D, Wilmore JR, Gaudette BT. The continuing story of T-cell independent antibodies. *Immunol Rev*. 2019;288(1):128-135.

48. Mond JJ, Lees A, Snapper CM. T cell-independent antigens type 2. *Annu Rev Immunol*. 1995;13:655-692.

49. Obukhanych TV, Nussenzweig MC. T-independent type II immune responses generate memory B cells. *J Exp Med*. 2006;203(2):305-310.

50. Bortnick A, Chernova I, Quinn WJ, 3rd, Mugnier M, Cancro MP, Allman D. Long-lived bone marrow plasma cells are induced early in response to T cell-independent or T cell-dependent antigens. *J Immunol*. 2012;188(11):5389-5396.

51. Foote JB, Mahmoud TI, Vale AM, Kearney JF. Long-term maintenance of polysaccharide-specific antibodies by IgM-secreting cells. *J Immunol*. 2012;188(1):57-67.

52. Taillardet M, Haffar G, Mondiere P, et al. The thymus-independent immunity conferred by a pneumococcal polysaccharide is mediated by long-lived plasma cells. *Blood*. 2009;114(20):4432-4440.

53. Victora GD, Nussenzweig MC. Germinal centers. *Annu Rev Immunol*. 2012;30:429-457.

54. Berek C, Berger A, Apel M. Maturation of the immune response in germinal centers. *Cell*. 1991;67(6):1121-1129.

55. Muramatsu M, Kinoshita K, Fagarasan S, Yamada S, Shinkai Y, Honjo T. Class switch recombination and hypermutation require activation-induced cytidine deaminase (AID), a potential RNA editing enzyme. *Cell*. 2000;102(5):553-563.

56. Crotty S. T follicular helper cell differentiation, function, and roles in disease. *Immunity*. 2014;41(4):529-542.

57. Vinuesa CG, Linterman MA, Yu D, MacLennan IC. Follicular Helper T Cells. *Annu Rev Immunol*. 2016;34:335-368.

58. Nieuwenhuis P, Opstelten D. Functional anatomy of germinal centers. *Am J Anat*. 1984;170(3):421-435.

59. Kennedy DE, Okoreeh MK, Maienschein-Cline M, et al. Novel specialized cell state and spatial compartments within the germinal center. *Nat Immunol*. 2020;21(6):660-670.

60. De Silva NS, Klein U. Dynamics of B cells in germinal centres. *Nat Rev Immunol*. 2015;15(3):137-148.

61. Depoil D, Zaru R, Guiraud M, et al. Immunological synapses are versatile structures enabling selective T cell polarization. *Immunity*. 2005;22(2):185-194.

62. Shulman Z, Gitlin AD, Weinstein JS, et al. Dynamic signaling by T follicular helper cells during germinal center B cell selection. *Science*. 2014;345(6200):1058-1062.

63. Victora GD, Dominguez-Sola D, Holmes AB, Deroubaix S, Dalla-Favera R, Nussenzweig MC. Identification of human germinal center light and dark zone cells and their relationship to human B-cell lymphomas. *Blood*. 2012;120(11):2240-2248.

64. Vinuesa CG, Tangye SG, Moser B, Mackay CR. Follicular B helper T cells in antibody responses and autoimmunity. *Nat Rev Immunol*. 2005;5(11):853-865.

65. Gitlin AD, Shulman Z, Nussenzweig MC. Clonal selection in the germinal centre by regulated proliferation and hypermutation. *Nature*. 2014;509(7502):637-640.

66. Victora GD, Schwickert TA, Fooksman DR, et al. Germinal center dynamics revealed by multiphoton microscopy with a photoactivatable fluorescent reporter. *Cell*. 2010;143(4):592-605.

67. Dominguez-Sola D, Victora GD, Ying CY, et al. The proto-oncogene MYC is required for selection in the germinal center and cyclic reentry. *Nat Immunol*. 2012;13(11):1083-1091.

68. Finkin S, Hartweger H, Oliveira TY, Kara EE, Nussenzweig MC. Protein Amounts of the MYC Transcription Factor Determine Germinal Center B Cell Division Capacity. *Immunity*. 2019.

69. Zotos D, Tarlinton DM. Determining germinal centre B cell fate. *Trends Immunol*. 2012;33(6):281-288.

70. Shlomchik MJ, Weisel F. Germinal center selection and the development of memory B and plasma cells. *Immunol Rev*. 2012;247(1):52-63.

71. Forthal DN. Functions of Antibodies. *Microbiol Spectr*. 2014;2(4):AID-0019-2014.

72. Shi W, Liao Y, Willis SN, et al. Transcriptional profiling of mouse B cell terminal differentiation defines a signature for antibody-secreting plasma cells. *Nat Immunol*. 2015;16(6):663-673.

73. Aronov M, Tirosh B. Metabolic Control of Plasma Cell Differentiation- What We Know and What We Don't Know. *J Clin Immunol*. 2016;36 Suppl 1:12-17.

74. Wiggins KJ, Scharer CD. Roadmap to a plasma cell: Epigenetic and transcriptional cues that guide B cell differentiation. *Immunol Rev*. 2021;300(1):54-64.

75. Waffarn EE, Baumgarth N. Protective B cell responses to flu--no fluke! *J Immunol*. 2011;186(7):3823-3829.

76. Woodruff MC, Ramonell RP, Nguyen DC, et al. Extrafollicular B cell responses correlate with neutralizing antibodies and morbidity in COVID-19. *Nat Immunol*. 2020;21(12):1506-1516.

77. Vose BM, Bonnard GD. Limiting dilution analysis of the frequency of human T cells and large granular lymphocytes proliferating in response to interleukin 2. I. The effect of lectin on the proliferative frequency and cytotoxic activity of cultured lymphoid cells. *J Immunol*. 1983;130(2):687-693.

78. Boothby M, Rickert RC. Metabolic Regulation of the Immune Humoral Response. *Immunity*. 2017;46(5):743-755.

79. Dufort FJ, Bleiman BF, Gumina MR, et al. Cutting edge: IL-4-mediated protection of primary B lymphocytes from apoptosis via Stat6-dependent regulation of glycolytic metabolism. *J Immunol*. 2007;179(8):4953-4957.

80. Price MJ, Patterson DG, Scharer CD, Boss JM. Progressive Upregulation of Oxidative Metabolism Facilitates Plasmablast Differentiation to a T-Independent Antigen. *Cell Rep*. 2018;23(11):3152-3159.

81. Weisel FJ, Mullett SJ, Elsner RA, et al. Germinal center B cells selectively oxidize fatty acids for energy while conducting minimal glycolysis. *Nat Immunol*. 2020;21(3):331-342.

82. Saijo K, Mecklenbrauker I, Santana A, Leitger M, Schmedt C, Tarakhovsky A. Protein kinase C beta controls nuclear factor kappaB activation in B cells through selective regulation of the IkappaB kinase alpha. *J Exp Med*. 2002;195(12):1647-1652.

83. Su TT, Guo B, Kawakami Y, et al. PKC-beta controls I kappa B kinase lipid raft recruitment and activation in response to BCR signaling. *Nat Immunol*. 2002;3(8):780-786.

84. Sanchez WY, McGee SL, Connor T, et al. Dichloroacetate inhibits aerobic glycolysis in multiple myeloma cells and increases sensitivity to bortezomib. *Br J Cancer*. 2013;108(8):1624-1633.

85. Shen YC, Ou DL, Hsu C, et al. Activating oxidative phosphorylation by a pyruvate dehydrogenase kinase inhibitor overcomes sorafenib resistance of hepatocellular carcinoma. *Br J Cancer*. 2013;108(1):72-81.

86. Stockwin LH, Yu SX, Borgel S, et al. Sodium dichloroacetate selectively targets cells with defects in the mitochondrial ETC. *Int J Cancer*. 2010;127(11):2510-2519.

87. Sil P, Muse G, Martinez J. A ravenous defense: canonical and non-canonical autophagy in immunity. *Curr Opin Immunol*. 2018;50:21-31.

88. Cenci S. Autophagy, a new determinant of plasma cell differentiation and antibody responses. *Mol Immunol*. 2014;62(2):289-295.

89. Pengo N, Scolari M, Oliva L, et al. Plasma cells require autophagy for sustainable immunoglobulin production. *Nat Immunol*. 2013;14(3):298-305.

90. Hetz C, Zhang K, Kaufman RJ. Mechanisms, regulation and functions of the unfolded protein response. *Nat Rev Mol Cell Biol*. 2020;21(8):421-438.

91. Ron D, Walter P. Signal integration in the endoplasmic reticulum unfolded protein response. *Nat Rev Mol Cell Biol*. 2007;8(7):519-529.

92. Harding HP, Zhang Y, Ron D. Protein translation and folding are coupled by an endoplasmic-reticulum-resident kinase. *Nature*. 1999;397(6716):271-274.

93. Harding HP, Novoa I, Zhang Y, et al. Regulated translation initiation controls stress-induced gene expression in mammalian cells. *Molecular cell*. 2000;6(5):1099-1108.

94. Ma Y, Shimizu Y, Mann MJ, Jin Y, Hendershot LM. Plasma cell differentiation initiates a limited ER stress response by specifically suppressing the PERK-dependent branch of the unfolded protein response. *Cell Stress Chaperones*. 2010;15(3):281-293.

95. Gass JN, Jiang HY, Wek RC, Brewer JW. The unfolded protein response of B-lymphocytes: PERK-independent development of antibody-secreting cells. *Mol Immunol*. 2008;45(4):1035-1043.

96. Masciarelli S, Fra AM, Pengo N, et al. CHOP-independent apoptosis and pathway-selective induction of the UPR in developing plasma cells. *Mol Immunol*. 2010;47(6):1356-1365.

97. Marciniak SJ, Yun CY, Oyadomari S, et al. CHOP induces death by promoting protein synthesis and oxidation in the stressed endoplasmic reticulum. *Genes Dev*. 2004;18(24):3066-3077.

98. Puthalakath H, O'Reilly LA, Gunn P, et al. ER stress triggers apoptosis by activating BH3-only protein Bim. *Cell*. 2007;129(7):1337-1349.

99. Aragon IV, Barrington RA, Jackowski S, Mori K, Brewer JW. The specialized unfolded protein response of B lymphocytes: ATF6alpha-independent development of antibody-secreting B cells. *Mol Immunol*. 2012;51(3-4):347-355.

100. Yoshida H, Matsui T, Yamamoto A, Okada T, Mori K. XBP1 mRNA is induced by ATF6 and spliced by IRE1 in response to ER stress to produce a highly active transcription factor. *Cell*. 2001;107(7):881-891.

101. Sriburi R, Jackowski S, Mori K, Brewer JW. XBP1: a link between the unfolded protein response, lipid biosynthesis, and biogenesis of the endoplasmic reticulum. *J Cell Biol*. 2004;167(1):35-41.

102. Shaffer AL, Shapiro-Shelef M, Iwakoshi NN, et al. XBP1, downstream of Blimp-1, expands the secretory apparatus and other organelles, and increases protein synthesis in plasma cell differentiation. *Immunity*. 2004;21(1):81-93.

103. McGehee AM, Dougan SK, Klemm EJ, et al. XBP-1-deficient plasmablasts show normal protein folding but altered glycosylation and lipid synthesis. *J Immunol*. 2009;183(6):3690-3699.

104. Taubenheim N, Tarlinton DM, Crawford S, Corcoran LM, Hodgkin PD, Nutt SL. High rate of antibody secretion is not integral to plasma cell differentiation as revealed by XBP-1 deficiency. *J Immunol*. 2012;189(7):3328-3338.

105. Gaudette BT, Jones DD, Bortnick A, Argon Y, Allman D. mTORC1 coordinates an immediate unfolded protein response-related transcriptome in activated B cells preceding antibody secretion. *Nat Commun*. 2020;11(1):723.

106. Schebesta A, McManus S, Salvagiotto G, Delogu A, Busslinger GA, Busslinger M. Transcription factor Pax5 activates the chromatin of key genes involved in B cell signaling, adhesion, migration, and immune function. *Immunity*. 2007;27(1):49-63.

107. Muto A, Ochiai K, Kimura Y, et al. Bach2 represses plasma cell gene regulatory network in B cells to promote antibody class switch. *EMBO J*. 2010;29(23):4048-4061.

108. Muto A, Tashiro S, Nakajima O, et al. The transcriptional programme of antibody class switching involves the repressor Bach2. *Nature*. 2004;429(6991):566-571.

109. Ochiai K, Katoh Y, Ikura T, et al. Plasmacytic transcription factor Blimp-1 is repressed by Bach2 in B cells. *The Journal of biological chemistry*. 2006;281(50):38226-38234.

110. Vilagos B, Hoffmann M, Souabni A, et al. Essential role of EBF1 in the generation and function of distinct mature B cell types. *J Exp Med*. 2012;209(4):775-792.

111. Fukuda T, Yoshida T, Okada S, et al. Disruption of the Bcl6 gene results in an impaired germinal center formation. *J Exp Med*. 1997;186(3):439-448.

112. Shaffer AL, Yu X, He Y, Boldrick J, Chan EP, Staudt LM. BCL-6 represses genes that function in lymphocyte differentiation, inflammation, and cell cycle control. *Immunity*. 2000;13(2):199-212.

113. Tunyaplin C, Shaffer AL, Angelin-Duclos CD, Yu X, Staudt LM, Calame KL. Direct repression of prdm1 by Bcl-6 inhibits plasmacytic differentiation. *J Immunol*. 2004;173(2):1158-1165.

114. Dent AL, Shaffer AL, Yu X, Allman D, Staudt LM. Control of inflammation, cytokine expression, and germinal center formation by BCL-6. *Science*. 1997;276(5312):589-592.

115. Huang C, Geng H, Boss I, Wang L, Melnick A. Cooperative transcriptional repression by BCL6 and BACH2 in germinal center B-cell differentiation. *Blood*. 2014;123(7):1012-1020.

116. Xu H, Chaudhri VK, Wu Z, et al. Regulation of bifurcating B cell trajectories by mutual antagonism between transcription factors IRF4 and IRF8. *Nat Immunol*. 2015;16(12):1274-1281.

117. Carotta S, Willis SN, Hasbold J, et al. The transcription factors IRF8 and PU.1 negatively regulate plasma cell differentiation. *J Exp Med*. 2014;211(11):2169-2181.

118. Klein U, Casola S, Cattoretti G, et al. Transcription factor IRF4 controls plasma cell differentiation and class-switch recombination. *Nat Immunol*. 2006;7(7):773-782.

119. Sciammas R, Shaffer AL, Schatz JH, Zhao H, Staudt LM, Singh H. Graded expression of interferon regulatory factor-4 coordinates isotype switching with plasma cell differentiation. *Immunity*. 2006;25(2):225-236.

120. Ochiai K, Maienschein-Cline M, Simonetti G, et al. Transcriptional regulation of germinal center B and plasma cell fates by dynamical control of IRF4. *Immunity*. 2013;38(5):918-929.

121. Brass AL, Kehrli E, Eisenbeis CF, Storb U, Singh H. Pip, a lymphoid-restricted IRF, contains a regulatory domain that is important for autoinhibition and ternary complex formation with the Ets factor PU.1. *Genes Dev*. 1996;10(18):2335-2347.

122. Brass AL, Zhu AQ, Singh H. Assembly requirements of PU.1-Pip (IRF-4) activator complexes: inhibiting function in vivo using fused dimers. *EMBO J*. 1999;18(4):977-991.

123. Eisenbeis CF, Singh H, Storb U. Pip, a novel IRF family member, is a lymphoid-specific, PU.1-dependent transcriptional activator. *Genes Dev*. 1995;9(11):1377-1387.

124. Escalante CR, Brass AL, Pongubala JM, et al. Crystal structure of PU.1/IRF-4/DNA ternary complex. *Mol Cell*. 2002;10(5):1097-1105.

125. Glasmacher E, Agrawal S, Chang AB, et al. A genomic regulatory element that directs assembly and function of immune-specific AP-1-IRF complexes. *Science*. 2012;338(6109):975-980.

126. Ciofani M, Madar A, Galan C, et al. A validated regulatory network for Th17 cell specification. *Cell*. 2012;151(2):289-303.

127. Li P, Spolski R, Liao W, et al. BATF-JUN is critical for IRF4-mediated transcription in T cells. *Nature*. 2012;490(7421):543-546.

128. Sciammas R, Li Y, Warmflash A, Song Y, Dinner AR, Singh H. An incoherent regulatory network architecture that orchestrates B cell diversification in response to antigen signaling. *Mol Syst Biol*. 2011;7:495.

129. Krishnamoorthy V, Kannanganat S, Maienschein-Cline M, et al. The IRF4 Gene Regulatory Module Functions as a Read-Write Integrator to Dynamically Coordinate T Helper Cell Fate. *Immunity*. 2017;47(3):481-497 e487.

130. Zhao GN, Jiang DS, Li H. Interferon regulatory factors: at the crossroads of immunity, metabolism, and disease. *Biochim Biophys Acta*. 2015;1852(2):365-378.

131. Shaffer AL, Lin KI, Kuo TC, et al. Blimp-1 orchestrates plasma cell differentiation by extinguishing the mature B cell gene expression program. *Immunity*. 2002;17(1):51-62.

132. Lin Y, Wong K, Calame K. Repression of c-myc transcription by Blimp-1, an inducer of terminal B cell differentiation. *Science*. 1997;276(5312):596-599.

133. Lin KI, Lin Y, Calame K. Repression of c-myc is necessary but not sufficient for terminal differentiation of B lymphocytes in vitro. *Mol Cell Biol*. 2000;20(23):8684-8695.

134. Lin KI, Angelin-Duclos C, Kuo TC, Calame K. Blimp-1-dependent repression of Pax-5 is required for differentiation of B cells to immunoglobulin M-secreting plasma cells. *Mol Cell Biol*. 2002;22(13):4771-4780.

135. Kallies A, Hasbold J, Tarlinton DM, et al. Plasma cell ontogeny defined by quantitative changes in blimp-1 expression. *J Exp Med*. 2004;200(8):967-977.

136. Sciammas R, Davis MM. Modular nature of Blimp-1 in the regulation of gene expression during B cell maturation. *J Immunol*. 2004;172(9):5427-5440.

137. Piskurich JF, Lin KI, Lin Y, Wang Y, Ting JP, Calame K. BLIMP-I mediates extinction of major histocompatibility class II transactivator expression in plasma cells. *Nat Immunol*. 2000;1(6):526-532.

138. Minnich M, Tagoh H, Bonelt P, et al. Multifunctional role of the transcription factor Blimp-1 in coordinating plasma cell differentiation. *Nat Immunol*. 2016;17(3):331-343.

139. Tellier J, Shi W, Minnich M, et al. Blimp-1 controls plasma cell function through the regulation of immunoglobulin secretion and the unfolded protein response. *Nat Immunol*. 2016;17(3):323-330.

140. Liu GJ, Jaritz M, Wohner M, et al. Repression of the B cell identity factor Pax5 is not required for plasma cell development. *J Exp Med*. 2020;217(11).

141. Pridans C, Holmes ML, Polli M, et al. Identification of Pax5 target genes in early B cell differentiation. *J Immunol*. 2008;180(3):1719-1728.

142. Decker T, Pasca di Magliano M, McManus S, et al. Stepwise activation of enhancer and promoter regions of the B cell commitment gene Pax5 in early lymphopoiesis. *Immunity*. 2009;30(4):508-520.

143. Lu R, Medina KL, Lancki DW, Singh H. IRF-4,8 orchestrate the pre-B-to-B transition in lymphocyte development. *Genes Dev*. 2003;17(14):1703-1708.

144. Pongubala JM, Nagulapalli S, Klemsz MJ, McKercher SR, Maki RA, Atchison ML. PU.1 recruits a second nuclear factor to a site important for immunoglobulin kappa 3' enhancer activity. *Mol Cell Biol*. 1992;12(1):368-378.

145. Eisenbeis CF, Singh H, Storb U. PU.1 is a component of a multiprotein complex which binds an essential site in the murine immunoglobulin lambda 2-4 enhancer. *Mol Cell Biol*. 1993;13(10):6452-6461.

146. Ma S, Turetsky A, Trinh L, Lu R. IFN regulatory factor 4 and 8 promote Ig light chain kappa locus activation in pre-B cell development. *J Immunol*. 2006;177(11):7898-7904.

147. Nemazee D. Mechanisms of central tolerance for B cells. *Nat Rev Immunol*. 2017;17(5):281-294.

148. Halverson R, Torres RM, Pelanda R. Receptor editing is the main mechanism of B cell tolerance toward membrane antigens. *Nat Immunol*. 2004;5(6):645-650.

149. Pathak S, Ma S, Trinh L, Lu R. A role for interferon regulatory factor 4 in receptor editing. *Mol Cell Biol*. 2008;28(8):2815-2824.

150. Bevington S, Boyes J. Transcription-coupled eviction of histones H2A/H2B governs V(D)J recombination. *EMBO J*. 2013;32(10):1381-1392.

151. Shukla V, Lu R. IRF4 and IRF8: Governing the virtues of B Lymphocytes. *Front Biol (Beijing)*. 2014;9(4):269-282.

152. Mittrucker HW, Matsuyama T, Grossman A, et al. Requirement for the transcription factor LSIRF/IRF4 for mature B and T lymphocyte function. *Science*. 1997;275(5299):540-543.

153. Willis SN, Good-Jacobson KL, Curtis J, et al. Transcription factor IRF4 regulates germinal center cell formation through a B cell-intrinsic mechanism. *J Immunol*. 2014;192(7):3200-3206.

154. Durandy A. Activation-induced cytidine deaminase: a dual role in class-switch recombination and somatic hypermutation. *Eur J Immunol*. 2003;33(8):2069-2073.

155. Ye BH, Cattoretti G, Shen Q, et al. The BCL-6 proto-oncogene controls germinal-centre formation and Th2-type inflammation. *Nat Genet*. 1997;16(2):161-170.

156. Klein U, Tu Y, Stolovitzky GA, et al. Transcriptional analysis of the B cell germinal center reaction. *Proc Natl Acad Sci U S A*. 2003;100(5):2639-2644.

157. Price MJ, Scharer CD, Kania AK, Randall TD, Boss JM. Conserved Epigenetic Programming and Enhanced Heme Metabolism Drive Memory B Cell Reactivation. *J Immunol*. 2021.

158. Low MSY, Brodie EJ, Fedele PL, et al. IRF4 Activity Is Required in Established Plasma Cells to Regulate Gene Transcription and Mitochondrial Homeostasis. *Cell Rep*. 2019;29(9):2634-2645 e2635.

159. Pathak S, Ma S, Trinh L, et al. IRF4 is a suppressor of c-Myc induced B cell leukemia. *PLoS One*. 2011;6(7):e22628.

160. Ma S, Shukla V, Fang L, Gould KA, Joshi SS, Lu R. Accelerated development of chronic lymphocytic leukemia in New Zealand Black mice expressing a low level of interferon regulatory factor 4. *J Biol Chem*. 2013;288(37):26430-26440.

161. Shukla V, Ma S, Hardy RR, Joshi SS, Lu R. A role for IRF4 in the development of CLL. *Blood*. 2013;122(16):2848-2855.

162. Chang CC, Lorek J, Sabath DE, et al. Expression of MUM1/IRF4 correlates with clinical outcome in patients with B-cell chronic lymphocytic leukemia. *Blood*. 2002;100(13):4671-4675.

163. Alizadeh AA, Eisen MB, Davis RE, et al. Distinct types of diffuse large B-cell lymphoma identified by gene expression profiling. *Nature*. 2000;403(6769):503-511.

164. Mandelbaum J, Bhagat G, Tang H, et al. BLIMP1 is a tumor suppressor gene frequently disrupted in activated B cell-like diffuse large B cell lymphoma. *Cancer Cell*. 2010;18(6):568-579.

165. Saito M, Gao J, Basso K, et al. A signaling pathway mediating downregulation of BCL6 in germinal center B cells is blocked by BCL6 gene alterations in B cell lymphoma. *Cancer Cell*. 2007;12(3):280-292.

166. Kuppers R, Sousa AB, Baur AS, Strickler JG, Rajewsky K, Hansmann ML. Common germinal-center B-cell origin of the malignant cells in two composite lymphomas, involving classical Hodgkin's disease and either follicular lymphoma or B-CLL. *Mol Med*. 2001;7(5):285-292.

167. Aldinucci D, Celegato M, Borghese C, Colombatti A, Carbone A. IRF4 silencing inhibits Hodgkin lymphoma cell proliferation, survival and CCL5 secretion. *Br J Haematol*. 2011;152(2):182-190.

168. Shaffer AL, Emre NC, Romesser PB, Staudt LM. IRF4: Immunity. Malignancy! Therapy? *Clin Cancer Res*. 2009;15(9):2954-2961.

169. Shaffer AL, Emre NC, Lamy L, et al. IRF4 addiction in multiple myeloma. *Nature*. 2008;454(7201):226-231.

170. Jelinek DF, Lipsky PE. The role of B cell proliferation in the generation of immunoglobulin-secreting cells in man. *J Immunol*. 1983;130(6):2597-2604.

171. Quah BJ, Parish CR. New and improved methods for measuring lymphocyte proliferation in vitro and in vivo using CFSE-like fluorescent dyes. *J Immunol Methods*. 2012;379(1-2):1-14.

172. Heinzel S, Marchingo JM, Horton MB, Hodgkin PD. The regulation of lymphocyte activation and proliferation. *Curr Opin Immunol*. 2018;51:32-38.

173. Tangye SG, Hodgkin PD. Divide and conquer: the importance of cell division in regulating B-cell responses. *Immunology*. 2004;112(4):509-520.

174. Barwick BG, Scharer CD, Bally APR, Boss JM. Plasma cell differentiation is coupled to division-dependent DNA hypomethylation and gene regulation. *Nat Immunol*. 2016;17(10):1216-1225.

175. Scharer CD, Barwick BG, Guo M, Bally APR, Boss JM. Plasma cell differentiation is controlled by multiple cell division-coupled epigenetic programs. *Nat Commun*. 2018;9(1):1698.

176. Scharer CD, Patterson DG, Mi T, Price MJ, Hicks SL, Boss JM. Antibody-secreting cell destiny emerges during the initial stages of B-cell activation. *Nat Commun*. 2020;11(1):3989.

177. Deenick EK, Hasbold J, Hodgkin PD. Switching to IgG3, IgG2b, and IgA is division linked and independent, revealing a stochastic framework for describing differentiation. *J Immunol*. 1999;163(9):4707-4714.

178. Dowling MR, Kan A, Heinzel S, et al. Stretched cell cycle model for proliferating lymphocytes. *Proc Natl Acad Sci U S A*. 2014;111(17):6377-6382.

179. Hasbold J, Corcoran LM, Tarlinton DM, Tangye SG, Hodgkin PD. Evidence from the generation of immunoglobulin G-secreting cells that stochastic mechanisms regulate lymphocyte differentiation. *Nat Immunol*. 2004;5(1):55-63.

180. Hawkins ED, Turner ML, Wellard CJ, Zhou JH, Dowling MR, Hodgkin PD. Quantal and graded stimulation of B lymphocytes as alternative strategies for regulating adaptive immune responses. *Nat Commun*. 2013;4:2406.

181. Heinzel S, Binh Giang T, Kan A, et al. A Myc-dependent division timer complements a cell-death timer to regulate T cell and B cell responses. *Nat Immunol*. 2017;18(1):96-103.

182. Hodgkin PD, Lee JH, Lyons AB. B cell differentiation and isotype switching is related to division cycle number. *J Exp Med*. 1996;184(1):277-281.

183. Zhou JHS, Markham JF, Duffy KR, Hodgkin PD. Stochastically Timed Competition Between Division and Differentiation Fates Regulates the Transition From B Lymphoblast to Plasma Cell. *Frontiers in immunology*. 2018;9:2053.

184. Duffy KR, Wellard CJ, Markham JF, et al. Activation-induced B cell fates are selected by intracellular stochastic competition. *Science*. 2012;335(6066):338-341.

185. Lister R, Pelizzola M, Dowen RH, et al. Human DNA methylomes at base resolution show widespread epigenomic differences. *Nature*. 2009;462(7271):315-322.

186. Jjingo D, Conley AB, Yi SV, Lunyak VV, Jordan IK. On the presence and role of human gene-body DNA methylation. *Oncotarget*. 2012;3(4):462-474.

187. Okano M, Bell DW, Haber DA, Li E. DNA methyltransferases Dnmt3a and Dnmt3b are essential for de novo methylation and mammalian development. *Cell*. 1999;99(3):247-257.

188. Hermann A, Goyal R, Jeltsch A. The Dnmt1 DNA-(cytosine-C5)-methyltransferase methylates DNA processively with high preference for hemimethylated target sites. *J Biol Chem*. 2004;279(46):48350-48359.

189. Greenberg MVC, Bourc'his D. The diverse roles of DNA methylation in mammalian development and disease. *Nat Rev Mol Cell Biol*. 2019;20(10):590-607.

190. Kitamura D, Roes J, Kuhn R, Rajewsky K. A B cell-deficient mouse by targeted disruption of the membrane exon of the immunoglobulin mu chain gene. *Nature*. 1991;350(6317):423-426.

191. Smith KG, Hewitson TD, Nossal GJ, Tarlinton DM. The phenotype and fate of the antibody-forming cells of the splenic foci. *Eur J Immunol*. 1996;26(2):444-448.

192. Caron G, Hussein M, Kulis M, et al. Cell-Cycle-Dependent Reconfiguration of the DNA Methylome during Terminal Differentiation of Human B Cells into Plasma Cells. *Cell Rep*. 2015;13(5):1059-1071.

193. Willis SN, Nutt SL. New players in the gene regulatory network controlling late B cell differentiation. *Curr Opin Immunol*. 2019;58:68-74.

194. Qi T, Sun M, Zhang C, Chen P, Xiao C, Chang X. Ascorbic Acid Promotes Plasma Cell Differentiation through Enhancing TET2/3-Mediated DNA Demethylation. *Cell Rep*. 2020;33(9):108452.

195. Barwick BG, Scharer CD, Martinez RJ, et al. B cell activation and plasma cell differentiation are inhibited by de novo DNA methylation. *Nat Commun*. 2018;9(1):1900.

196. Allis CD, Jenuwein T. The molecular hallmarks of epigenetic control. *Nat Rev Genet*. 2016;17(8):487-500.

197. Buenrostro JD, Wu B, Chang HY, Greenleaf WJ. ATAC-seq: A Method for Assaying Chromatin Accessibility Genome-Wide. *Curr Protoc Mol Biol*. 2015;109:21 29 21-29.

198. Scharer CD, Blalock EL, Barwick BG, et al. ATAC-seq on biobanked specimens defines a unique chromatin accessibility structure in naive SLE B cells. *Sci Rep*. 2016;6:27030.

199. Singh H, Glasmacher E, Chang AB, Vander Lugt B. The molecular choreography of IRF4 and IRF8 with immune system partners. *Cold Spring Harb Symp Quant Biol*. 2013;78:101-104.

200. Haines RR, Barwick BG, Scharer CD, Majumder P, Randall TD, Boss JM. The Histone Demethylase LSD1 Regulates B Cell Proliferation and Plasmablast Differentiation. *J Immunol*. 2018;201(9):2799-2811.

201. Guo M, Price MJ, Patterson DG, et al. EZH2 Represses the B Cell Transcriptional Program and Regulates Antibody-Secreting Cell Metabolism and Antibody Production. *J Immunol*. 2018;200(3):1039-1052.

202. Taylor JJ, Pape KA, Steach HR, Jenkins MK. Humoral immunity. Apoptosis and antigen affinity limit effector cell differentiation of a single naive B cell. *Science*. 2015;347(6223):784-787.

203. Di Pietro A, Good-Jacobson KL. Disrupting the Code: Epigenetic Dysregulation of Lymphocyte Function during Infectious Disease and Lymphoma Development. *J Immunol*. 2018;201(4):1109-1118.

204. Papalexi E, Satija R. Single-cell RNA sequencing to explore immune cell heterogeneity. *Nat Rev Immunol*. 2018;18(1):35-45.

205. Kunz DJ, Gomes T, James KR. Immune Cell Dynamics Unfolded by Single-Cell Technologies. *Front Immunol*. 2018;9:1435.

206. Halliley JL, Tipton CM, Liesveld J, et al. Long-Lived Plasma Cells Are Contained within the CD19(-)CD38(hi)CD138(+) Subset in Human Bone Marrow. *Immunity*. 2015;43(1):132-145.

207. Hou B, Reizis B, DeFranco AL. Toll-like receptors activate innate and adaptive immunity by using dendritic cell-intrinsic and -extrinsic mechanisms. *Immunity*. 2008;29(2):272-282.

208. Robinson MD, McCarthy DJ, Smyth GK. edgeR: a Bioconductor package for differential expression analysis of digital gene expression data. *Bioinformatics*. 2010;26(1):139-140.

209. Trapnell C, Cacchiarelli D, Grimsby J, et al. The dynamics and regulators of cell fate decisions are revealed by pseudotemporal ordering of single cells. *Nat Biotechnol*. 2014;32(4):381-386.

210. Subramanian A, Tamayo P, Mootha VK, et al. Gene set enrichment analysis: a knowledge-based approach for interpreting genome-wide expression profiles. *Proc Natl Acad Sci U S A*. 2005;102(43):15545-15550.

211. Lam WY, Bhattacharya D. Metabolic Links between Plasma Cell Survival, Secretion, and Stress. *Trends Immunol*. 2018;39(1):19-27.

212. Adamson B, Norman TM, Jost M, et al. A Multiplexed Single-Cell CRISPR Screening Platform Enables Systematic Dissection of the Unfolded Protein Response. *Cell*. 2016;167(7):1867-1882 e1821.

213. Aibar S, Gonzalez-Blas CB, Moerman T, et al. SCENIC: single-cell regulatory network inference and clustering. *Nat Methods*. 2017;14(11):1083-1086.

214. Betz BC, Jordan-Williams KL, Wang C, et al. Batf coordinates multiple aspects of B and T cell function required for normal antibody responses. *J Exp Med*. 2010;207(5):933-942.

215. Venturi GM, Tu L, Kadono T, et al. Leukocyte migration is regulated by L-selectin endoproteolytic release. *Immunity*. 2003;19(5):713-724.

216. Yoon HS, Scharer CD, Majumder P, et al. ZBTB32 is an early repressor of the CIITA and MHC class II gene expression during B cell differentiation to plasma cells. *J Immunol*. 2012;189(5):2393-2403.

217. Kawasaki T, Kawai T. Toll-like receptor signaling pathways. *Front Immunol*. 2014;5:461.

218. Mesin L, Ersching J, Victora GD. Germinal Center B Cell Dynamics. *Immunity*. 2016;45(3):471-482.

219. Cyster JG, Allen CDC. B Cell Responses: Cell Interaction Dynamics and Decisions. *Cell*. 2019;177(3):524-540.

220. Hodgkin PD. Modifying clonal selection theory with a probabilistic cell. *Immunol Rev*. 2018;285(1):249-262.

221. Barkhausen T, Krettek C, van Griensven M. L-selectin: adhesion, signalling and its importance in pathologic posttraumatic endotoxemia and non-septic inflammation. *Exp Toxicol Pathol*. 2005;57(1):39-52.

222. Iwakoshi NN, Lee AH, Glimcher LH. The X-box binding protein-1 transcription factor is required for plasma cell differentiation and the unfolded protein response. *Immunol Rev*. 2003;194:29-38.

223. Rickert RC, Roes J, Rajewsky K. B lymphocyte-specific, Cre-mediated mutagenesis in mice. *Nucleic Acids Res*. 1997;25(6):1317-1318.

224. Shapiro-Shelef M, Lin KI, McHeyzer-Williams LJ, Liao J, McHeyzer-Williams MG, Calame K. Blimp-1 is required for the formation of immunoglobulin secreting plasma cells and pre-plasma memory B cells. *Immunity*. 2003;19(4):607-620.

225. Kim D, Pertea G, Trapnell C, Pimentel H, Kelley R, Salzberg SL. TopHat2: accurate alignment of transcriptomes in the presence of insertions, deletions and gene fusions. *Genome Biol*. 2013;14(4):R36.

226. Hsu F, Kent WJ, Clawson H, Kuhn RM, Diekhans M, Haussler D. The UCSC Known Genes. *Bioinformatics*. 2006;22(9):1036-1046.

227. Baker SC, Bauer SR, Beyer RP, et al. The External RNA Controls Consortium: a progress report. *Nat Methods*. 2005;2(10):731-734.

228. Lawrence M, Huber W, Pages H, et al. Software for computing and annotating genomic ranges. *PLoS Comput Biol*. 2013;9(8):e1003118.

229. van Dijk D, Sharma R, Nainys J, et al. Recovering Gene Interactions from Single-Cell Data Using Data Diffusion. *Cell*. 2018;174(3):716-729 e727.

230. Mitchell S. What Will B Will B: Identifying Molecular Determinants of Diverse B-Cell Fate Decisions Through Systems Biology. *Front Cell Dev Biol*. 2020;8:616592.

231. Fernandez D, Ortiz M, Rodriguez L, Garcia A, Martinez D, Moreno de Alboran I. The proto-oncogene c-myc regulates antibody secretion and Ig class switch recombination. *J Immunol*. 2013;190(12):6135-6144.

232. Perez-Olivares M, Trento A, Rodriguez-Acebes S, et al. Functional interplay between c-Myc and Max in B lymphocyte differentiation. *EMBO Rep*. 2018;19(10).

233. Walter P, Ron D. The unfolded protein response: from stress pathway to homeostatic regulation. *Science*. 2011;334(6059):1081-1086.

234. Bettigole SE, Glimcher LH. Endoplasmic reticulum stress in immunity. *Annu Rev Immunol*. 2015;33:107-138.

235. Turner ML, Hawkins ED, Hodgkin PD. Quantitative regulation of B cell division destiny by signal strength. *J Immunol*. 2008;181(1):374-382.

236. Vignon C, Debeissat C, Georget MT, et al. Flow cytometric quantification of all phases of the cell cycle and apoptosis in a two-color fluorescence plot. *PLoS One*. 2013;8(7):e68425.

237. Jin L, Chun J, Pan C, et al. Phosphorylation-mediated activation of LDHA promotes cancer cell invasion and tumour metastasis. *Oncogene*. 2017;36(27):3797-3806.

238. Chang YC, Yang YC, Tien CP, Yang CJ, Hsiao M. Roles of Aldolase Family Genes in Human Cancers and Diseases. *Trends Endocrinol Metab*. 2018;29(8):549-559.

239. Xiong Y, Lu J, Fang Q, et al. UBE2C functions as a potential oncogene by enhancing cell proliferation, migration, invasion, and drug resistance in hepatocellular carcinoma cells. *Biosci Rep*. 2019;39(4).

240. Huang L, Wang HY, Li JD, et al. KPNA2 promotes cell proliferation and tumorigenicity in epithelial ovarian carcinoma through upregulation of c-Myc and downregulation of FOXO3a. *Cell Death Dis*. 2013;4:e745.

241. Gao Z, Man X, Li Z, et al. PLK1 promotes proliferation and suppresses apoptosis of renal cell carcinoma cells by phosphorylating MCM3. *Cancer Gene Ther*. 2020;27(6):412-423.

242. Zhu J, Cui K, Cui Y, Ma C, Zhang Z. PLK1 Knockdown Inhibits Cell Proliferation and Cell Apoptosis, and PLK1 Is Negatively Regulated by miR-4779 in Osteosarcoma Cells. *DNA Cell Biol*. 2020;39(5):747-755.

243. Heikkila R, Schwab G, Wickstrom E, et al. A c-myc antisense oligodeoxynucleotide inhibits entry into S phase but not progress from G0 to G1. *Nature*. 1987;328(6129):445-449.

244. Wickstrom EL, Bacon TA, Gonzalez A, Freeman DL, Lyman GH, Wickstrom E. Human promyelocytic leukemia HL-60 cell proliferation and c-myc protein expression are inhibited by an antisense pentadecadeoxynucleotide targeted against c-myc mRNA. *Proc Natl Acad Sci U S A*. 1988;85(4):1028-1032.

245. Bretones G, Delgado MD, Leon J. Myc and cell cycle control. *Biochim Biophys Acta*. 2015;1849(5):506-516.

246. Buenrostro JD, Giresi PG, Zaba LC, Chang HY, Greenleaf WJ. Transposition of native chromatin for fast and sensitive epigenomic profiling of open chromatin, DNA-binding proteins and nucleosome position. *Nat Methods*. 2013;10(12):1213-1218.

247. Heinz S, Benner C, Spann N, et al. Simple combinations of lineage-determining transcription factors prime cis-regulatory elements required for macrophage and B cell identities. *Mol Cell*. 2010;38(4):576-589.

248. Stone SL, Peel JN, Scharer CD, et al. T-bet Transcription Factor Promotes Antibody-Secreting Cell Differentiation by Limiting the Inflammatory Effects of IFN-gamma on B Cells. *Immunity*. 2019;50(5):1172-1187 e1177.

249. Hann SR. Role of post-translational modifications in regulating c-Myc proteolysis, transcriptional activity and biological function. *Semin Cancer Biol*. 2006;16(4):288-302.

250. Saxton RA, Sabatini DM. mTOR Signaling in Growth, Metabolism, and Disease. *Cell*. 2017;169(2):361-371.

251. Liu P, Ge M, Hu J, et al. A functional mammalian target of rapamycin complex 1 signaling is indispensable for c-Myc-driven hepatocarcinogenesis. *Hepatology*. 2017;66(1):167-181.

252. Gao S, Chen M, Wei W, et al. Crosstalk of mTOR/PKM2 and STAT3/c-Myc signaling pathways regulate the energy metabolism and acidic microenvironment of gastric cancer. *J Cell Biochem*. 2018.

253. Lin CJ, Cencic R, Mills JR, Robert F, Pelletier J. c-Myc and eIF4F are components of a feedforward loop that links transcription and translation. *Cancer Res*. 2008;68(13):5326-5334.

254. Pourdehnad M, Truitt ML, Siddiqi IN, Ducker GS, Shokat KM, Ruggero D. Myc and mTOR converge on a common node in protein synthesis control that confers synthetic lethality in Myc-driven cancers. *Proc Natl Acad Sci U S A*. 2013;110(29):11988-11993.

255. Schmidt EV, Ravitz MJ, Chen L, Lynch M. Growth controls connect: interactions between c-myc and the tuberous sclerosis complex-mTOR pathway. *Cell Cycle*. 2009;8(9):1344-1351.

256. Negishi H, Ohba Y, Yanai H, et al. Negative regulation of Toll-like-receptor signaling by IRF-4. *Proc Natl Acad Sci U S A*. 2005;102(44):15989-15994.

257. Boddicker RL, Kip NS, Xing X, et al. The oncogenic transcription factor IRF4 is regulated by a novel CD30/NF-kappaB positive feedback loop in peripheral T-cell lymphoma. *Blood*. 2015;125(20):3118-3127.

258. Chaudhri VK, Dienger-Stambaugh K, Wu Z, Shrestha M, Singh H. Charting the cis-regulome of activated B cells by coupling structural and functional genomics. *Nat Immunol*. 2020;21(2):210-220.

259. Man K, Miasari M, Shi W, et al. The transcription factor IRF4 is essential for TCR affinity-mediated metabolic programming and clonal expansion of T cells. *Nat Immunol*. 2013;14(11):1155-1165.

260. Chapman NM, Zeng H, Nguyen TM, et al. mTOR coordinates transcriptional programs and mitochondrial metabolism of activated Treg subsets to protect tissue homeostasis. *Nat Commun*. 2018;9(1):2095.

261. Raybuck AL, Cho SH, Li J, et al. B Cell-Intrinsic mTORC1 Promotes Germinal Center-Defining Transcription Factor Gene Expression, Somatic Hypermutation, and Memory B Cell Generation in Humoral Immunity. *J Immunol*. 2018;200(8):2627-2639.

262. Yao S, Buzo BF, Pham D, et al. Interferon regulatory factor 4 sustains CD8(+) T cell expansion and effector differentiation. *Immunity*. 2013;39(5):833-845.

263. Laplante M, Sabatini DM. Regulation of mTORC1 and its impact on gene expression at a glance. *J Cell Sci*. 2013;126(Pt 8):1713-1719.

264. Wall M, Poortinga G, Hannan KM, Pearson RB, Hannan RD, McArthur GA. Translational control of c-MYC by rapamycin promotes terminal myeloid differentiation. *Blood*. 2008;112(6):2305-2317.

265. Hay N, Sonenberg N. Upstream and downstream of mTOR. *Genes Dev*. 2004;18(16):1926-1945.

266. Magnuson AM, Kiner E, Ergun A, et al. Identification and validation of a tumor-infiltrating Treg transcriptional signature conserved across species and tumor types. *Proc Natl Acad Sci U S A*. 2018;115(45):E10672-E10681.

267. Naviaux RK, Costanzi E, Haas M, Verma IM. The pCL vector system: rapid production of helper-free, high-titer, recombinant retroviruses. *J Virol*. 1996;70(8):5701-5705.

268. Kawauchi D, Robinson G, Uziel T, et al. A mouse model of the most aggressive subgroup of human medulloblastoma. *Cancer Cell*. 2012;21(2):168-180.

269. Dobin A, Davis CA, Schlesinger F, et al. STAR: ultrafast universal RNA-seq aligner. *Bioinformatics*. 2013;29(1):15-21.

270. Langmead B, Trapnell C, Pop M, Salzberg SL. Ultrafast and memory-efficient alignment of short DNA sequences to the human genome. *Genome Biol*. 2009;10(3):R25.

271. Zhang Y, Liu T, Meyer CA, et al. Model-based analysis of ChIP-Seq (MACS). *Genome Biol*. 2008;9(9):R137.

272. Tomayko MM, Anderson SM, Brayton CE, et al. Systematic comparison of gene expression between murine memory and naive B cells demonstrates that memory B cells have unique signaling capabilities. *J Immunol*. 2008;181(1):27-38.

273. Laidlaw BJ, Schmidt TH, Green JA, Allen CD, Okada T, Cyster JG. The Eph-related tyrosine kinase ligand Ephrin-B1 marks germinal center and memory precursor B cells. *J Exp Med*. 2017;214(3):639-649.

274. Laidlaw BJ, Cyster JG. Transcriptional regulation of memory B cell differentiation. *Nat Rev Immunol*. 2021;21(4):209-220.

275. Wang Y, Shi J, Yan J, et al. Germinal-center development of memory B cells driven by IL-9 from follicular helper T cells. *Nat Immunol*. 2017;18(8):921-930.

276. Suan D, Krautler NJ, Maag JLV, et al. CCR6 Defines Memory B Cell Precursors in Mouse and Human Germinal Centers, Revealing Light-Zone Location and Predominant Low Antigen Affinity. *Immunity*. 2017;47(6):1142-1153 e1144.

277. Carter RH. B cells in health and disease. *Mayo Clin Proc*. 2006;81(3):377-384.

278. Moens L, Tangye SG. Cytokine-Mediated Regulation of Plasma Cell Generation: IL-21 Takes Center Stage. *Front Immunol*. 2014;5:65.

279. Yaqoob P, Newsholme EA, Calder PC. Comparison of cytokine production in cultures of whole human blood and purified mononuclear cells. *Cytokine*. 1999;11(8):600-605.

280. Costalonga M, Zell T. Lipopolysaccharide enhances in vivo interleukin-2 production and proliferation by naive antigen-specific CD4 T cells via a Toll-like receptor 4-dependent mechanism. *Immunology*. 2007;122(1):124-130.

281. du Plessis WJ, Kleynhans L, du Plessis N, et al. The Functional Response of B Cells to Antigenic Stimulation: A Preliminary Report of Latent Tuberculosis. *PLoS One*. 2016;11(4):e0152710.

282. Arango Duque G, Descoteaux A. Macrophage cytokines: involvement in immunity and infectious diseases. *Front Immunol*. 2014;5:491.

283. Patterson DG, Kania AK, Zuo Z, Scharer CD, Boss JM. Epigenetic gene regulation in plasma cells. *Immunol Rev*. 2021.

284. Akkaya M, Kwak K, Pierce SK. B cell memory: building two walls of protection against pathogens. *Nat Rev Immunol*. 2020;20(4):229-238.

285. Kurosaki T, Kometani K, Ise W. Memory B cells. *Nat Rev Immunol*. 2015;15(3):149-159.

286. Price MJ, Scharer CD, Kania AK, Randall TD, Boss JM. Conserved Epigenetic Programming and Enhanced Heme Metabolism Drive Memory B Cell Reactivation. *J Immunol*. 2021;206(7):1493-1504.

287. Zuccarino-Catania GV, Sadanand S, Weisel FJ, et al. CD80 and PD-L2 define functionally distinct memory B cell subsets that are independent of antibody isotype. *Nat Immunol*. 2014;15(7):631-637.

288. Saelens W, Cannoodt R, Todorov H, Saeys Y. A comparison of single-cell trajectory inference methods. *Nat Biotechnol*. 2019;37(5):547-554.

289. Nowotschin S, Setty M, Kuo YY, et al. The emergent landscape of the mouse gut endoderm at single-cell resolution. *Nature*. 2019;569(7756):361-367.

290. Kawabe T, Naka T, Yoshida K, et al. The immune responses in CD40-deficient mice: impaired immunoglobulin class switching and germinal center formation. *Immunity*. 1994;1(3):167-178.

291. Renshaw BR, Fanslow WC, 3rd, Armitage RJ, et al. Humoral immune responses in CD40 ligand-deficient mice. *J Exp Med*. 1994;180(5):1889-1900.

292. Takahashi Y, Dutta PR, Cerasoli DM, Kelsoe G. In situ studies of the primary immune response to (4-hydroxy-3-nitrophenyl)acetyl. V. Affinity maturation develops in two stages of clonal selection. *J Exp Med*. 1998;187(6):885-895.

293. Xu J, Foy TM, Laman JD, et al. Mice deficient for the CD40 ligand. *Immunity*. 1994;1(5):423-431.

294. Luo W, Weisel F, Shlomchik MJ. B Cell Receptor and CD40 Signaling Are Rewired for Synergistic Induction of the c-Myc Transcription Factor in Germinal Center B Cells. *Immunity*. 2018;48(2):313-326 e315.

295. Ersching J, Efeyan A, Mesin L, et al. Germinal Center Selection and Affinity Maturation Require Dynamic Regulation of mTORC1 Kinase. *Immunity*. 2017;46(6):1045-1058 e1046.

296. Ise W, Fujii K, Shiroguchi K, et al. T Follicular Helper Cell-Germinal Center B Cell Interaction Strength Regulates Entry into Plasma Cell or Recycling Germinal Center Cell Fate. *Immunity*. 2018;48(4):702-715 e704.